Working session: Bridge design issues. Papers and posters

Working Session

Bridge Design Issues

Papers and Posters

Leere Seite
Blank page
Page vide

Vibration Measurement of Tsing Ma Bridge Deck Units during Erection

Tommy CHAN
Assist. Prof.
Hong Kong Polytechnic Univ.
Hong Kong, China

Jan Ming KO
Chair and Head
Hong Kong Polytechnic Univ.
Hong Kong, China

Ching Kwong LAU
Deputy Director
Highways Dept, Hong Kong Gov.
Hong Kong, China

Kai Yuen WONG
Senior Eng.
Highways Dept, Hong Kong Gov.
Hong Kong, China

Summary

The Tsing Ma Suspension Bridge in Hong Kong has a main span of 1377m and an overall length of 2160m. During its construction, ambient vibration measurements were carried out to study the dynamic behaviour of the bridge at various construction stages. This paper reports the random vibration measurements of the first few suspeneded deck units. Two measurements were conducted with the first measurement on the first twin-deck-unit module suspended on the main cables and the second on the three partially connected twin-deck-units suspended on the main cables. The identified lowest 15 natural frequencies of the two systems are within the frequency range 0~0.3 Hz and are very closely distributed. The modal frequencies identified and the corresponding analytical results for both systems are in close agreement with the maximum relative difference being less than 10%.

1. Introduction

The Tsing Ma Bridge, a long suspension bridge with a main span of 1377m and a total length of 2160m, spans the Ma Wan Channel between the islands of Tsing Yi and Ma Wan. It carrys both road and rail transportation on two decks under a harsh marine environment and typhoon conditions. Construction of the Tsing Ma Bridge commenced in May 1992. The towers were completed in November 1993. Anchorages were erected for cable construction in July 1994. Spinning of the main cables commenced in July 1994 and completed in April 1995. The first twin-deck-unit module was lifted into position at the center of the main span of the bridge on 9 August 1995. The construction of the whole bridge was completed and opened to traffic in April 1997. During its construction, ambient vibration measurements were carried out to study the dynamic behaviour of the bridge at various construction stages. Previous studies which included measurements of the two bridge-towers (Law et al 1995) and bridge-towers with the erected cables (Xu et al 1997) had been carried out. This paper presents the third study of the series, in which the global dynamic characteristics of the suspended deck units were investigated by in-situ vibration measurement. The suspended deck structure was composed of 95 units plus two special end modules and were erected from the centre of main span towards the bridge-towers. Most (97%) of the units were of 18m in length and 500t in weight. Each lifting module consisted of two deck units welded together. The first measurement was made from 16-17 August 1995 to measure the ambient vibration response of the single twin-deck-unit module. Then the second measurement was made from 29-30 August 1995 after the other two twin-deck-units had been installed.

2. The Main Cable and the Deck Units

The main cables, which are 36m apart, were built up wire by wire by the in-situ aerial spinning technique. Each of the cables is of cross-sectional area 0.759m^2 for the main span. The mass density per unit of cable length is 5.832 t/m. The cables are approximately 1.1m in diameter after compaction. The cables are accommodated with saddles located at the top of the tower legs and at the main anchorages and adjacent piers, and transfer the loadings into the towers and anchorages. The suspenders are at 18m centers and are attached to the deck by cast steel sockets.

Each deck unit consists of two 6.3m deep longitudinal trusses, spaced at 27 m centers. These act compositely with the orthotropic deck plates supporting the carriageways to provide bending stiffness. Plan diagonal bracing spans the upper and lower vents and acts with the orthotropic plates to provide lateral stiffness. Vierendeel cross frames are located at 4.5m centers. Figure 1 (Beard 1993) shows a typical cross frame of a deck unit. Each basic deck unit, weighing approximately 500 t, is 18 m long with an overall depth of 7.7 m.

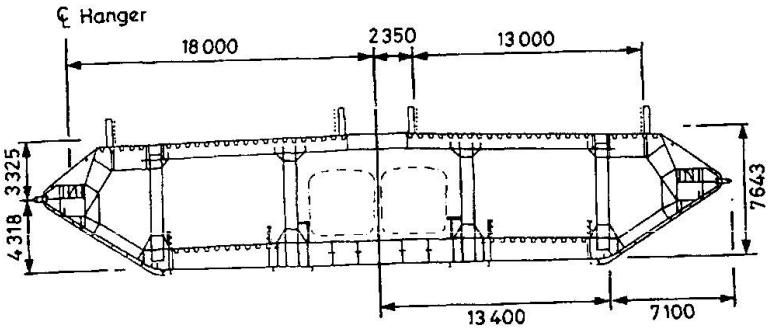

Figure 1 Typical Cross-section of Deck Unit (Beard 1993)

Each lifting deck module consists of two 18m deck units welded together to form a 36m module (twin-deck-unit). Figure 2 shows the numbering system of the deck units. The deck units measured in the present study are described as follows.

I) *Single Twin-Deck-Unit* : The twin-deck-unit Nos. {58, 59} with a total length of 36m was the first lifting module being installed to the main cables. They are the center-most suspended deck units.

II) *Three Temporarily Connected Twin-Deck-Units* : The testing section consisted of three twin-deck-units (lifting modules), i.e. Nos. {60 , 61}, Nos. {58, 59} and Nos. {56, 57}. The three modules were temporarily bolted together to form a single section with a total length of 108m.

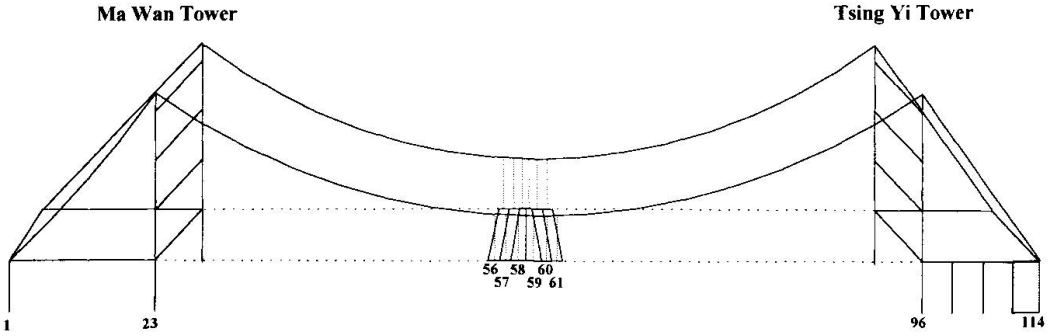

Figure 2 Number System of Deck Units

3. Finite Element Modelling

Based on previous studies (Xu et al 1997), it is valid to assume that the main span cables are suspended on two fixed end-supports at the same level by neglecting the influence of the bridge towers. Cable is a flexible structural element which has hardly any bending resistance. Cable structures are generally elastic in nature but are nonlinear in the geometric sense. In the present study, each cable is modelled by a number of two-node cable elements with six-degree-of-freedoms, i.e. three translational movements in horizontal, vertical and transverse directions for each node. This kind of elements takes account of the cable tension and the geometric deflection. The 6x6 stiffness matrix, which includes linear elastic stiffness, geometric stiffness and large deflection stiffness, and the consistent mass matrix are established by considering the static equilibrium state as initial state. The bridge deck units are freely suspended on the main cables through suspenders. The suspenders are also modelled as cable elements. As the motion of the bridge deck units normally follows the motion of the cables and the objective of the analysis is to find out the global modal characteristics of the suspended bridge-deck units, each twin-deck-unit module is modelled as a rigid body. The temporary site joints between each twin-deck-unit module are treated as such connection that the two adjacent twin-deck-units can rotate freely in vertical direction, but move together in the in-plane direction. In the present analysis, each main span cable is represented by 25 finite elements with different lengths and the bridge deck units are represented by rigid deck units. The finite element models are shown in Figure 3.

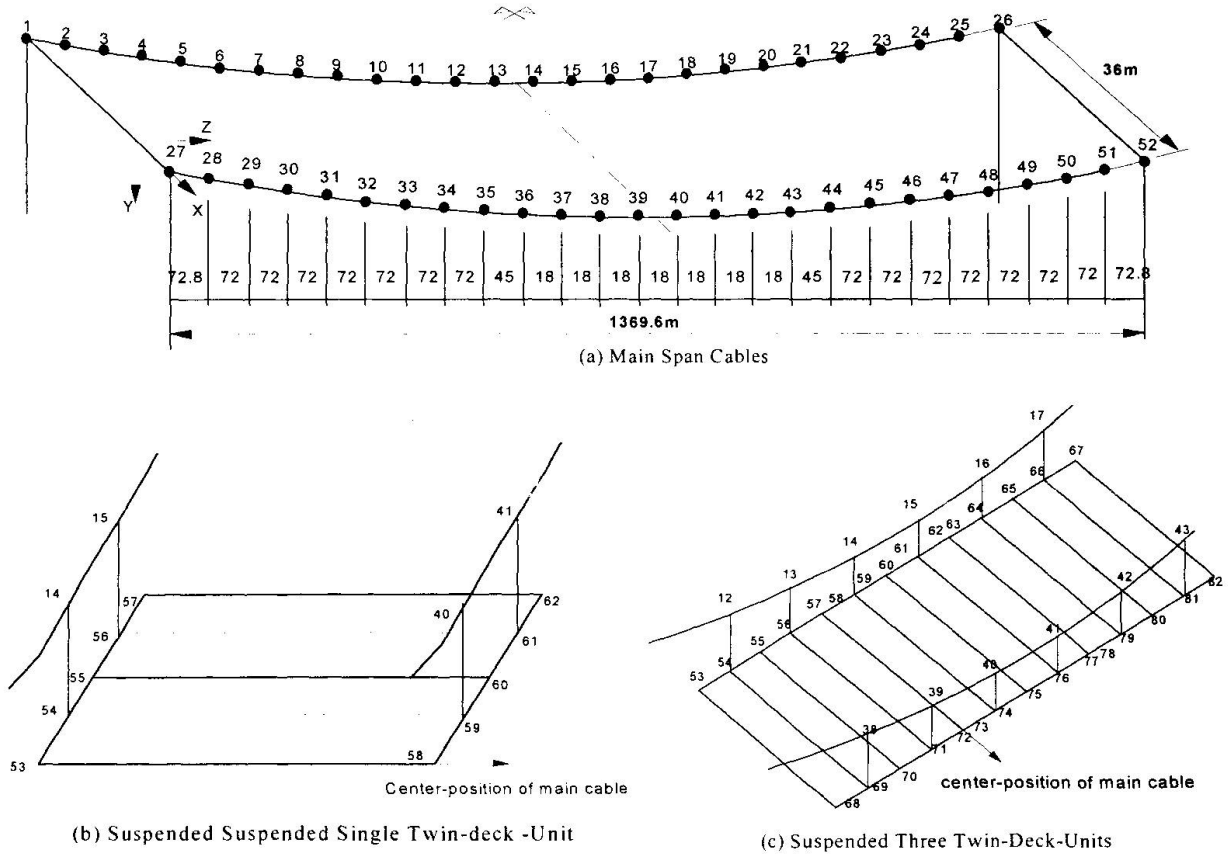

(a) Main Span Cables

(b) Suspended Suspended Single Twin-deck -Unit

(c) Suspended Three Twin-Deck-Units

Figure 3 Finite Element Models with Node Numbering

4. The Field Measurement and Signal Processing

It was originally planned to conduct the two measurements in 2 two-day programmes. However, because of the tight schedule of construction and the multitude of construction activities on site, only one full day was allowed for each measurement.

The location of sensors is a very important aspect in modal testing. In general, the more the sensors the more the information can be got and the more complete the modal parameters can be obtained. However, the number of sensors are always limited. The philosophy of locating sensors is to simulate the test, and to choose locations that give maximum responses. Since the global natural frequencies and mode shapes are essential for the updating of the system parameters, the sensors will be so located such that the bending, torsional and side-sway modes of the suspended deck units and the cables will be measured separately. With the help of the theoretical mode shapes (Ko et al 1996), the locations of 12 sensors in each recording were arranged in such a way so that the measured results could be effectively used to describe each mode. The arrangements of the sensors for the measurement of the single twin-deck-unit system are shown in Figure 4. Similar arrangements were made for the measurements of the three twin-deck-units system.

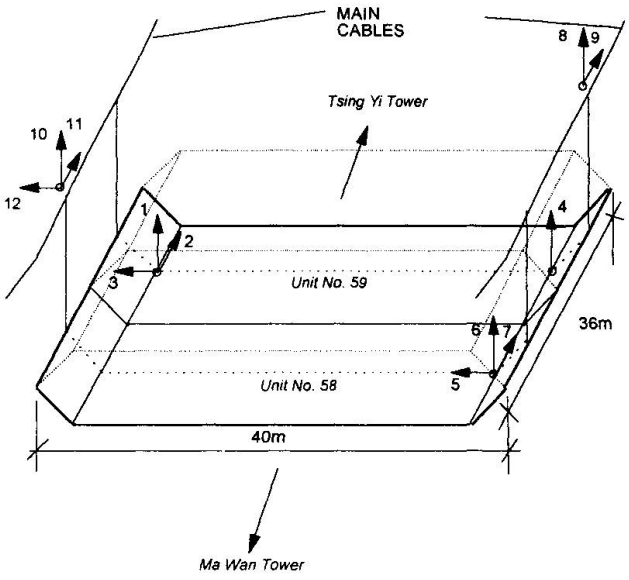

Figure 4 Layout of Sensors for the Measurement of the Single Twin-Deck-Unit System

There were totally five recordings made. The first measurement, in which one recording was made, was for the dynamic response of the single twin-deck-unit system (Nos. {58, 59}). The other four recordings were made for the second measurement. They were carried out after the other two twin-deck-units modules (Nos. {60, 61} and Nos. {56, 57}) had been suspended and the three modules were temporarily bolted together. In general, the sensors in the deck units, which were mounted on magnetic stands fixed on the floor of the deck, were oriented in three directions to measure the vertical, lateral, longitudinal and torsional motions. On the other hand, the sensors on the main cables, which were mounted on magnetic stands fixed to the cable bands of the cables, were to identify the interaction between bridge deck units and the cables.

Theoretical analysis indicated that the natural frequencies of the suspended bridge deck units with main cables were closely spaced in the low frequency range (Ko et al 1996). Therefore the signal processing was performed in the frequency range of 0~1.56 Hz. In order to identify the very closely spaced natural frequencies, a fine frequency resolution of 0.00195Hz, which is the finest frequency resolution set in the B&K 3550 Multichannel Analysis System, was adopted in the spectral analysis. It was found that under the above frequency resolution, some vibration modes were still difficult to identify, therefore the recorded signals on the tapes were played back with a speed of 4 times faster than the original recorded tape speed in the same frequency range of 0~1.56 Hz. In this way, a finer frequency resolution could be achieved and the natural frequencies were obtained by dividing the calcuated values by 4.

5. Results

Comparison between the natural frequencies obtained by the ambient vibration measurement and those obtained by the finite element analysis are shown in Table 1. It is seen that the measured and computed natural frequencies are all in close agreement. The relative difference are within

10%. These comparisons indicate that the finite element modelling established in the theoretical analysis is reasonable and acceptable for predicting the modal properties of the suspended deck units. It also implied that there is a good agreement between the measured structural stiffness and that predicted in the finite element modelling.

Mode of Vibration	Single Twin-Deck-Unit			Three Twin-Deck-Units		
	Theoretical (Hz)	Measured (Hz)	Relative Difference (%)	Theoretical (Hz)	Measured (Hz)	Relative Difference (%)
1st lateral sway mode	0.0510	0.051	0.0	0.0495	0.049	1.0
2nd lateral sway mode	0.1102	0.112	-1.6	0.1195	0.117	2.1
3rd lateral sway mode	0.1478	0.152	-2.8	0.1493	0.150	-0.5
4th lateral sway mode	0.2162	0.209	3.4	0.2369	0.223	6.2
5th lateral sway mode	0.2259	0.234	-3.5	0.2443	0.256	-4.6
1st lift mode	0.1073	0.107	0.3	0.1161	0.113	2.7
2nd lift mode	0.1438	0.139	3.5	0.1474	0.141	4.5
3rd lift mode	0.2165	0.219	-1.1	0.2286	0.230	-0.6
4th lift mode	0.2454	0.258	-4.9	0.2568	0.269	-4.5
1st torsional mode[1]	0.1088	0.110	-1.1	0.1264	---	---
2nd torsional mode[2]	0.1439	0.150	-4.1	0.1486	0.164	-9.4
3rd torsional mode[1]	0.2192	0.223	-1.7	0.2494	0.248	0.6
4th torsional mode[2]	0.2456	0.269	-8.7	0.2615	0.285	-8.2
deck rot. sway mode	0.2105	0.203	3.7	0.1971	0.207	-4.9
deck long. sway mode	0.2229	0.226	-1.4	0.2177	0.225	-3.2

1 - antisymetric mode; 2 - symetric mode

Table1: Theoretical and Measured Natural Frequencies of the two systems

It has to be pointed out that although a fine frequency resolution was taken in the spectral analysis, the first antisymmetric torsional mode of the suspended three twin-deck-units system was still not able to be identified.

From the measured modal vectors of suspended three twin-deck-units system, it can be observed that, in the in-plane direction of the bridge deck (lateral and longitudinal direction), the three twin-deck-units are basically vibrating as a rigid plate, i.e. no large relative motions occurred at the temporary bolted joints between two adjacent twin-deck-units. Therefore the three twin-deck-units can be regarded as one rigid deck section in the in-plane direction. However, in the vertical direction, some relative rotations are observed between two adjacent twin-deck-units, such as that in the fourth lift mode. The above results are consistent with the finite element modelling established in the theoretical analysis.

It is noticed that most of the measured natural modes of the suspended bridge deck units always vibrate together with the main cables. For each system, only one deck rotational sway mode and one deck longitudinal sway mode, which are dominated by deck vibration, are identified at the frequency range of 0~0.3 Hz. This is agreeable to the theoretical predictions.

By comparing the measured modal vectors with the theoretical mode shapes, it can be concluded that the measured modal motions are basically in accord with the theoretically predicted mode shapes. However, it is also noticed that some inconsistency still exists between the measured and

the computed modal vectors, such as the fourth and the fifth lateral sway modes of the suspended three twin-deck-units system as well as the second lateral sway mode and the deck rotational sway mode of the suspended single twin-deck-unit system.

6. Conclusions

1. The measurement of the structural response to ambient vibration from wind load and ground micro-tremor has proved to be an effective means for identification of the dynamic properties of a full-scale flexible structure with low natural frequencies. The dynamic properties identified include natural frequencies and mode shapes.
2. Careful planning and execution of the field work is a key factor in the collection of high quality data. Preliminary finite element dynamic analysis is useful in the design and planning of the ambient vibration test programme to achieve appropriate deployment and orientation of the motion-sensing instruments, to determine the reference point and to select appropriate filter setting and the sampling frequency.
3. For both the single twin-deck-unit system and the three twin-deck-unit system, many closely-spaced natural frequencies were found in the low frequency range of 0~0.3 Hz.
4. The modal frequencies identified and the corresponding analytical results for both systems are in close agreement with the maximum relative difference being less than 10 %. These comparisons indicate that the finite element modelling established in the theoretical analysis is reasonable and acceptable for predicting the modal properties of the suspended deck units.
5. It is found that, in the in-plane direction of the three twin-deck-units, no large relative motions occurred at the temporary bolted joints between two adjacent twin-deck-units. Therefore the three twin-deck-units can be regarded as one rigid deck section in the in-plane direction. However, in the vertical direction, some relative rotations are observed between two adjacent twin-deck-units for the suspended three twin-deck-units system.
6. The measured modal vectors are basically agreeable to the theoretically predicted mode shapes, but some inconsistency still exists between the measured and the computed modal vectors for some modes. This is due to the difficulty in representing the actual site conditions in the finite element modelling and the possible coupling of the closely distributed modes.

7. Acknowlegements

The authors wish to express their thanks to the Hong Kong Director of Highways, Mr. K.S. Leung for his permission to publish this paper. Any opinion expressed or conclusion made in the text are entirely those of the authors.

8. References

Beard. A.S. (1993). "Development of the Tsing Ma Bridge." The Structural Engineers, Vol. 71 No. 11, p. 192-195.

Ko, J.M. and Xue S.D. (1996). "Dynamic Behaviors of Suspended Bridge-Deck Units During Construction", Proceedings of *International Conference on Advances in Steel Structures,* Hong Kong, p. 497-503.

Law, S.S., Ko, J.M., Lau, C.K., and Wong, K.Y. (1995). "Ambient Vibration Measurement of the Tsing Ma Bridge Towers", Proceedings of *Internation Conference on Bridges into the 21st Century,* Impressions Design and Printed Ltd., Hong Kong, p. 585-592.

Xu, Y.L., Ko, J.M., and Yu, Z. (1997). "Model Analysis of Tower-Cable System of Tsing Ma Long Suspension Bridge", Engineering Structures, Vol. 19 No. 10, p. 857-867.

Static and Dynamic Instability Analyses of 1400-meter Long-Span Cable-Stayed Bridges

Masatsugu NAGAI
Prof.
Nagaoka Univ. of Technology
Nagaoka, Japan

Xu XIE
Research Assoc.
Saitama Univ.
Urawa, Japan

Hiroki YAMAGUCHI
Prof.
Saitama Univ.
Urawa, Japan

Yozo FUJINO
Prof.
Univ. of Tokyo
Tokyo, Japan

Summary

This paper describes static and dynamic instability analyses of long-span cable-stayed bridges. They are elasto-plastic finite displacement analysis under in-plane load, finite displacement analysis under displacement-dependent wind load and flutter analysis. Using a 1400-meter cable-stayed bridge model, in which four types of cross-sectional shapes of the girder are selected, static and dynamic instability analyses are carried out. Finally, the design materials for identifying a minimum cross sectional shape of the girder, which ensures safety against above instabilities, are presented.

1. Introduction

In the design of long-span cable-stayed bridges, ensuring safety against static and dynamic instabilities is an important issue, because the shape and dimension of the girder are controlled by the above instabilities. However, static and dynamic instability phenomena of long-span cable-stayed bridges based on analytical procedures have not been made clear so far. In this paper, using a 1400-meter cable-stayed bridge model, static and dynamic instability analyses such as elasto-plastic finite displacement analysis under in-plane load, finite displacement analysis under displacement-dependent wind load and flutter analysis based on modal coordinate are carried out. Four types of cross section of the box girder are chosen. The span/width ratio is 56 and 47, and the span/depth ratio is 400 and 350, respectively. It is recommended, for ensuring safety against out-of-plane instability under wind load, that the span/width ratio should be less than 40. However, in this study, the larger values are employed. The employed cross sections are preliminary designed, in which the yield point of the material only is selected to be instability criterion. By carrying out the above instability analyses, the factor of safety under in-plane load, critical wind velocity of lateral torsional buckling and flutter onset wind velocity are presented. Finally, the design materials for obtaining minimum cross-sectional shape and dimension of the girder is presented

2. Analytical procedure

2.1 Elasto-plastic finite displacement analysis under vertical load [1)]

For evaluating load carrying capacity of the cable-stayed bridges, not only geometrical but also material nonlinear behaviors should be taken into account. The fundamental equation of elasto-plastic finite displacement analysis is given by

$$([K_{ep}] + [K_\sigma])\{\Delta u\}^e = \{\Delta f\}^e \quad (1)$$

$$[K_{ep}] = \int_v [B]^T [D_{ep}][B] dv \quad (2)$$

$$[K_\sigma] = \int_v [G]^T [\sigma][G] dv \quad (3)$$

where, $[K_{ep}]$ and $[K_\sigma]$ are elasto-plastic and initial stress matrices, $\{\Delta u\}^e$ and $\{\Delta f\}^e$ are incremental displacement and force vectors of the element, [B] and [G] are matrices consisted of interpolation functions, $[D_{ep}]$ is matrix relating to the constitutive law, $[\sigma]$ is matrix consisted of initial stress resultants.

In this formulation, the constitutive law of elastic perfect-plastic material is derived based on the Prandtle-Reuss equation. The yield condition is given by

$$\sqrt{\sigma^2 + 3\tau^2} - \sigma_y = 0 \quad (4)$$

Where, σ_y is the yield point of the material.

2.2 Finite displacement analysis under wind load [2)]

In this analysis, the girder is subjected to the following three components of wind load, such as the drag force (D), lift force (L) and aerodynamic moment (M), which are given by

$$D(\alpha) = 0.5\,\rho\, U_Z^2 A_n C_D(\alpha)$$
$$L(\alpha) = 0.5\,\rho\, U_Z^2 B C_L(\alpha) \quad (5)$$
$$M(\alpha) = 0.5\,\rho\, U_Z^2 B^2 C_M(\alpha)$$

where, ρ is the air density, A_n is the vertical projection of the girder, B is the total width of the girder and C_D, C_L and C_M are aerodynamic coefficients.

U_Z is the design wind velocity at the height of z, and is given by

$$U_Z = (z/10)^{1/7} U_{10} \quad (6)$$

Where, U_{10} is the wind velocity at the height of 10 meters.

When the girder is subjected to the wind load, it displaces in the lateral direction and, at some wind velocity, it starts rotating. Due to the rotation of the girder, three components of aerodynamic forces above defined change, because they are dependent on an angle of attack (α) of the wind. This phenomenon should be taken into account[3)]. In this analysis, 4-node isoparametoric cable element is used, thus the wind load acting on the cable is taken into account. In addition, the change of the tension in cables and its direction is considered. With respect to aerodynamic coefficients, the values of the Meiko-chuo bridge (590-meter cable-stayed bridge)[3)] which were obtained from wind tunnel test, are used.

2.3 Flutter analysis based on modal coordinate[4)]

A fundamental equation of flutter analysis is derived based on modal coordinate and the effect of the cable local vibration on flutter onset wind velocity is taken into account. The unsteady drag

force of the girder is derived based on quasi-steady state theory, and the unsteady lift and aerodynamic moment are derived based on flat plate theory. The unsteady drag and lift forces of the cables are derived based on quasi-steady state theory.

The following is the fundamental equation of flutter analysis, which is expressed using both physical and modal coordinates.

$$[(M_{BC} - F_R) - iF_I]\begin{Bmatrix} \ddot{d} \\ \ddot{q}_C \end{Bmatrix} + [K_{BC}]\begin{Bmatrix} d \\ q_C \end{Bmatrix} = \{0\} \tag{7}$$

where, $\{d\}$ is the displacement of the girder and towers, $\{q_C\}$ is the generalized displacement of the cables, which corresponds to the cable local vibration, $[M_{BC}]$ and $[K_{BC}]$ are mass and stiffness matrices, respectively and $[F_R]$ and $[F_I]$ are real and imaginary parts of unsteady aerodynamic forces.

Carrying out eigenvalue analysis of the whole structure, in which cable local vibration is neglected, we obtain the modal matrix $[\phi]$. Using this matrix, eq.(10) is transformed into eq.(11). Where, $\{q\}$ is the generalized displacement, which corresponds to the global vibration.

$$[\phi]^T[(M_{BC} - F_R) - iF_I][\phi]\begin{Bmatrix} \ddot{q} \\ \ddot{q}_C \end{Bmatrix} + [\phi]^T[K_{BC}][\phi]\begin{Bmatrix} q \\ q_C \end{Bmatrix} = \{0\} \tag{8}$$

Assuming the reduced frequency, complex eigenvalue analysis is carried out, then we obtain complex eigenvalue of $\lambda = \lambda_R \pm i\,\lambda_I$. When the sign of the damping ($\xi = \lambda_R / \sqrt{\lambda_R^2 + \lambda_I^2}$) changes from plus to minus, flutter occurs.

3. BRIDGE MODEL

Fig.1(a) shows a side-view of a cable-stayed bridge model. Center and side spans are 1400 and 680 meters, respectively. In the side span, three intermediate piers are installed at a distance of 100 meters in order to increase in-plane flexural rigidity. Fig.1(b) is a front view of the tower, and the height of it from the deck level is one fifth of the center span length. Fig.1(c) shows the cross sectional shape of the girder. Four types of cross sections are used. In the Fig., Bu of 25 and 30 meters and h_w of 3.5 and 4.0 meters are selected. When calculating the stress from wind load, the design wind velocities of the girder and cables are assumed to be 60 and 70m/s, respectively. Those of them at the stage of erection are 70% of the above values. The drag coefficient (C_D) of them are assumed to be 0.8 and 0.7, respectively.

Dimension of the girder is determined by using the following criteria

$$\sigma_D + \sigma_L < \sigma_y / \gamma_1 \qquad (\gamma_1 = 1.7) \tag{13}$$

$$\sigma_D + \sigma_W < \sigma_y / \gamma_2 \qquad (\gamma_2 = 1.15) \tag{14}$$

where, σ_D, σ_L and σ_W are stresses from dead, live and wind loads, respectively, σ_y (= 451MPa) is the yield point of the employed material and γ is the factor of safety.

To satisfy eq.(14), the thickness of the plate is increased as shown in Fig.1(d). In the bridge axis direction, the section of Xu as shown in Fig.1(a) is reinforced. Table 1 shows the cross-sectional properties of the girder preliminary designed. In the table, the figures in the parenthesis are for the reinforced girder.

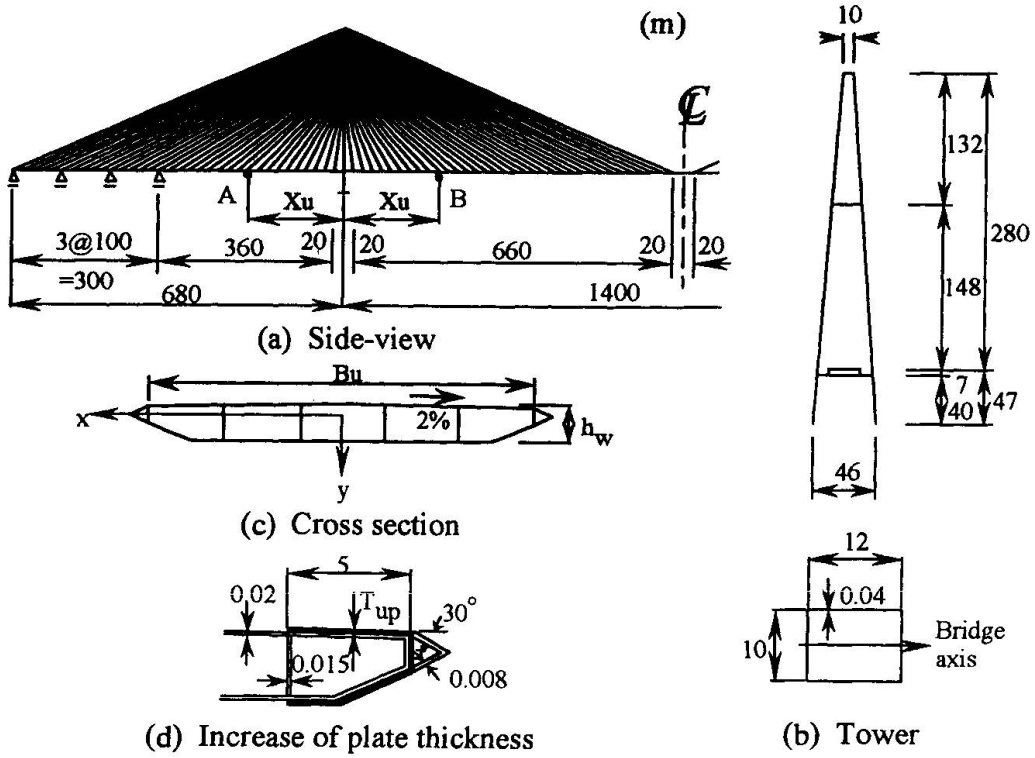

Figure1: Bridge model

Table1 : Cross sectional properties of the girder and tower

	Bu (m)	hw (m)	A (m^2)	Ix (m^4)	Iy (m^4)	J (m^4)	Iw (m^6)	W (tf/m)	Xu (m)
Girder	25	3.5	1.314 (2.243)	2.56 (4.050)	75.653 (177.323)	5.767 (9.395)	90.431 (314.397)	21.441 (28.871)	260
	25	4.0	1.348 (2.359)	3.291 (5.130)	76.932 (187.140)	7.133 (11.333)	106.659 (404.954)	21.815 (29.751)	200
	30	3.5	1.563 (2.134)	3.083 (3.987)	127.201 (222.835)	7.08 (9.615)	173.351 (369.716)	24.177 (28.871)	120
	30	4.0	1.605 (2.182)	4.002 (5.051)	129.658 (225.990)	8.889 (11.728)	210.045 (452.920)	24.639	140
Tower			1.76	30.667	40.32	39.273	—	19.342	—

4. RESULTS AND DISCUSSIONS

4.1 Load carrying capacity under in-plane load

Fig.2 shows incremental displacements of the bridge at ultimate state. In all cases, at points A and B, where the cross sectional properties are changed, the rapid increase of the vertical displacement is observed. In this region, the displacement in the bridge axis direction also increases rapidly. Hence, this is thought to be elaso-plastic global buckling of the girder. When in-plane instability occurs, the applied load of each model is from 2.75 to 2.90 times the dead load intensity. The large values are obtained. Since the effect of the local buckling of the stiffened plate is not taken into account in this analysis, it is predicted that the unstable behavior of the bridge models is controlled by the local buckling.

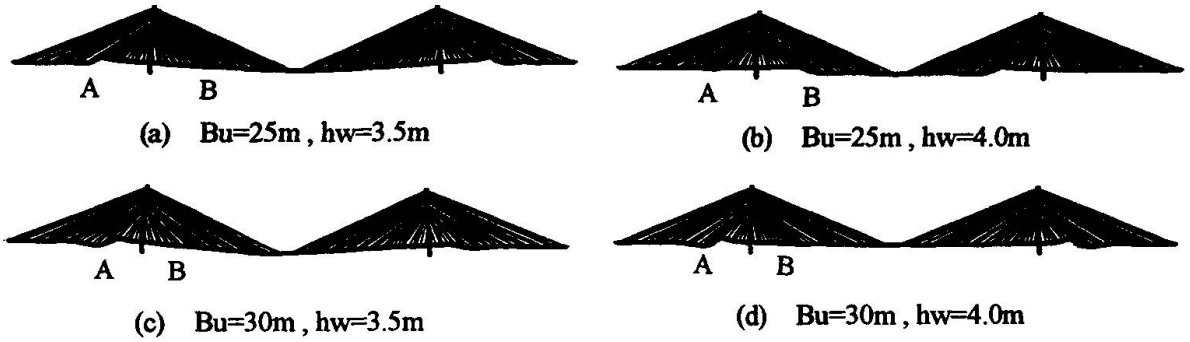

Figure2: Incremental displacement at ultimate state

4.2 Lateral torsional buckling instability under wind load

Fig.3 shows the lateral displacement, vertical displacement and rotational angle at the middle of the center span of the completed bridges. Fig.4 shows those at the tip of the cantilevered girder. In case of the completed bridges, at wind velocity of around 60m/s, nonlinear behavior of vertical displacement and rotational angle becomes prominent, and at the wind velocity from 77 to 80m/s, they diverges. This is lateral torsional buckling. In case of the bridge under construction, since the system is flexible, the larger lateral displacement is obtained. At the wind velocity of around 50m/s, nonlinear behavior of the vertical displacement becomes prominent and, at the wind velocity from 66 to 70m/s, the girder becomes unstable. The critical wind velocities calculated are enough high compared with the design wind velocities.

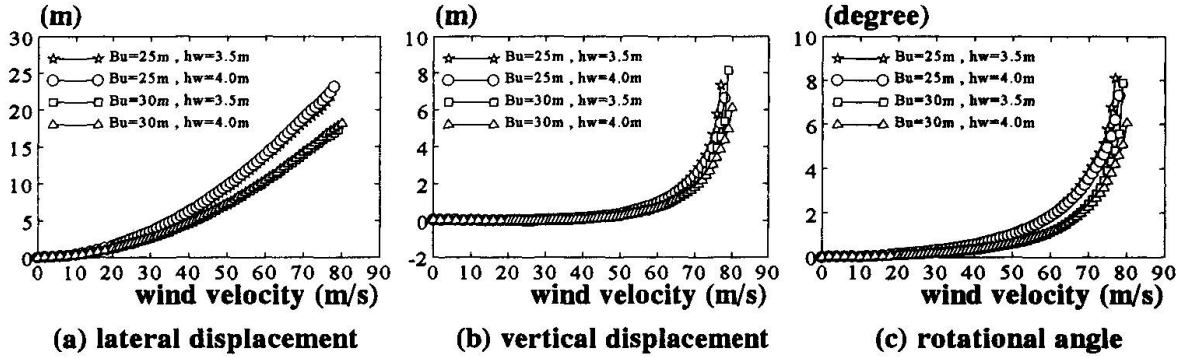

Figure3 : Displacement at the middle of the center span (after completion)

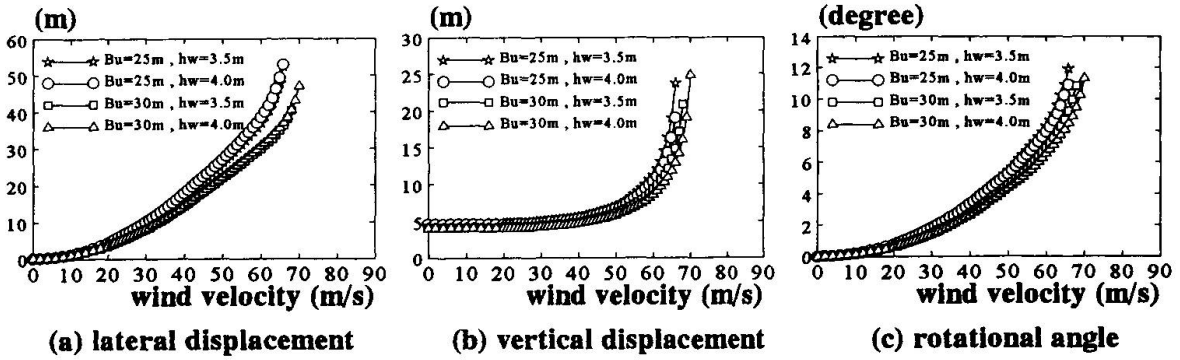

Figure4 : Displacement at the tip of the girder (under construction)

4.3 Flutter onset wind velocity

Table 2 shows the flutter onset wind velocity of the completed bridge and the bridge under construction, respectively. In the table, the figures in the parenthesis are wind velocities when the cable local vibration is taken into account. It is found that the flutter onset wind velocity is higher than the critical wind velocity under static wind load. It is also found that the effect of the cable local vibration on flutter onset wind velocity is prominent. From this result, it is concluded that the dimension of the girder is controlled by static instability.

Table2: Flutter onset wind verocity

(m/s)

Model	Completed [30-mode]	Under Construction [20-mode]
Bu=25m , hw=3.5m	120 (144)	100 (151)
Bu=25m , hw=4.0m	127	118
Bu=30m , hw=3.5m	120	102
Bu=30m , hw=4.0m	126 (151)	105 (168)

5. CONCLUDING REMARKS

We explained instability analyses of long-span cable-stayed bridges. The followings are main results obtained from this study.

1).In all cases, the factor of safety from 2.75 to 2.90 is obtained.

2).Flutter onset wind velocity exceeds 100 meters and is higher than the critical wind velocity of lateral torsional buckling under static load. It is found, among instability issues, that static instabilities under in-plane load and displacement-dependent wind load control the dimension of the girder.

3).On condition that the bridge is designed based on the procedure explained in Sec.3, the girder with the span/width ratio of around 60 and the span/depth ratio of around 400 can be used.

References

1)X.Xie, M.Nagai and H.Yamaguchi : Ultimate strength analysis and behavior of long-span cable-stayed bridges, Jour. of JSCE (in Japanese, under contribution)

2)X.Xie, H.Yamaguchi and M.Nagai : Static behaviors of self-anchored and partially erath-anchored long-span cable-stayed bridges, Int. Jour. of Structural Engineering and Mechanics, Vol.5, No.6, pp.767-774, 1997

3)V.Boonyapinyo, H.Yamada and T.Miyata : Nonlinear buckling insatiability analysis of long-span cable-stayed bridges under displacement-dependent wind load, Jour. of Structural Engineering, JSCE, Vol.39A, pp.923-936, 1993

4)M.Nagai, T.Ishida, X.Xie, H.Yamaguchi and Y.Fujino : Minimum girder width ensuring safety against static and dynamic instabilities of long-span cable-stayed bridges under wind load, Jour. of Structural Engineering, JSCE, 1998 (in Japanese, to appear)

On the Limit Span of Cable-Stayed Structures

Paolo CLEMENTE
Research Structural Eng.
ENEA - C.R. Casaccia
Roma, Italy

Paolo Clemente, born 1959, received his civil engineering degree and his Ph.D in structural engineering from the Univ. of Naples. In 1985 he joined ENEA, where he is currently responsible for experimental dynamic analysis of structures and system identification.

Summary

The self-weight of the cable plays a fundamental role in the behaviour of very-long span cable-stayed structures. In fact, as span becomes longer, cable stays become longer and heavier. So a large percentage of their capacity is required to carry their own self-weight. In the present paper the behaviour of a cable-stay under a fixed load is studied in an "exact" theory by evaluating the actual stress and axial stiffness. The limit span of a steel cable-stay is determined by means of a numerical procedure. The results can be easily extended to cables of new composite materials, which will allow to cover very-long spans in the next future.

1. Introduction

Even thought the first cable-stayed structures were built in the seventeenth century, only in the last forty years the growth of such structures has been phenomenal. Since 1955, when the Strömsund Bridge in Sweden was built, cable-stayed structure span growth has first been gradual and steadily. A terrific increase has occurred in the last decade: first the 602 *m* span Yang Pu Bridge in Shanghai, then the 856 *m* span Normandie Bridge and finally the 890 *m* Tatara Bridge in Japan have been completed.
Leonhardt suggested that cable-stayed spans of 1200 to 1500 *m* were feasible (Billington and Nazmy 1990) and proposed a span of 1472 *m* for the Messina Strait Bridge. A hybrid variety with spans of 5000 *m* was designed for the Gibraltar Strait Crossing (Lin and Chow 1991).
The reasons for increased spans were individualised by Podolny (1995) very well. Among these were the increase of the horizontal navigation clearances, in order to accommodate the increasing size and volume of marine traffic; the economic trade off of span length cost of deep water foundations, as opposed to shallow water foundations; the risk of ship collision with piers.
The feasibility of longer spans is related to the implementation of new high-strength light-weight materials. As spans become longer, cable stays become longer and heavier and therefore their installation becomes very difficult. The structure will show a low stiffness because of the low stiffness of the cables due to their sag. A long and heavy stay is also difficult to put in tension and a high percentage if its stress is related to its self-weight. Stays with large diameter also determine the wind drag forces to be higher.
In this paper the feasibility of very long-span cable-stayed structures is investigated. The behaviour of a single cable-stay, subject to vertical loads only, is analysed in order to find out the theoretical limit span. The slope of the cable is fixed to 0.4, which represents the optimum ratio between the height of the pylon and the half span of the girder from an economical point of view (Clemente and D'Apuzzo 1995).

2. The cable in the actual configuration

The behaviour of the stays under dead loads depends on the erection procedure. The girder is usually cantilever erected and forces in the stays are controlled, so that, in the configuration under dead loads, there are no bending moments in the structure. The bending moment in the girder has to be considered as a local stress related to the distance between the cables. Therefore the analysis of the structure under dead load can be carried out by referring to the statically determinate truss scheme, in which hinges are placed at nodes. To analyse the structural behaviour under live loads, the bending stiffness of the girder must be taken into account (Clemente and D'Apuzzo 1990). Its influence on the structural behaviour becomes negligible for very long-span structures. On the other hand the ratio *p/w* between live and dead loads becomes very low when the span length approaches to its limit value. So stresses due to live loads are very low with respect to those due to dead loads.
For all these reasons a suitable model for the stay is that of Figs. 1 and 2. The cable is fixed at left end and its right end can move in the vertical direction only. The pylon bending stiffness is supposed to be infinite. Actually, a the displacement of the pier top due to its deformability, can be neglected when evaluating the slope angle α. The girder is supposed to have an infinite axial stiffness.

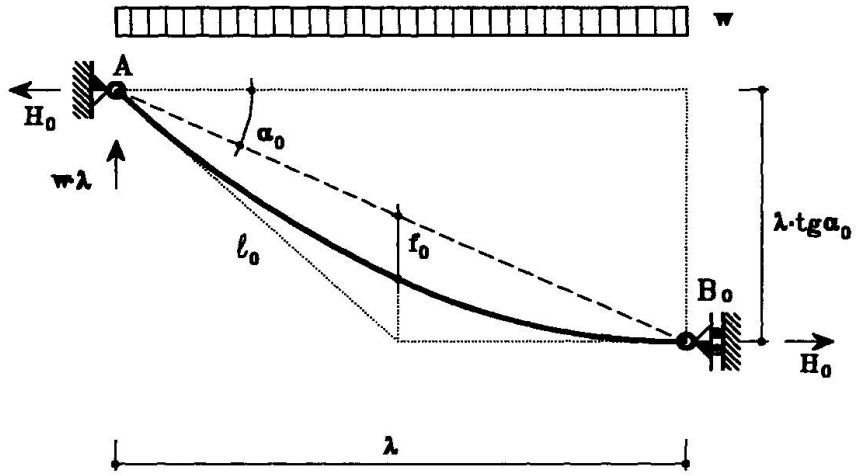

Fig. 1 Cable subject to the self weight only

Consider first the cable subject to the self-weight only, whose length in the actual configuration is ℓ_0 (Fig. 1). It assumes a configuration with horizontal tangent at B_0. The shape of the cable is supposed to be parabolic, and its self weight w uniformly distributed:

$$w = \gamma_c \cdot A_c \cdot \ell_0 / \lambda \tag{1}$$

γ_c and A_c being the weight per unit volume and the cross-section area, respectively. As will be shown later, these hypotheses cause negligible errors in the determination of the cable geometry. Tension at B_0 is:

$$H_0 = \frac{w \cdot (2\lambda)^2}{8 \cdot \lambda \tan\alpha_0} = \frac{W}{2 \tan\alpha_0} \tag{2}$$

where $W = w \cdot \lambda$ is the total weight of the stay. The vertical component of the reaction at A is $(w \cdot \lambda)$. If the force P acts at the lower end, the cable assumes a new equilibrium configuration (Fig. 2). This being closer to the straight line connecting A and B, the assumed hypothesis about w is better satisfied than in the case of self-weight only. The vertical component of the reaction at A is

$$V = W + P \tag{3}$$

and the horizontal component of the tension is

$$H = (P + W/2)/\tan\alpha \tag{4}$$

For a given γ_c, the actual configuration depends on A_c and ℓ_0, which determine the value of W. It can be found by using the iteration procedure shown in the next section.

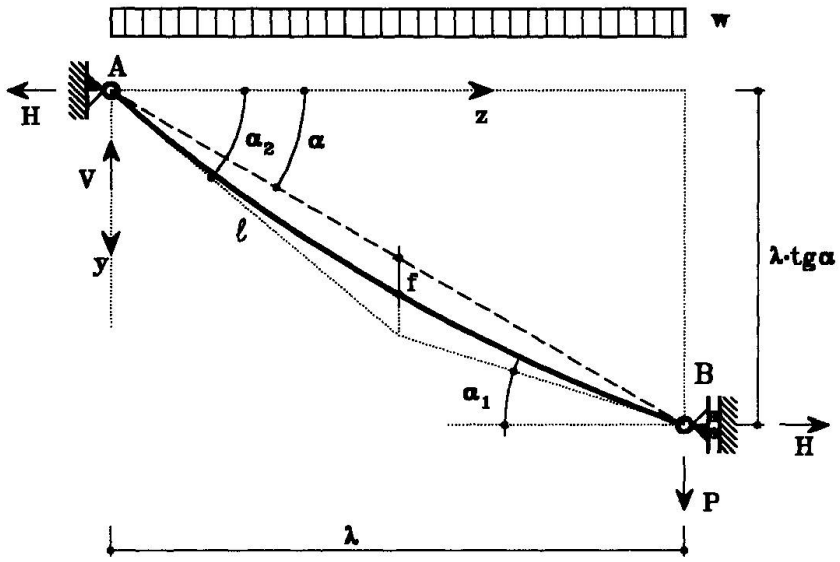

Fig. 2 Cable in the actual configuration

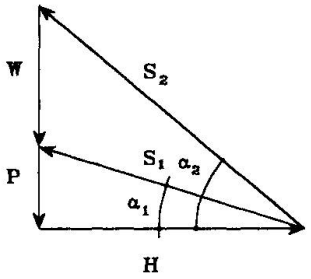

Fig.3 Equilibrium at A and B

3. The Limit Span

While the direct solution of the equilibrium of the cable is almost hard, stresses in the cable can be found, for a fixed configuration, in a simplest way. Consider the cable of Fig. 2, subject to its self-weight and to load P at its lower end B. Suppose the geometrical configuration of the cable to be fixed. In the hypothesis of parabolic shape, it is defined by the sag f at the mid-span:

$$y = -\left(4f/\lambda^2\right)\cdot z^2 + \left[tan\alpha + \left(4f/\lambda\right)\right]\cdot z \tag{5}$$

and the angles at A and B are defined, respectively, by the relations:

$$tan\alpha_1 = tan\alpha - 4f/\lambda \qquad tan\alpha_2 = tan\alpha + 4f/\lambda \tag{6}$$

The actual length of the cable, in this configuration, can be approximately estimated with the relation-ship

$$\ell \approx \lambda\cdot\left[1+\frac{8}{3}\left(\frac{f}{\lambda}\right)^2 + \frac{tan^2\alpha}{2} - \frac{32}{5}\left(\frac{f}{\lambda}\right)^4 + \frac{tan^4\alpha}{8}\right] \tag{7}$$

The horizontal component of the tension

$$H = P/tan\alpha_1 \tag{8}$$

is independent of the span λ. It depends only on the geometrical shape of the cable. The resultant of the self-weight W is applied at a horizontal distance from A equal to

$$z_W = \frac{\int_0^\lambda z\cdot\left[1+y'^2\right]^{1/2}dz}{\int_0^\lambda\left[1+y'^2\right]^{1/2}dz} \tag{9}$$

which, in the assumption of uniformly distributed self-weight, can be supposed to be equal to $\lambda/2$. From the rotational equilibrium equation around A, the total weight of the cable can be deduced

$$W = \left(\lambda/z_W\right)\cdot\left(H\cdot tan\alpha - P\right) \tag{10}$$

and, from this, the stay cross-sectional area

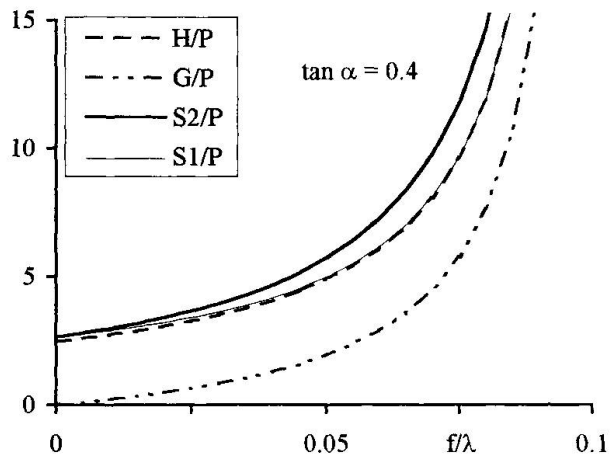

Fig. 4 H/P, G/P, S_1/P, and S_2/P versus f/λ

$$A_c = W/\gamma_c \ell \qquad (11)$$

It is worth to note that, the ratio λ/z_W depending on f/λ only, W is independent of λ and so is A_c.
The force in the cable varies from the minimum value at the bottom (Fig. 3)

$$S_1 = H/cos\alpha_1 \qquad (12)$$

to the maximum value at the top

$$S_2 = H/cos\alpha_2 \qquad (13)$$

Also S_1 and S_2, are independent of λ. They are correlated to the horizontal component of the tension H and to the shape of the cable.
In Fig. 4 the diagrams of non-dimensional parameters H/P, W/P, S_2/P and S_1/P versus f/λ are plotted for the case $tan\alpha$=0.4. They all are independent of λ and γ_c. As one can see all the parameters increase very much for f/λ>0.05. For f/λ=0, it is $S_1=S_2=H/\cos\alpha=P/\sin\alpha$. This relations, which are usually used for the preliminary design, are approximately valid only for very low values of f/λ, i.e. when W is negligible. When f/λ increases, W becomes comparable to P and the stresses in the cable get higher. The difference between S_1 and S_2 increases and $S_1 \rightarrow H$. When $f/\lambda \rightarrow 0.1$ all the parameters tend to infinite. In fact if f/λ=0.1 then α_1=0, and the equilibrium at B is impossible. The minimum and maximum stresses are respectively:

$$\sigma_1 = S_1/A_c \qquad \sigma_2 = S_2/A_c \qquad (14)$$

The stresses can be evaluated in all the sections. So the variation $\Delta\ell$ of the cable length and finally the natural length of the cable can be calculated.
The described procedure is very suitable to find out the limit span λ_{lim} of a cable-stay, this being the span for which the whole capacity of the cable is required to carry its own self-weight. If λ is fixed, for each value of f/λ the corresponding maximum stress $\sigma=\sigma_2$ can be calculated and so the apparent tangent modulus E^*:

$$E^* = E \cdot \left[1 + E/12\sigma \cdot (\gamma\lambda/\sigma_m)^2\right]^{-1/2} \qquad (15)$$

where $\sigma_m = (\sigma_1 + \sigma_2)/2$.
The following assumption were made: γ_c=0.078 *MN/m³* and E=200000 *MPa* and P=1 *MN*. In Fig. 5 the curves of σ versus f/λ are plotted, for different values of λ. First of all it is to note that all the curves stop at f/λ=0.1, that is the limit value for the assumed value of α. If $f/\lambda \rightarrow 0.1$, $\alpha_1 \rightarrow 0$ and $H \rightarrow \infty$. If f/λ>0.1, then α_1 becomes negative. As a result H is negative too, and a negative value of W would be needed for the equilibrium. With regard to this limit case, the limit value of the span λ can be defined. In fact, only one curve intersects the straight line f/λ=0.1 in correspondence of the fixed maximum value of σ. The value of λ, which characterises the individualised curve is the limit value of λ, for the given σ.
Fig. 6 shows the diagrams of E^*/E versus f/λ. The deterioration of the apparent modulus is more evident for high values of f/λ and low values of λ. This paradox can be explain with the following consideration: for high values of λ, W being independent of λ, A_c must be lower and therefore σ_m is higher. As a result the stay behaves harder.
In Fig. 5 the curves relative to given values of E^*/E are also plotted. From a technical point of view it is important to fix a minimum value of E^*/E. So the technical limit value λ of can be defined as follows. Suppose that a value of σ has been fixed and a value of E^*/E has been chosen. These two values define a point in the diagram. The curve $\sigma(f/\lambda)$ passing through this point is the curve relative to the maximum value of λ.
The assumed hypothesis about the cable shape were tested with reference to the limit case f/λ=0.1. The difference between the co-ordinate y at mid-span between the assumed parabolic shape and the catenary is 1.15%. The error in evaluating z_W is about 1.7%. Obviously the errors are lower when f/λ<0.1.

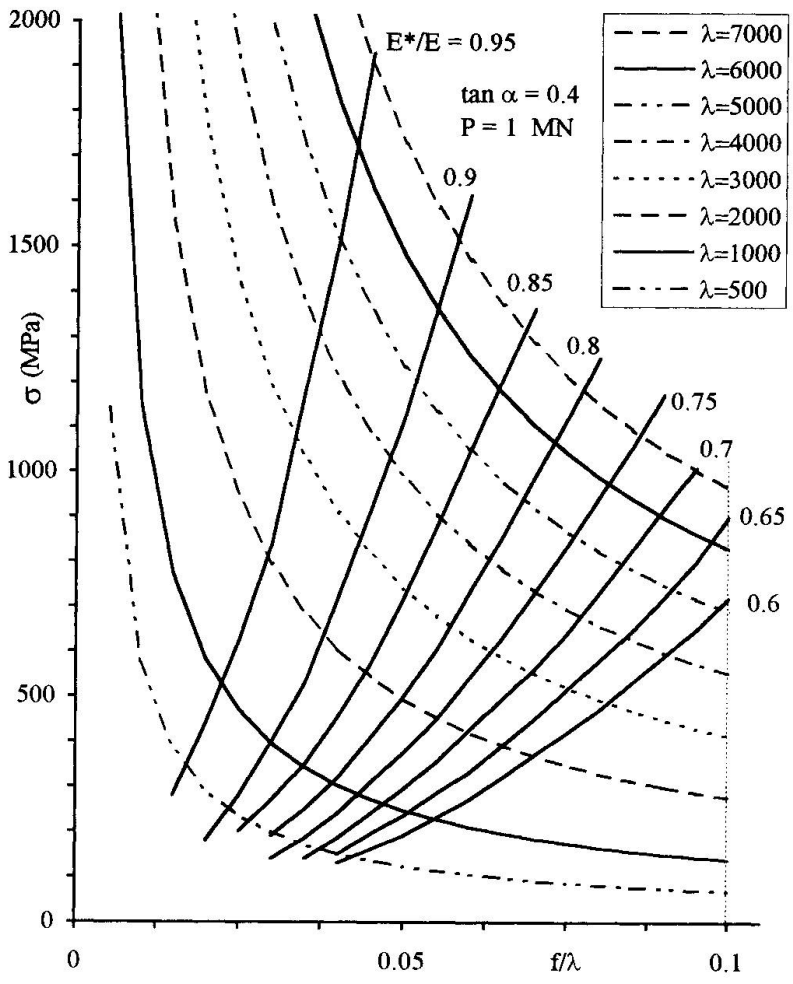

Fig. 5 σ versus f/λ

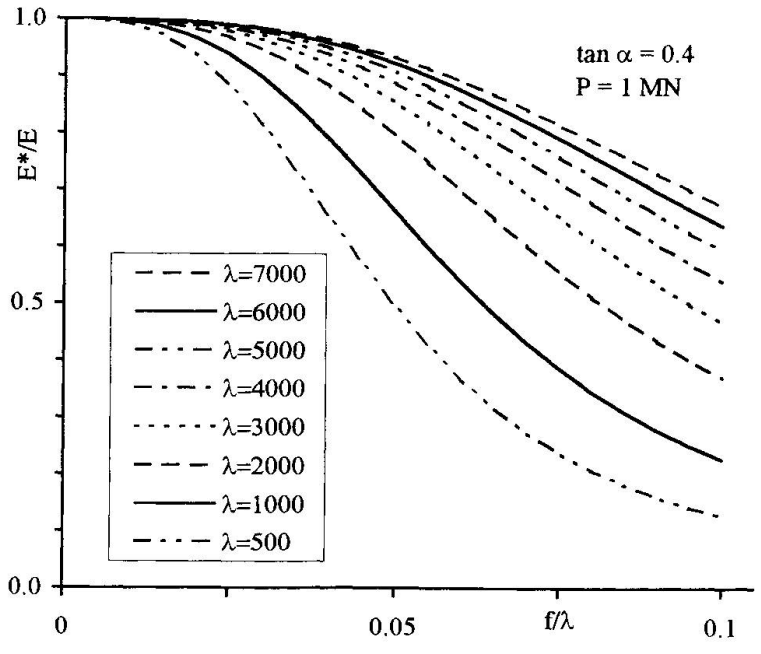

Fig. 6 E^*/E versus f/λ

The limit value of the span λ depends mainly on the stress σ. The value of σ, which can be assumed for the preliminary design, is related to the ratio *p/w* between live and dead loads. If f_s is the limit stress of the cable, the allowable stress is between $f_s/3$ and $f_s/2$. This study being relative to the analysis of very long-span cable-stays, low values of *p/w* were considered. Therefore values of σ very close to the allowable ones were assumed.

In Fig. 7 the diagrams of the deflection *f*/λ versus λ are plotted, for different values of σ. It is apparent that *f*/λ varies almost linearly with λ and significant reduction of it can be obtained by increasing σ. The sag ratio *f*/λ is correlated to the deformability of the cable and so is the ratio E^*/E, which is also plotted in Fig. 7 versus λ, for usual values of σ. As obvious E^*/E decreases when λ gets higher. It decreases more rapidly for lower values of the stress σ.

In Fig. 8 the diagram of the cable cross-section area A_c versus λ is plotted for different values of σ. All the curves show a slight increment of A_c with λ, that becomes very rapid for high values of λ. The value of λ, for which the slope in the diagram changes, increases with λ. It is evident that to obtain a reduction of A_c, σ must be increased. For a given value of A_c the curves show the same tangent, which happens to be independent of λ. Therefore fixing a value of $\Delta A_c/\Delta\lambda$ is equivalent to fix a value of A_c.

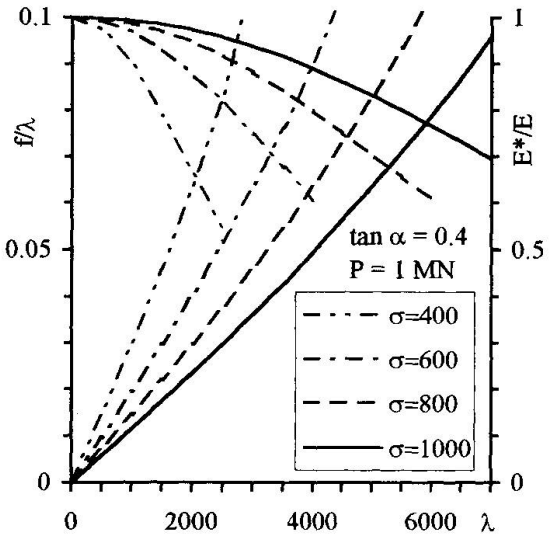

Fig. 7 f/λ and E^*/E versus λ

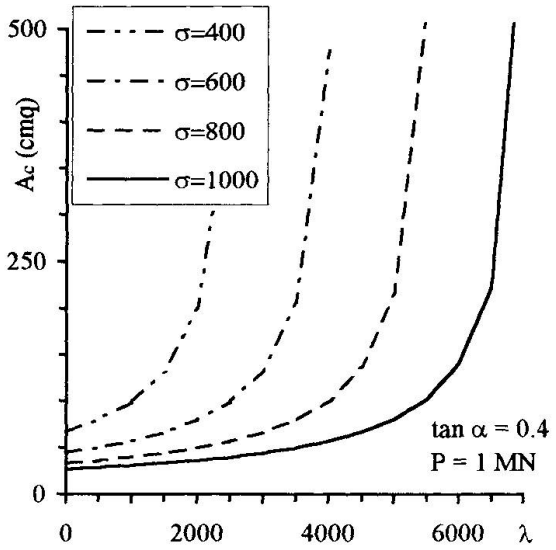

Fig. 8 A_c versus λ

4. Conclusions

In the design of a cable-stay its own self-weight is usually ignored and the actual configuration is confused with the straight line connecting A and B. As a result the force in the cable is supposed to be constant and equal to $P/\sin\alpha$. This assumption is acceptable only if $f/\lambda \approx 0$ and, therefore, if W is very low. This condition is satisfied only for short spans.

In the case of very long-spans the cable weight becomes very high and the sag ratio f/λ is not negligible. The force in the cable is everywhere higher than $P/\sin\alpha$. Both the differences $S_1 - P/\sin\alpha$ and $S_2 - S_1$ increase with f/λ. As a result the self-weight of the stay cannot be ignored in the cable design. It is worth to point out that stress in the cable being higher than $P/(A_c \sin\alpha)$ the apparent modulus is higher than one could expect.

The numerical results shown in this paper are relative to steel cables, but they can be easily generalised to other materials. In particular, from the values of σ in Fig. 5, those of the ratio σ/γ_c can be deduced, γ_c being equal to 0.078 MN/m^3.

Materials, characterised by low values of σ/γ_c, have the potential to cover longer distances in the next future. Carbon fiber composite cables seem to be very good because of their high strength ($\approx$2000 MPa) and their very low unit weight (0.015 MN/m^3), but may have a lower Young's modulus. The aerodynamic behaviour of light stays is also to be investigated. New high performance materials are available also for the beam and pylon, which translate to reduced weight and thus loading but they are too expensive at the present time.

References

Billington D.P. and A. Nazmy (1991). "History and Aesthetics of Cable-Stayed Bridges." *Journal of Structural Engineering*, ASCE, Vol. 117, No. 10, October, 3103-3134.

Clemente P. and D'Apuzzo M. (1990). "Analisi del modello generalizzato di ponte strallato." *Fondazione Politecnica per il Mezzogiorno d'Italia*, Giannini, Napoli, No. 162, (in Italian).

Clemente P. and D'Apuzzo M. (1995). "Design of cable-stayed roofs." *Proc., 15th Italian Conference on Steel Structures* (Riva del Garda), C.T.A., Milano.

Lin T.Y. and Chow P. (1991). "Gibraltar Strait Crossing - A Challenge to Bridge and Structural Engineers." *Structural Engineering International Journal of IABSE*, Vol. 1, No. 2.

Podolny W. (1995). "Future trends in cable-stayed bridges." *Proc., IASS Symposium Spatial Structures: Heritage, Present and Future* (Milan), SGE Padova, Vol. 2, 985-994.

Assessment and Strengthening of Two Cantilever-Type Concrete Bridges

Jan TEIGEN
Principal Eng.
Det Norske Veritas
Hovik, Norway

Jan Teigen, born 1951, received his civil engineering degree from Norwegian Institute of Technology in 1974, Master of Science degree form Univ. of Colorado in 1990 and Dr Phil. degree from Univ. of Oslo in 1994. He is currently Principal Engineer in Section for Fixed Structures at Det Norske Veritas.

Steinar FJELDHEIM
Principal Eng.
Norwegian Public Roads Adm.
Oslo, Norway

Steinar Fjeldheim, born 1944, received his civil engineering degree from Univ. of Denver in 1968. He is currently Principal Engineer in Bridge Maintenance Division of Bridge Department at Norwegian Public Roads Administration.

Summary

For both Puttesund and Sørsund Bridge, excessive sag has developed over time resulting in a severe slope-discontinuity at the hinge in the centre of the main span. Both bridges are also found to have insufficient capacity in some regions of the main span, Puttesund basically related to shear and Sørsund mainly to bending. The purpose of this paper is to present some of the design work and evaluations carried out for various alternatives to raise and strengthen the bridges. Generally, it proved difficult to find efficient and economic methods for raising the girders to a significant proportion of the existing deflections. Thus, for the final upgrading procedures priorities were instead given to weight saving actions, improvements of traffic comfort and, of course, the necessary strengthening of the girders. Analyses were based on nonlinear FE-technique. Also in situ measurements of concrete stresses have been carried out.

1. Introduction

Puttesund Bridge (Fig. 1) was completed in 1970. It is a prestressed concrete single cell box girder bridge built by the cantilever construction. The main span of 138 m is counterbalanced by two 28 m rock-filled abutments. Sørsund Bridge (Fig. 2) was completed in 1962. It consists of two approach spans and three cantilever constructed main spans with single cell box girder of lengths 50 m + 100 m + 50 m. In the centre of the (largest) main span of both bridges is located a hinge that transfers shear and torsion and allows for axial movements. In common is also the weight saving opening in the bottom slab on adjacent sides of the hinge. Over the years the main span has deflected about 0.4 - 0.5 m on the bridges resulting in a severe slope-discontinuity at the hinge. On Sørsund some remedial actions to improve the traffic comfort have been taken in the form of adding further surfacing in the region of the hinge, the maximum thickness being 18 cm. This substantial increase in weight has again amplified the deflection, and today the rotation capacity is exceeded implying the joint is permanently closed at the top. This malfunction has however probably prevented the arms from further sagging. On Puttesund measurements have shown a steady increase in deflection over the last 15 years, but at a somewhat decreasing rate. Also cracks have been recorded. Around the quarter-points of the span inclined cracks at the upper part of the webs are observed, indicating a potential shear capacity problem.

2. Program review, modelling considerations and types of analysis

Since the computer program used initially on Puttesund gave poor agreement with the observed behaviour of the bridge, it was decided to employ the state-of-the-art *computer program DARC*. This is a nonlinear finite element program that originally was developed as a part of a doctoral study by the first author. The key ingredient of the program is a new 3D shear-beam element that allows for analysing the response of reinforced and prestressed concrete beams in arbitrary combinations of the axial, bending, shear and torsion modes. All significant nonlinear material and time dependent effects are taken into account like cracking, crushing, creep, shrinkage and ageing of the concrete and yielding and relaxation of the reinforcement. Also the segmental construction capability is included. The 3D element mentioned is formulated on so-called hierarchical form, which makes it possible to suppress the shear effect so that the axial/bending behaviour can be represented alone. For Puttesund having a shear capacity problem, this option became particularly useful since it clarified at an early stage the maximum effect by shear-strengthening the bridge.

Generally the element mesh of the girders is chosen in accordance with the division of casting segments used in the construction. Each element is based on the dimensions at the midlength of the corresponding segment. The bottom slab is however sloped to achieve the arch effect in girders of variable height, still using only one element per segment. Due to symmetry, only half the bridges were initially analysed based on free-edge boundary condition at the hinge. For Sørsund, part of the corresponding approach span was also omitted, giving a 120 m model of the total 408 m bridge. The assumed symmetry is valid only for symmetric configurations of traffic loading. For Puttesund the whole system had to be taken into account in a final analysis when maximum shear in the critical segment was studied.

Two kinds of analysis are performed. The *time analysis* simulates the bridge behaviour from start of construction and up to the current year of the analysis ('today') when usually some kind of remedial action is introduced. Finally the analysis continues for another 25 years. The construction sequences and corresponding times are based on drawings and other documents available. Unless otherwise noted only permanent loading is considered (dead weight, prestress, etc.). The purpose of the time analysis is primarily to investigate the deflection-state of the bridge 'today' and in the future with or without the various remedial actions for raising and strengthening the girder. Material properties are based on characteristic code values or best estimates in absence of such. The *capacity analysis* is a short-term analysis under combination of permanent and traffic loading. The purpose of the analysis is to determine the load carrying capacity of the bridge at a given state. The prestress level for the state is taken from the time analysis. Material properties and loading are based on factored ULS design values. The current class of traffic loading is used in the analysis, although both bridges originally were designed according to a lower load class. Instead, the required factor of traffic loading is now reduced to 0.87, which is two third of the current code value of 1.3. The analysis is carried out by first applying the permanent loading up to its factored load level, usually with load factor 1.2 except for 1.0 on prestressing. Then the traffic loading is gradually introduced until the failure load of the bridge is reached.

3. Puttesund Bridge

The *time analysis* of the **existing bridge** gave for the situation of 'today' per Sept. 1995, a resulting position of the cantilever tip about 29 cm below the prescribed road line. For further 25 years ahead the predicted sag will exceed 32 cm. In these figures the precamber used for

construction has been subtracted. In comparison, the observed sag of 'today' is about 41 cm, thus 12 cm more than computed. Four years after completion of the bridge, in 1974, this difference was about 2.5 cm, while in 1980 it had increased to 4.6 cm. From this trend it is good reason to expect that the additional sag for the bridge in the next 25 years will become a lot more than the computed 3 cm. Among reasons for this discrepancy may be cyclic effects from heavy vehicles, impact loading at the hinge due to the growing slope-discontinuity and uncertainties in long-term material properties. Only permanent loading is considered in this analysis. To investigate the effect of one occurrence of heavy traffic loading, an additional analysis was performed where the characteristic traffic loading was applied shortly after completion of the bridge and then removed. This gave an immediate permanent contribution to the tip deflection of 2 cm, but no additional long-term effect was detected. Also an analysis with the purpose of investigating the sensitivity with respect to long-term material properties was carried out. Here the assumption was made that the 28-day code values were not reached before 'today'. Using the same ageing function as before implies quite weaker concrete at the early years. The impact on computed sag was dramatic, now becoming about 55 cm 'today', compared to 29 cm formerly. Finally, the contribution to the sag from shear deformations was investigated. At the tip this was about 15 %. Getting closer to the abutment the shear contribution increases, eventually becoming dominant. The *capacity analysis* was run with prestress level corresponding to the state of 'today' as taken from the time analysis. Failure occurred by yielding in the stirrups accompanied by crushing of concrete in the lower part of the webs in the segment closest to the quarter-point of the span, where also the inclined cracks are observed. At failure the factor of traffic loading was 0.75, thus below the required value 0.87.

An obvious way of raising the girder is by application of **external prestressing along the bridge**. Here a total of six cables are placed at the soffit of the bridge deck flanges (Fig. 3), each with a tensioning force of 2 MN applied behind the abutments. In the *time analysis*, the tensioning performed 'today' gave an immediate uplift of the cantilever tip of 8.5 cm. After three months 1 cm additional uplift was gained. However, for the next 25 years the tip gets almost the same additional long-term sag as if no external prestressing is applied. Also a time analysis including extra weight in the hinge area to improve traffic comfort was made, reducing the uplift to 6 cm. The *capacity analysis* was run with prestress level corresponding to 25 years ahead of 'today' and with the extra weight included. The analysis gave a factor of traffic loading at failure of 0.70, thus slightly less than obtained without longitudinal external prestressing and extra weight. Since failure is governed by shear, longitudinal prestressing has very little influence on the capacity. Also an identical analysis, but with shear effect suppressed, was carried out. The factor of traffic loading at failure then became 1.45, expressing the capacity of the bridge in the axial and bending modes. This indicates that the bridge may pass the required safety level with ample margin using an efficient shear strengthening method. A preliminary analysis confirmed that a promising remedy then is vertical prestressing of the webs.

A less traditional alternative for raising the girder is by means of **pretensioning the bottom slab**. This may be obtained by jacking compression into steel tubes placed on the slab (Fig. 4). Besides giving uplift, the method will also reduce the shear forces due to the inclination of the bottom slab. All work is carried out inside the box girder undisturbed by the traffic. Analysed here are four steel tubes with a total jacking force of only 2.4 MN. Due to the wide opening in the bottom slab, this is about the maximum tensile force that can be transferred to the cross section without any strengthening. The *time analysis* gave an immediate uplift of the cantilever tip of 3 cm. The uplift is now more concentrated to the hinge area, giving an almost horizontal tip tangent and thus eliminating the demand for extra traffic comfort. The *capacity analysis* showed very little impact from this solution. However, with increased pretensioning the method is still interesting, either as a separate means or in combination with others.

Since the methods considered so far did not give the desired uplift without substantially increasing the prestressing forces, it was decided to investigate the effect of a **pseudo cable stayed solution** (Fig. 5). A simple steel tower, supporting two cables anchored 9 m and 33 m from the cantilever tip, is placed at the front of each counterbalance abutment. The proportion between the forces in outer and inner cable is 1.0 : 0.7, which means that the vertical components will be almost of same magnitude. A simplified analysis was made based on treating the cable forces as external loading on the existing bridge. The intention was to find the approximate magnitude of the cable forces that would bring the arms back to their original level. The result was somewhat surprising, since cable forces of only 4.0 MN and 2.8 MN in outer and inner cable respectively, became sufficient. At this stage the shear force in the critical segment is almost zero. Thus, the solution appears to elegantly solve both the sag and shear problem. However, since a more comprehensive analysis was not run, some unforeseen problems may come forward.

An **evaluation of the various alternatives** may be summarised as follows:

- Use of longitudinal external cables will require a substantial increase in prestressing force if significant uplift shall be achieved. This means that the superstructure will require more strengthening locally in the anchoring zones of the cables and thereby also a corresponding increase in weight and costs. The prestressing will not help to obtain the desired load class, but is first of all a means to improve the traffic comfort and make a better appearance.
- Pretensioning the bottom slab has much the same features as using longitudinal external cables.
- The pseudo cable stayed solution appears to solve both the sag and the shear problem, but is found too expensive.
- Application of vertical prestressing improves the shear capacity but does not give any uplift.

Since the **upgrading procedure** had to solve the shear capacity problem, it was decided to optimise further the solution for transverse prestressing. The various means to actively raise the girder were all abandoned because of their high costs. Instead a relatively simple way of improving the traffic comfort was called for, which basically consists of replacing the sidewalks of concrete with aluminium, removing existing asphalt and building up a wearing course of variable thickness in the hinge area using leca concrete. To avoid bumps, the transition curve is based on the existing deflection taking into account the minimum allowable vertical road radius for the design speed in question. On top is placed a 3 cm layer of high quality asphalt. The final weight saving on each arm becomes 21 MN, which is advantageous in view of keeping future deflections at a minimum. Also the temporary removal of the guardrail makes it possible to adjust its alignment in the sagging area.

So far, all attention has been given to the analysis of the bridge in the longitudinal direction. Since shear was found critical in a region of each arm, it was deemed necessary also to carry out a *transverse analysis*. The web moments from traffic and weight of bottom and top slab will utilise the same reinforcement as required by the global shear forces, and thus possibly amplify the shear capacity problem. The transverse analysis showed that the web moments occupied a substantial part of the stirrup-capacity. Based on this, **vertical prestressing** equal to 2 MPa in the webs was assumed along the whole bridge span. In order to have the prestressing effective over the whole height of the webs, the bars are anchored at the soffit of the bottom slab and as close to the top surface of the deck as possible (Fig. 6). The spacing of the bars is determined so that the concrete stresses become uniformly distributed in the longitudinal direction. Since DARC is based on a beam model it cannot account for the transverse effects in the box girder directly. Instead the area of existing stirrups were reduced in the model by the amount of reinforcement required to carry the transverse moments. This approach is believed to be on the safe side, and consequently also

the amount of prestressing found on this basis to obtain the required shear capacity. For the **final analysis** two different locations of heavy traffic loading are now considered for the global analysis. One symmetric condition giving maximum moment over the whole span, and one asymmetric that gives maximum shear in the critical segment. In the latter case the model must comprise the whole bridge system. The analysis confirmed that vertical prestressing became necessary along the whole bridge span due to the combined effect of global shear and transverse moments. However, the strengthening changed the type of failure from shear to bending, the factor of traffic loading now being 1.35. No final time analysis was made.

4. Sørsund Bridge

The *time analysis* of the **existing bridge** showed that the cantilever tip for the situation of 'today' per July 1996, was positioned 27 cm below the prescribed road line, and for the next 25 years an additional 1 cm is predicted. In these figures an assumed precamber profile that brought the superstructure into correct position at completion has been subtracted. Again, there is a distinct discrepancy between calculated and measured values since the observed sag of 'today' is about 50 cm. However, later measurements of the asphalt layer showed that the thickness varied between 12-18 cm, which is two to three times more than assumed in the analysis. The *capacity analysis* was run with a prestress level for the state of 'today' as taken from the time analysis. Failure occurred at a factor of traffic loading of 0.30, thus quite far from the required value 0.87. The failure mode was crushing of concrete in the lower region of the girder at a segment in the main span with wide opening in the bottom slab, about 20 m from the hinge. This indicates the opening causes insufficient compression capacity, and that bending and not shear is governing the failure.

In the critical segment the transverse web moments are not pronounced because the cross section here basically consists of two individual beams due to the wide opening in the bottom slab. Consequently the stirrups can mainly be utilised for global shear transfer. For the closed box areas, a *transverse analysis* has however been made. Since bending failure is found critical, the use of longitudinal external cables may now become a relevant means not only for giving uplift but also for strengthening the bridge. However, again facing a modest budget of rehabilitation, load class requirements must have top priority in the **upgrading procedure** and actively lifting the cantilever arms is left out. The strengthening consists of casting the inner 12 m of the open bottom slab (Fig. 7). Improved traffic comfort is solved in a way similar to Puttesund.

Before running the final analysis, certain input data were correlated to **measurements made on the bridge**. One intention was to compare in situ stresses in concrete at selected points with values obtained from the analysis. The measurements of concrete stresses were carried out using the so-called stress-relief coring technique. Generally, measured stresses were found to be higher than computed in the top slab and vice versa for the bottom slab, indicating the actual prestress level may be higher than assumed in the analyses. Thus, the prestress was adjusted so that better agreement with measured stresses was obtained. In addition to stress measurements, also the concrete strength and modulus of elasticity were tested, allowing for a 33 % increase in concrete strength. Since moment and not shear is deemed critical, the original symmetry-based model was retained for the **final analysis**. The 12 m casting of the open bottom slab was introduced in the analysis by separate elements after the application of permanent loading, but before the traffic loading. Again bending became critical, but now failure took place in the corresponding region with open bottom slab in the side span at a factor of traffic loading of 1.05, confirming sufficient capacity of the bridge. No final time analysis was made.

5. Conclusions

The nonlinear analysis program DARC proved to be a successful tool to identify critical failure modes and to investigate the various strengthening and lifting alternatives for the two sag-deteriorated bridges. Both structures were found to have insufficient capacity, one related to shear failure and the other to bending. It proved difficult however to find efficient and economic uplift methods. For the chosen upgrading procedures, priorities had to be given to strengthening of the girders, weight reductions and improvements of traffic comfort. Vertical prestressing of the webs and casting a region of the open bottom slab were the adopted strengthening methods for the shear-weak and bending-weak bridge, respectively. Computed sag has generally been less than observed. It seems difficult to point out one main cause for this since long-term deformations are dependent on many factors. For bridges with a hinge in the centre of the main span, however, it is believed that the traffic impacts there due to the growing slope-discontinuity are particularly detrimental. The improved traffic comfort and weight reductions may thus become mitigating. Future performance of the bridges should be carefully recorded. To improve the analysis concept, more effort should be paid to clarify the interaction between global and local load effects.

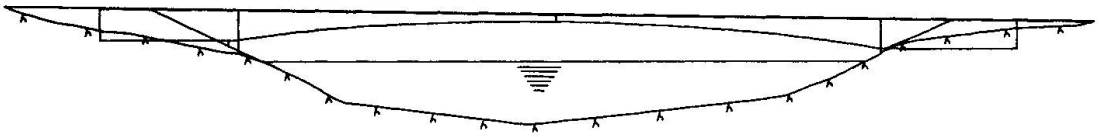

Fig.1 Overview of Puttesund Bridge

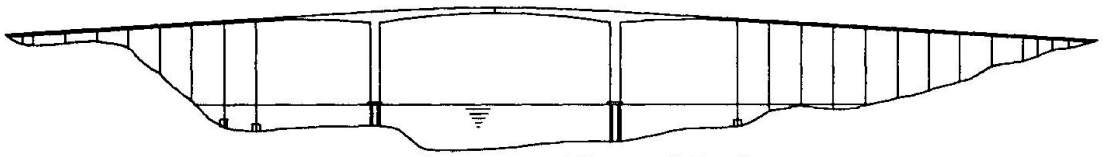

Fig. 2 Overview of Sørsund Bridge

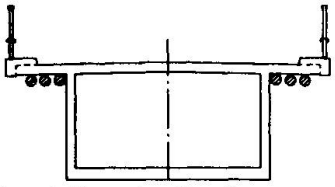

Fig. 3 Longitudinal external cables

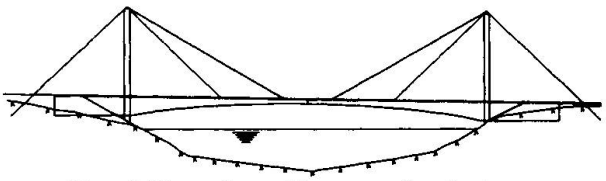

Fig. 5 Pseudo cable stayed solution

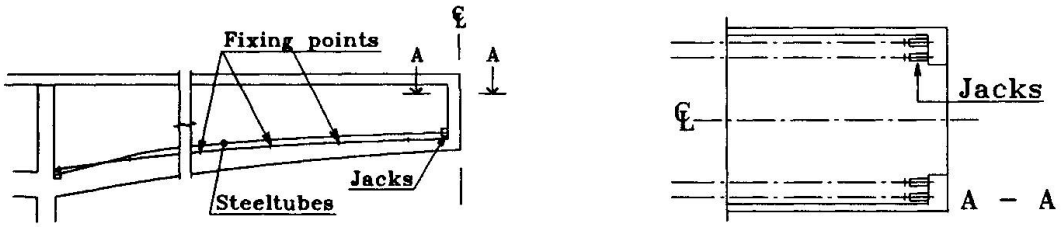

Fig.4 Pretensioning of bottom slab

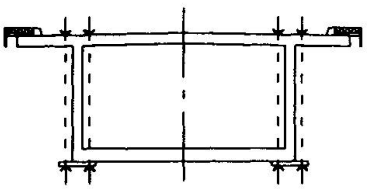

Fig.6 Vertical prestressing

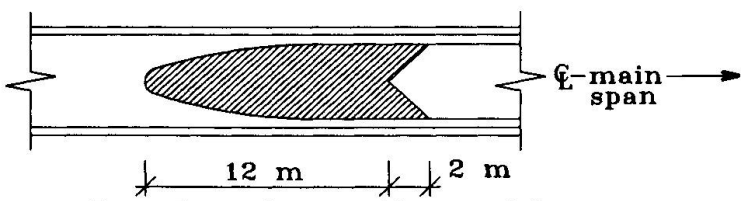

Fig. 7 Strengthening of bottom slab

Study on Stress Transfer Mechanism of Hybrid Rigid-Frame Bridge

Mochammad AFIFUDDIN
Doctoral Student
Saitama Univ.
Urawa, Japan

Atsuhiko MACHIDA
Prof. Dr
Saitama Univ.
Urawa, Japan

Toru SATO
Struct. Eng.
Miyazi Iron Works Co. Ltd
Tokyo, Japan

Takao SUGIYAMA
Struct. Eng.
Hokaido Branch of JH
Sapporo, Japan

Summary

This paper explains about the research on stress transfer mechanism of hybrid rigid frame bridge. The behavior of stress transfer mechanism was clarified through experiments and analysis. In experimental work, two specimens of hybrid rigid frame bridge in which the super structure is rigidly connected to reinforced concrete piers were tested. Two dimensional finite element method was used to analyze the structure to clarified the result analytically. From this study it was found that the studs on the stiffener, effectively transfer the loads to the stiffener. Since the strains of inner and outer surface of the flange in the connection are within reasonable range, it is recommended that this type of connection method can be used if stud shear connectors are properly provided on the stiffeners.

1. Introduction

Hybrid rigid frame bridge structure is a structure in which the super structure is rigidly connected to reinforced concrete piers of the bridge. This type of structure now becomes famous in Japan due to some advantages. The main advantage of this type of structure is the structure can carry the seismic response more safety than the ordinary structure. On the other hand, as an economical effect, due to the reduction of bearing to handle the structure, this type of structure also cheaper than ordinary structure due to the reduction of weight of super structure. Also some damage originated from local damage in shoes and expansion joints in super structures can be eliminated[1].

Though such merits do exist, still few studies have been carried out to clarify the behavior of each component of the structures. So far the research only specified to strength and ductility of full structures [2], or studied on the properties of the corner section of the structures [3]. The objectives of this research are to study the stress transfer mechanism in developed steel-concrete hybrid rigid frame bridge and to study the mechanical behaviors including the load carrying capacity of individual elements in the structure. The experimental and analytical works were explained, and the results for each component of structures are observed analytically as well as experimentally.

It was found that the studs on the stiffener, effectively transfer loads to the stiffener. Since the strains of inner and outer surface of the flange in the connection are within reasonable range, it is recommended that this type of connection method can be used if stud shear connectors are properly provided on the stiffeners.

2. Experimental Work

2.1. Specimens

The specimens consist of steel girder, reinforced concrete column, stiffeners, main reinforcements, and stud shear connectors. Stiffeners are fixed in steel girder, and main reinforcements are continuous from the reinforced concrete column to the steel girder through the holes in the bottom flange. The reinforcements were anchored to the concrete within the space enclosed by top and bottom of flange, web plate, and stiffeners. As such, the steel girder and reinforced concrete column becomes a single structure. This type of mix hybrid structure is considered in this study using a T-shape specimen. The load transferred from RC column to steel girder can be considered as bending moment.

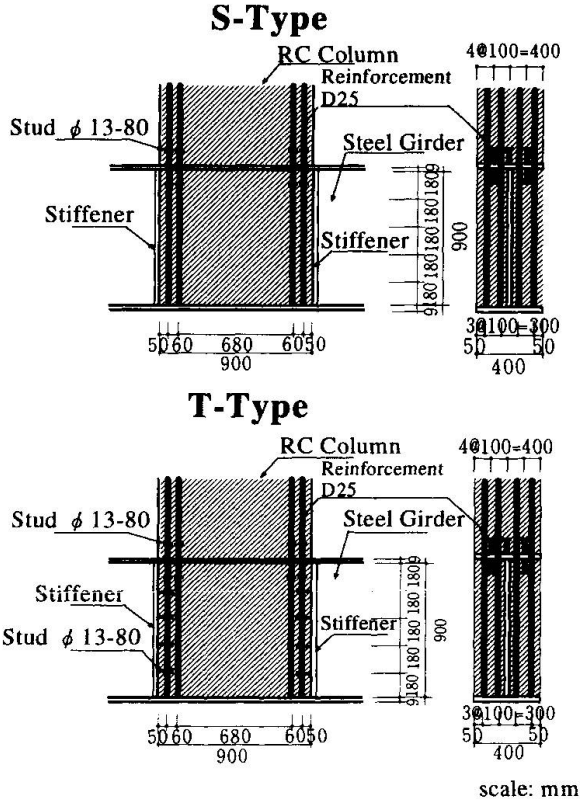

Fig. 1. Detail Specimens

Figure 1 shows the detail of connection for each specimen. In S- type specimen, studs exist only in the flange of the intersection of the connection part of RC column and steel girder. On the other hand, in T-type specimen, studs exist not only in the steel flange but also in the stiffeners of the connection part. The objective of T-type specimen is to determine the effect of stud shear connectors in the stiffener which have ability to transfer some additional loads through the connection. Detailed explanation concerning about experimental work can be referred to previous paper [4].

2.2. Testing program

The specimens were tested in inverted position compared to the ordinary structures. The load was applied at the top of reinforced concrete column. The data was measured from the strain gauges and displacement transducers attached to the specimen. The applied loading was cyclic and as for sign convention, the direction towards of actuator head is considered to be positive for tension load, and negative for compression load. At peak displacement of each cycle, the occurrence of crack was checked and the stresses in the reinforcement bars were observed for yielding condition.

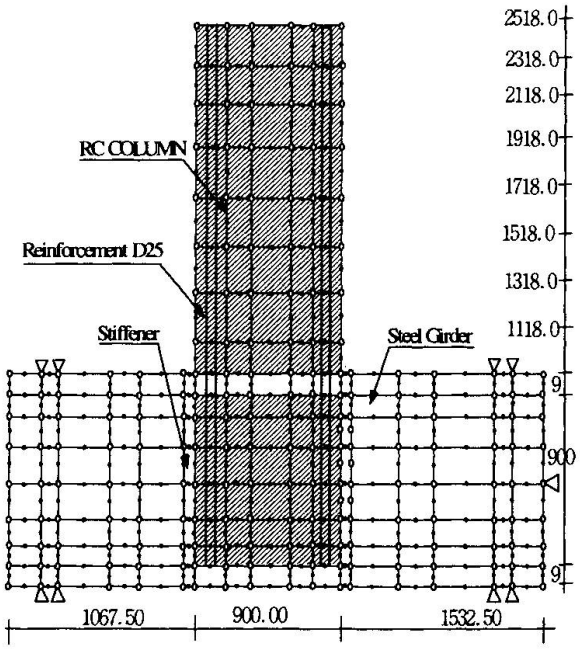

Fig. 2. Mesh generation of FEM

3. Analytical Work

The structures are analyzed by using finite element program MARC[5]. The structures are

divided into several elements, and the dimensions and the mesh generation of each element are shown in Figure 2. Plane stress element with 8 node element was used for modeling the concrete and steel plate, and truss element was used for modeling steel reinforcement and stud shear connectors. Detailed constitutive equation for concrete and steel can be referred to previous paper [6].

4. Result and Discussion

4.1. Behavior of the flanges

Behavior of the flanges monitored by strain distribution on inner and outer surface of the flange. Figure 3 shows the comparison result for strain distribution on inner surface of flange both for S-type and T-type. It can be recognized from the figure that the measured strain distributions agree well with the values obtained from analysis except the point in compression flange for S-type. The strain in the point located in compression flange of north side was 4211 micron. At the same point, the analytical result was about 1500 micron. Compare to another point in compression flange, the strain in north side has large value. Figure 4 also shows the same phenomena, where the largest strain distribution was also in the compression flange of north side. These phenomena might be due to the large moment in the connection part, so the strains in that part become large. Figure 5 shows the strain distribution on tension flange for each type. The figure shows that the largest stain value was in the south side. It means that the result is in contrast to the result for the compression flange. This behavior can be easily understood that when the load is applied to the RC Column, the compression load will be transferred to the steel girder through bonding between reinforcement and concrete. Also the load transferred from the stiffener to the tension flange of the girder in south side. On the other hand, in north side the load transferred through the bonding between steel and concrete to the compression flange of the girder. It can be understood from figure 3 to 5 that the analytical result shows good agreement with the experimental result. It can be seen also that the strain in inner and outer surface of the flange in T-type is not so large. It means that even if we reduce the thickness of the flange in the connection part of T-type specimen, the structures are still all right. Since the strains of inner and outer side of the flange in the connection are within reasonable range, it is recommended that this type of connection method can be used if stud shear connectors are properly provided on the stiffeners.

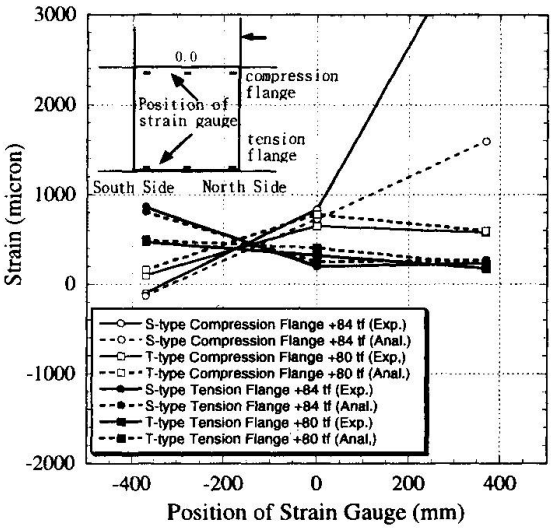

Fig. 3. Strain Distribution of Inner Surface of the Connection

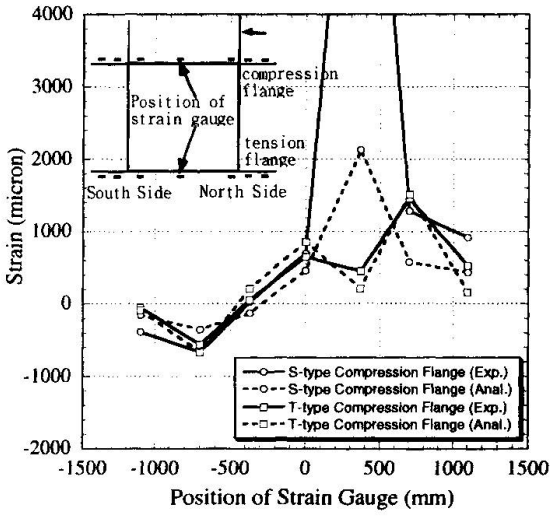

Fig. 4. Strain Distribution on Compression Flange for Each Type

4.2. Effect of the thickness of the flange in connection part on strain distribution

As mention in section 4.1 that the strain in inner and outer surface of the flange for specimen T-type was not so large. So it is possible to reduce the thickness of the flange in connection part. In analytical study, there are two cases have been studied to investigate the effect of the thickness of the flange in the connection part. In case A, the thickness in compression and tension flange of connection part reduce to 6 mm, and the thickness of stiffener is 9 mm. Case B, the thickness in compression and tension flange of connection part , and the thickness of stiffener are 6 mm. The result for inner surface of the compression and tension flange show in Figure 6 and 7, respectively. The results plotted in the figures are experimental result, analytical result for the original structure, and analytical result for case A and B. It can be investigated from the result that even if we reduce the thickness of flange in the connection part, the result still in the reasonable range. Figure 6 shows that in case-A, the strain in south and north side almost same with the result of the original structure, but the strain in the middle of connection part (in point 0.0) is larger than the original structure. This result shows a clear understanding about the effect of the thickness of the flange. Due to the reduction of the thickness, the flange will carry more strain. On the other hand in south and north side of the specimen, the value almost same due to the thickness of the stiffener same with the original structure. In case B, the strain in south and north side are larger than original structure, also the strain in the middle of connection part is larger compared to the original structure and case A. It can be understood from this study that in case A the strain in south and north side of the connection are smaller than case B, because some strain will be carried by the stiffener in the connection part. It can be concluded from these phenomena that the thickness of the flange in the compression flange and the stiffener in the connection has significant role in stress transfer.

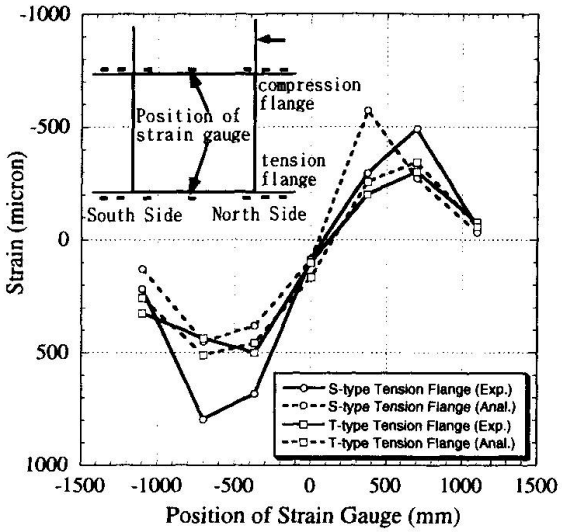

Fig.5. Strain Distribution on Tension Flange for Each Type

Figure 7 shows strain distribution on inner surface of tension flange in the connection. This figure shows the comparison result between experimental result, analytical result for original structure, and analytical for case A and B. The figure shows that the results for case A and B in every point get larger result compare to the original structure. In case A, even if the thickness of the stiffener is same as original structure, but the results in south and north side are larger than the original structure. It can be rationalized that when the load applied to the specimen, the

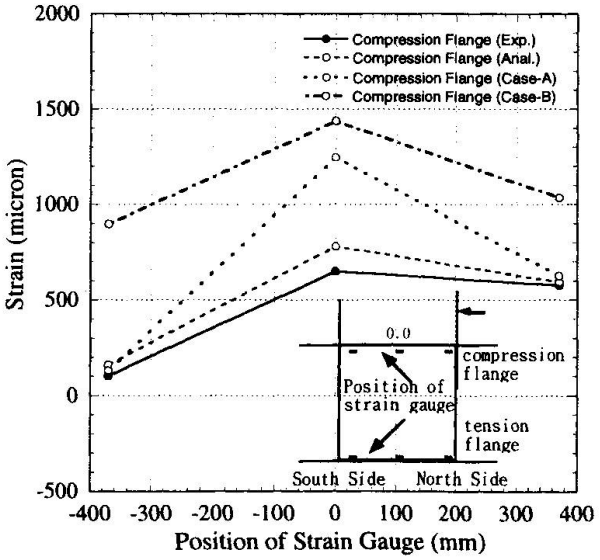

Fig. 6. Strain Distribution on inner surface of Compression Flange in the connection

tension flange will carry the load which is transferred through bonding between reinforcement and concrete. In case B, compare to the original structure and case A, the stain increase in south, north, as well as in the middle of the connection part (point 0.0). Analytical result shows that the result in all of the point almost same. This phenomena also as an effect of the reduction of the thickness of the flange and stiffener in the connection part. As a result from figure 6 and 7, the effect of the thickness of the flange in the connection part shows that the thickness in compression and tension flange has significant role on stress transfer. However, that effect in the compression flange is more significant compared to the tension flange.

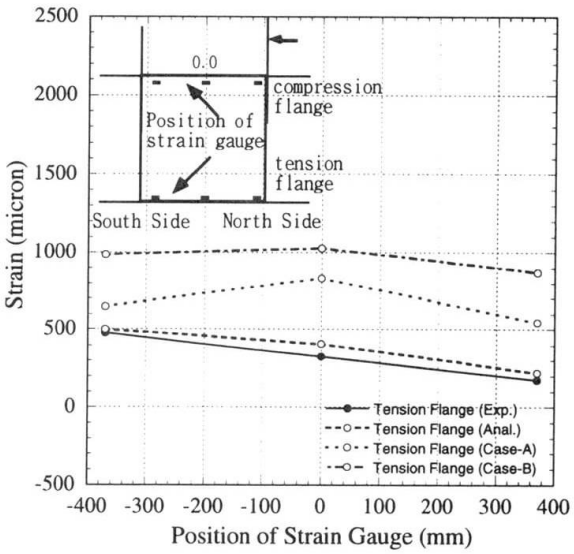

Fig. 7. Strain Distribution of Inner Surface of Tension Flange in The Connection

4.3. Behavior of the stiffener

Behavior of the stiffener monitored by checking the compression and tension force that carried by the stiffener. In experiment and analytical investigation, point a-b-c-d are used as investigation points. Point a-b located in the upper part of stiffener, and point c-d located in the lower part of stiffener. Load compression force relationship for stiffener and stud located in the investigation point a-b and c-d is shown in Figure 8 and 9. The purposes of these figures are to show the different phenomenon between S-type and T-type, to show phenomenon in the upper part and lower part of the stiffener, moreover to show good agreement between analytical and experimental result. From the figures we can see that S-type specimen carry more compression force than T-type. It can be investigated from the experimental work that when the load applied to the specimen S-type, in south side, the load directly transferred to the stiffener. Then in case of specimen T-type, the load will transferred to the stiffener and then transferred to stud shear connector. For investigation point a-b, the compression force from stiffener will transfer to stud i,

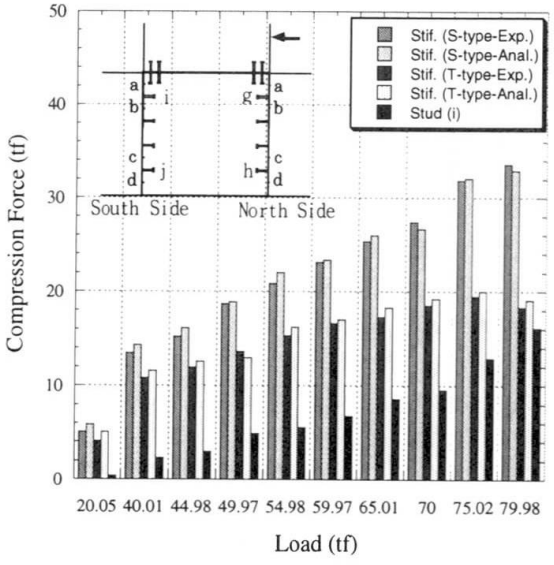

Fig. 8. Load-Compression Force Relationship in Point a-b and Stud i

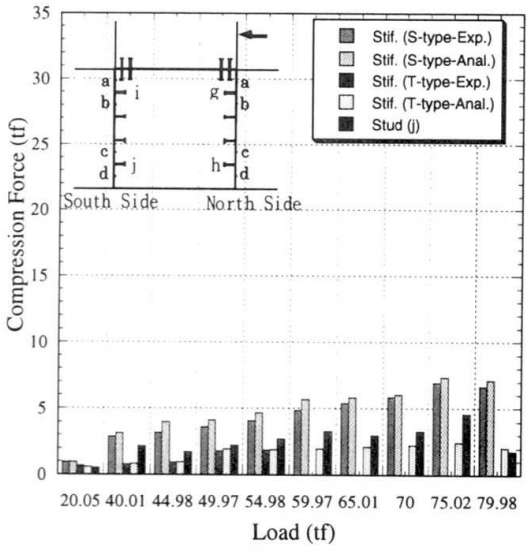

Fig.9. Load-Compression Force Relationship in Point c-d and Stud j

as shown in Figure 8. The result for investigation point c-d and stud j shows in Figure 9. This figure shows the same phenomenon with the previous figure, but the different is only in the total compression force can be carried is very small compare to the previous result. It can be concluded from these figures that the stud shear connector located in the upper part of stiffeners work effectively in transferring the stress in the connection part of hybrid rigid frame bridge. Considering the explanation from figure 8 and 9, the load transfer mechanism was drawn in Figure 10.

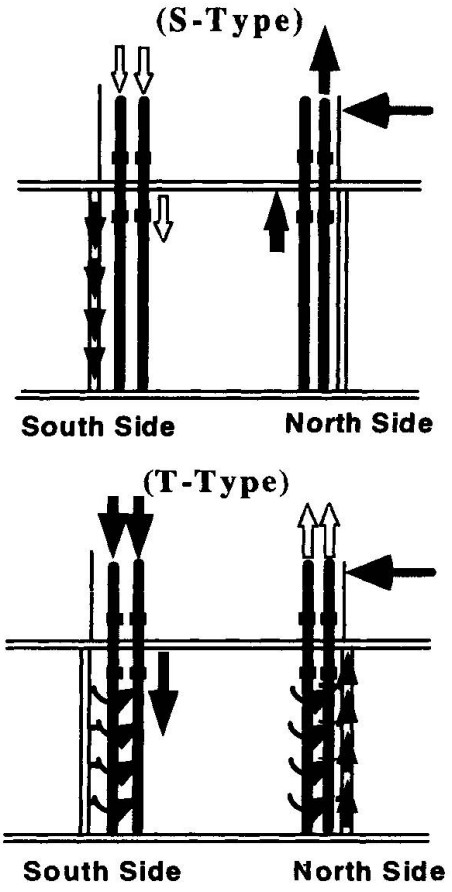

Fig. 10. Load Transfer Mechanism of Each Type

5. CONCLUSION

On the basis of the results in this study, the following conclusions may be drawn.

1. The strain in inner and outer surface of the flange in the connection of T-type is small. So it is possible to reduce the thickness of the flange for T-type specimen. Since the strains of inside and outside the flange in the connection are within reasonable range, it is recommended that this type of structure can be used if stud shear connectors are properly provided on the stiffeners.
2. Analytical results concerning the effect of the thickness of the flange in the connection part shows that the thickness in compression and tension flange has significant role on stress transfer. However, that effect in the compression flange is more significant compared to the tension flange.
3. The stud shear connectors in the upper part of the stiffener work effectively in transferring the stress in the connection part of hybrid rigid frame bridge.

REFERENCES:

1. Jiro Tajima, Yoshiniro Ito, and A. Machida, (1987)," Joints in Hybrid Bridge of Steel Girder and Concrete Pier", IABSE proceeding, pp. 425-430.
2. Shigeyuki MATSUI, Yasukuki YUKAWA, et.al., (1997)."Strength and Ductility of Beam-to-Column Connections in Hybrid Bridge", International Conference, Composite Structures, IABSE Proceeding, pp.469-474.
3. Nobuhito Okubo, Yoshifumi Maeda, et.al., (1998)."An Experimental Study on Structural Properties of a Steel-Concrete Hybrid Frame Bridge", The Sixth East Asia-Pacific Conference on Structural Engineering & Construction, EASEC-6 Proceeding, pp.513-519.
4. Mochammad Afifuddin, Takao Sugiyama, et.al., (1998)."A study on Connection mechanism of T-Joint in Steel-Concrete Hybrid Rigid Frame", Transaction of JCI Vol.20, 1998, (under published).
5. Marc Analysis Research Corporation., (1994). *Marc Manual, Vol: A - E*, California, USA.
6. Mochammad Afifuddin, Atsuhiko Machida, et.al., (1998)."Study on Behavior of Connection Mechanism on Hybrid-Rigid Frame Bridge Structure", Journal of Structural Engineering, Vol.44A, 1998, (under published).

Interaction of Moving Mass in Dynamic Analysis of Bridges

Mansour ZIYAEIFAR
Post doctoral fellow
Chiba Univ.
Chiba, Japan

Hiroshi NOGUCHI
Prof.
Chiba Univ.
Chiba, Japan

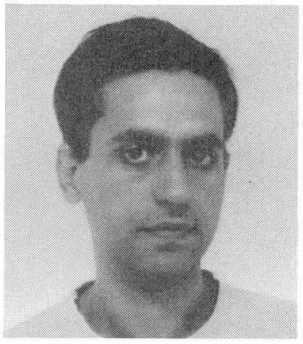

Mansour Ziyaeifar received his Ph.D. from Alberta Univ. in 1996. His current research are in the areas of finite element method, earthquake Eng. , bridge analysis and design.

Hiroshi Noguchi, received his Ph.D. from Tokyo Univ., in 1970. He has been involved in research in the area of concrete structures, seismic design and finite element method.

Summary

Application of new techniques in design of bridges although reduces the structural weight of the system but it may also result in a significant reduction in stiffness of the structure. In this case the bridge would be subjected to unprecedented dynamic behavior due to movement of traffic loads. In this study a simple but accurate method for dynamic analysis of bridges has been introduced to investigate the problems associated with interaction of mass and rotary inertia of traffic loads in dynamics of flexible bridges. The effect of suspension mechanism of vehicles on deformational aspects of the bridge is also integrated into this formulation. As an example for application of this technique, the results of a brief study on the effects of speed of traffic on dynamic behavior of simply supported rail-road bridges has been reported.

1. INTRODUCTION

Using new methods in design and construction of bridges, as well as application of advanced materials in bridge systems reduces, not only the structural weight of the system but in some cases it also affects the stiffness of the structure. Flexible bridges are more likely to experience severe dynamic responses due to passage of vehicles over the system. Dynamic behavior of a bridge due to traffic loads is a major concern in defining the functionality of a system and it is also considered as an important parameter in long term performance of the structure. An accurate dynamic analysis technique for flexible bridges needs incorporation of the effects of interaction between bridge and traffic loads. In a bridge, mass and rotary inertia of the system is continually changing by movement of traffic loads on the structure. Considering the fact that, mass of the traffic load is in contact with the bridge only through the suspension mechanism of vehicles, this parameter must also be included in an accurate representation for the bridge system and in investigation of dynamic behavior of the structure.

In this work a method based on Galerkin approximation has been developed which accounts for most of the required features expected from an accurate analysis technique. The method although is quite powerful in dealing with various parameters in interaction problem, it is simple in formulation and easy in programming.

2. DYNAMICS OF A VEHICLE ON A FLEXIBLE BRIDGE

To represent the case of an ordinary vehicle, it is considered as an object supported on two axles as shown in Fig. 1. Formulation was extended for a simple case in which bridge is horizontal and vehicle moves in a uniform speed. Following relationships are equilibrium conditions of vehicle on a flexible bridge system.

$$\begin{cases} \sum F_y = 0 \\ \sum M_c = 0 \end{cases} \Rightarrow \begin{cases} P + Q - mg + m\ddot{y}_c = 0 \\ P\,l_c - Q(l - l_c) - J\,\ddot{\alpha}_c = 0 \end{cases} \tag{1}$$

Where P and Q are reactions of axles of vehicle and l is the distance between two axles. Variables y_c and α_c are vertical and rotational acceleration of center of gravity of vehicle and l_c is the distance between center of gravity and reaction P. Parameter g is the gravitational constant, m is the mass of vehicle and J is its rotary inertia. Variables y_c and α_c can be replaced by the following expressions.

$$\ddot{y}_c = \ddot{y}_P + \frac{l_c}{l}(\ddot{y}_Q - \ddot{y}_P) \quad \text{and} \quad \ddot{\alpha}_c = \tan^{-1}\frac{\ddot{y}_Q - \ddot{y}_P}{l} \tag{2}$$

Where y_p and y_Q are local acceleration of bridge at the location of reactions P and Q respectively. By assuming small angle of rotation (i.e. small deformation of bridge) and in the case where center of gravity of vehicle is at the middle ($l_c = l/2$) of vehicle, solution of the equilibrium equations for P and Q results in the following expressions.

$$\begin{cases} P = \dfrac{mg}{2} + \ddot{y}_P\left[-\dfrac{J}{l^2} - \dfrac{m}{4}\right] + \ddot{y}_Q\left[\dfrac{J}{l^2} - \dfrac{m}{4}\right] \\ Q = \dfrac{mg}{2} + \ddot{y}_P\left[\dfrac{J}{l^2} - \dfrac{m}{4}\right] + \ddot{y}_Q\left[-\dfrac{J}{l^2} - \dfrac{m}{4}\right] \end{cases} \tag{3}$$

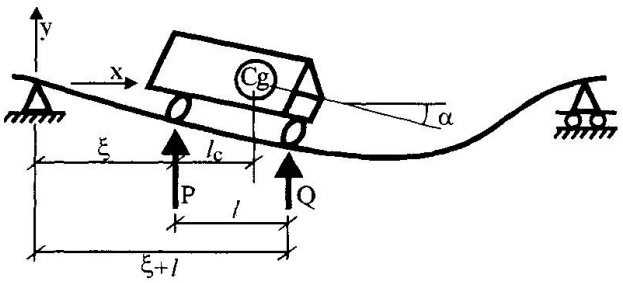

Fig. 1 - Bridge - vehicle representation

The first term in right hand side of the above equations represents the effect of static distribution of weight of vehicle on each axle. The second and third terms are representing the effects of local acceleration of bridge on reaction forces. The first term in brackets signifies the effect of mass rotary inertia while the second term (in brackets) indicates the effect of added mass of traffic load on reaction forces.

3. SUSPENSION MECHANISM

There is a similarity between suspension mechanism of vehicles and vibration isolator devices in mechanical systems. This similarity can be utilized to incorporate the effect of suspension mechanism of vehicles in dynamics of bridge by using force transmissibility factor ***TR*** (see, for example, Paz 1991). This factor in the case of bridge-vehicle system can be interpreted as the ratio between amplitude of dynamic force transmitted to the bridge with a flexible suspension mechanism and without it. Theoretically, transmissibility factor is a function of damping ratio of isolated system and frequency ratio of dynamic force, i.e.

$$TR = f(\zeta,\ \bar{\omega}/\omega) \tag{4}$$

Where ζ is damping ratio, ω is natural frequency of system and $\bar{\omega}$ is the frequency of harmonic force. In the case of bridge, ω is natural period of suspension system and $\bar{\omega}$ could be a function of both speed of vehicle and natural frequency of bridge. An easy way to implement this simple technique is to modify rotary inertia and mass of vehicle in the second and third terms of Eq.3 by the following expressions.

$$\begin{cases} J_{TR} = TR_P \,.J \\ m_{TR} = TR_H \,.m \end{cases} \tag{5}$$

In the above relationships parameters TR_P and TR_H are transmissibility coefficients for

pitching and heaving movement of vehicle and J_{TR} and m_{TR} are modified values for rotary inertia and mass of traffic load. Transmissibility coefficients in heaving and pitching are different due to distinct natural frequencies for each of these movements. Usually this factor for pitching (TR_P) is much smaller than for heaving movement (TR_H), predominantly because of the large rotary inertia of vehicles. This is considered a simplified approach because by scaling TR_P and TR_Q differently, the coupling effect between pitching and heaving movements of vehicle would be ignored.

Considering the above modification in mass and rotary inertia, the abbreviated form of reaction forces P and Q are as follows.

$$\begin{cases} P = A_0 + A_1 \ddot{y}_P + A_2 \ddot{y}_Q \\ Q = A_0 + A_2 \ddot{y}_P + A_1 \ddot{y}_Q \end{cases} \quad \text{Where: } A_0 = \frac{mg}{2}, \quad A_1 = \left[-\frac{J_{TR}}{l^2} - \frac{m_{TR}}{4} \right] \text{ and } A_2 = \left[\frac{J_{TR}}{l^2} - \frac{m_{TR}}{4} \right] \quad (6)$$

4. DYNAMICS OF BRIDGE

The simplified form of differential equation of a uniform bridge loaded with only one vehicle can be written as follows.

$$EI \frac{\partial^4 y}{\partial x^4} + \overline{m} \frac{\partial^2 y}{\partial t^2} = P\,\delta(\xi, x) + Q\,\delta(\xi + l, x) \qquad -l \le \xi \le L \qquad (7)$$

In which EI is flexural stiffness, $\overline{m}$ is mass per unit length. Forcing function in this equation consists of concentrated forces P and Q, which have been applied to the system by using Dirac-delta transformation functions represented by symbol δ (see, for example, Abramowitz et al. 1974). L is the total length of bridge and ξ is the distance of reaction P from the beginning of bridge (depicted in Fig.1). Based on the speed of vehicle and the elapsed time since the front axle of vehicle (reaction Q) has entered on the bridge, parameter ξ can be evaluated.

Forces P and Q are both functions of local acceleration of bridge y_p and y_Q as it is shown in Eq. 6. Interaction between load and deformational aspects of structure differentiate this problem from the ordinary problems in classical dynamic analysis. Therefore the available techniques in dynamic analysis of structures (modal analysis, for example) are not applicable to this particular case because of the interaction problem. In this study an algorithm based on Galerkin approximation (see, for example, Mikhlin 1964) has been chosen to address the problem. According to this approach deformation of the structure is approximated by a set of shape functions as follows.

$$y(x,t) = \sum_{i=1}^{n} \phi_i(x).q_i(t) \qquad (8)$$

In this equation $y(x,t)$ is vertical displacement of bridge while $\phi_i(x)$ are predefined displacement shape functions. Parameters $q_i(t)$ are shape function coefficients to be calculated at time t and n is the number of these shape functions. Replacing this approximation for deformation of the bridge into differential equation of system results in the following expression.

$$EI \sum_{i=1}^{n} \phi_i^{IV}(x) q_i(t) + \overline{m} \sum_{i=1}^{n} \phi_i(x) \ddot{q}_i(t) = \left[A_0 + A_1 \sum_{i=1}^{n} \phi_i(\xi) \ddot{q}_i(t) + A_2 \sum_{i=1}^{n} \phi_i(\xi + l) \ddot{q}_i(t) \right] \delta(\xi, x) + \left[A_0 + A_2 \sum_{i=1}^{n} \phi_i(\xi) \ddot{q}_i(t) + A_1 \sum_{i=1}^{n} \phi_i(\xi + l) \ddot{q}_i(t) \right] \delta(\xi + l, x) \qquad (9)$$

If shape functions ϕ_i are chosen to be a set of orthogonal functions, it can be shown that Dirac-delta equations are expandable based on the following relationships.

$$\delta(\xi,x)=\sum_{i=1}^{n}\phi_i(\xi)\phi_i(x) \qquad \text{and} \qquad \delta(\xi+l,x)=\sum_{i=1}^{n}\phi_i(\xi+l)\phi_i(x) \tag{10}$$

In a simplified approach, natural mode shapes of system can be used as shape functions for Galerkin approximation. By using the relational properties associated with application of a set of normalized modal shapes (see, for example, Paz.1991) and by pursuing Galerkin procedure, the final result will be the following set of equations.

$$\ddot{q}_m(t)+\omega_m^2.q_m(t)= \frac{1}{\overline{m}}\left\{\begin{array}{l}\left[A_0+A_1\sum_{i=1}^{n}\phi_i(\xi).\ddot{q}_i(t)+A_2\sum_{i=1}^{n}\phi_i(\xi+l).\ddot{q}_i(t)\right].\phi_m(\xi)+\\ \left[A_0+A_2\sum_{i=1}^{n}\phi_i(\xi).\ddot{q}_i(t)+A_1\sum_{i=1}^{n}\phi_i(\xi+l).\ddot{q}_i(t)\right].\phi_m(\xi+l)\end{array}\right\} \qquad m=1,2,..n \tag{11}$$

Where ω_m's are natural periods of the bridge. The above relationship is a set of n simultaneous coupled differential equations in time domain (ξ can be evaluated based on time).

The above relationships represents a case where only one vehicle with two axles is passing over the bridge. If the number of vehicles are more than one and system is subjected to damping forces, it can be easily shown that the system of equations will be changed to the following form.

$$\ddot{q}_m(t)+2\omega_m\zeta_m\dot{q}_m(t)+\omega^2{}_m q_m(t)= \sum_{j=1}^{k}\alpha_m(\xi_j)+\sum_{i=1}^{n}\ddot{q}_i(t)\sum_{j=1}^{k}\phi_i(\xi_j)\beta_m(\xi_j)+\sum_{i=1}^{n}\ddot{q}_i(t)\sum_{j=1}^{k}\phi_i(\xi_j+l)\lambda_m(\xi_j) \tag{12}$$

$$m=1,2,\ldots n$$

In which k is the number of vehicles on the bridge and parameters α , β and λ are defined as:

$$\left\{\begin{array}{l}\alpha_m(\xi)=A_0\left[\phi_m(\xi)+\phi_m(\xi+l)\right]/\overline{m}\\ \beta_m(\xi)=\left[A_1\phi_m(\xi)+A_2\phi_m(\xi+l)\right]/\overline{m}\\ \lambda_m(\xi)=\left[A_2\phi_m(\xi)+A_1\phi_m(\xi+l)\right]/\overline{m}\end{array}\right. \tag{13}$$

The following is the matrix form of the equation set No. 12.

$$[A_\xi]\{\ddot{q}_t\}+[2\omega\zeta]\{\dot{q}_t\}+[\omega^2]\{q_t\}=\{B_\xi\} \tag{14}$$

Where $[2\omega\,\zeta]$ is a diagonal matrix representing damping contribution in the system. Matrix $[A_\xi]$ and vector $\{B_\xi\}$are coefficient matrix and load vector, respectively. These two terms must be evaluated at time t based on location parameter ξ.

In comparison with classic dynamic analysis, in the above equation matrix $[A_\xi]$ is not a diagonal matrix. This clearly indicates that the equation set is in a coupled system. Among numerous time integration method applicable to this problem, a method based on Runge-Kutta formulas of order five and six (see Hull et al. 1976) has been adopted as the solution algorithm in this study. To be able to use Runge-Kutta formulas, differential equations must be transformed to a set of first order differential equations. It can be shown that, such transformation is possible by only using a simple change in the variables (see Hull et al. 1976).

8. CASE STUDY FOR HIGH-SPEED TRAINS

The capability of this technique is shown in an example in railway bridges. A train system as shown in Fig.2 is considered as traffic load on the bridge. Dynamic analysis was carried out for a bridge with 50 meters in length (shown in the same figure). The length of bridge is chosen less than the train, to investigate the case in which the whole bridge is loaded steadily with traffic. In this case, bridge is considered as simply supported single span structure.

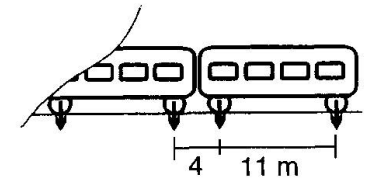

(a)- The train system :

Weight of each car :	1500.	KN
Rotary Inertia of each car :	3.E+9	$N\text{-}s^2.mm$
No. of cars in train system:	10	

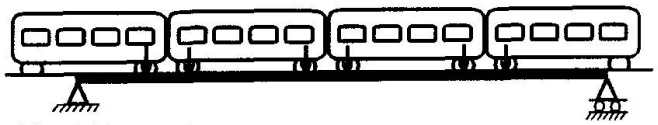

(c) - Bridge system :

Length:	50.	meter
Weight of bridge :	150.	KN/m
Stiffness (EI) :	1.E+17	$N.mm^2$

Fig. 2- The bridge - traffic model

It is assumed that all the natural modes have a damping ratio of 5% (ζ_m=0.05). The parameters TR_P and TR_H have been chosen intuitively to represent a system with characteristics of soft suspension mechanism (0.1 and 0.9 respectively). Figure 3 illustrates mid-span displacement of bridge when resonance occurs at speed of 73 Km/h. In this figure, horizontal axes represents the distance of front axle of the first car from the left support of the bridge (ξ+l). This figure is similar to classical *Influence Line* in bridge engineering. Figures with this type of horizontal axis hereinafter are referred to as ***Dynamic Influence Line***.

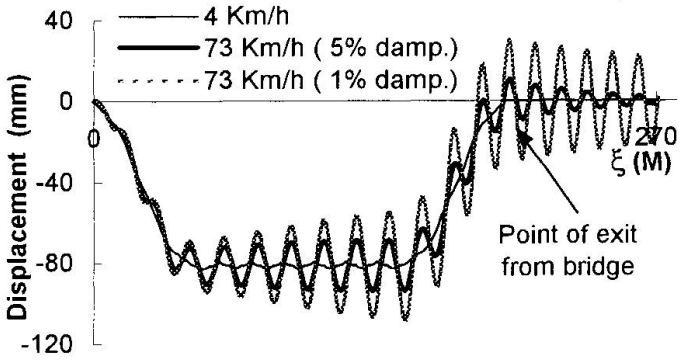

Fig. 3 - Displacement at mid-span during resonance

A case of low speed train (4Km/h) is also included in the same figure to simulate a behavior similar to static analysis of the bridge. As it is shown in the figure, a lower damping ratio causes larger amplitude of vibration in the structure. In the case of resonance the amplitude of vibration grows steadily with continuation of vibration process, thus its maximum magnitude depends on the number of cars in the train system.

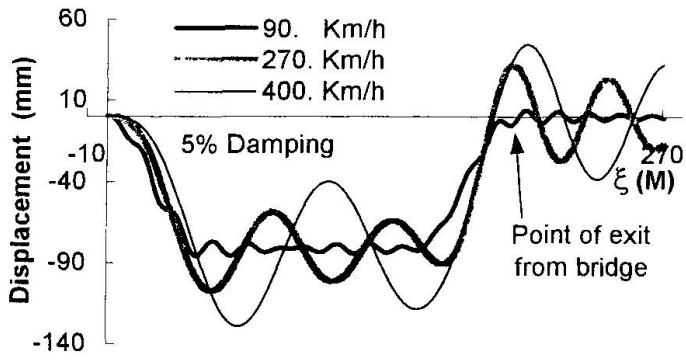

Fig. 4 - Displacement at mid-span at high speed

By further increase on the speed of train there will be a substantial increase on maximum displacement of bridge as it is shown in Fig. 4.

The result of analysis for shear force at a point close to support (at a distance of 1% of span from the left support) is illustrated in Fig. 5. The importance of traffic load

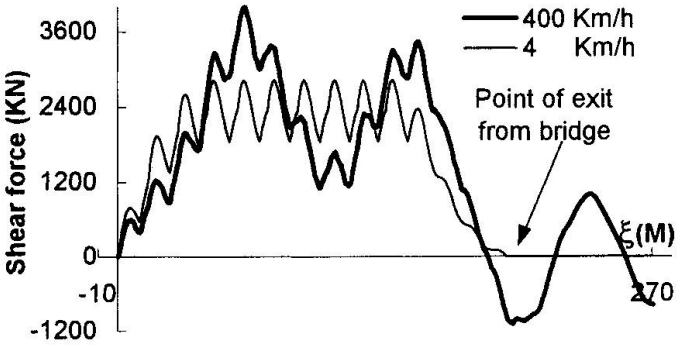

Fig. 5 - Shear force at a point close to support

representation as point loads in this formulation is illustrated in the same figure. According to this figure, even in the case of static loading (speed of 4Km/h) there is a periodic variation on the level of shear force in structure which aggravates by increase on the speed of traffic. If, for example, a detail information on stress cycle history of bridge for fatigue design is required, such accuracy in analysis is quite important.

9. CONCLUSION

To study the effects of reduction in stiffness of bridges on functionality and long term performance of these systems, a technique has been proposed for accurate dynamic analysis of these structures. This method is capable of representing the effects of movement of vehicles on bridge with a reasonable accuracy. The method is based on Galerkin approximation and it offers a phenomenal simplicity in formulation and also high efficiency in the computational efforts. However, since this method relies only on the general structural parameters of system (such as mass and flexural stiffness), it does not have the required generality to be applied to the detail analysis of bridges. In other words, this method can only provide a general view on dynamic behavior of those bridges with complicated structural system. In such cases the results of dynamic analysis by this approach can be used to extrapolate the response of the structure obtained from a detailed static analysis (by, for example, finite element method). It is believed that, this technique can be extended to a more general formulation to serve wider range of applications.

ACKNOWLEDGMENT

This work has been financially sponsored by the Japan Society for the Promotion of Science (JSPS) under the post doctoral fellowship No. P96026. The first author wishes to express his gratitude to Dr. M.M.Alishahi (Shiraz University, Shiraz, Iran) for his precious advice and valuable help on development of the basis of this subject. Authors are also in debt to Prof. N.Shirai (Nihon University, Tokyo, Japan) for his guidance and encouragement in the course of this study.

REFERENCES

Abramowitz, M. and Stegun, I.A. (1974). *Handbook of Mathematical Functions*. National Bureau of Standards, Dover Publications Inc., New York.

Hull, T.E., Enright, W.H. and Jackson, K.R. (1976). *User's guide for DVERK - A subroutine for solving non-stiff ODEs*. Department of Computer Science, Technical Report 100, University of Toronto.

Mikhlin, S.C. (1964). *Variational Methods in Mathematical Physics*. Macmillan.

Paz, M. (1991), *Structural Dynamics Theory and Computation*, Van Nostrand Reinhold.

System Fatigue Assessment of Orthotropic Steel Bridge Decks

Naxin ZHANG
Research Fellow
TU-Delft
Delft, The Netherlands

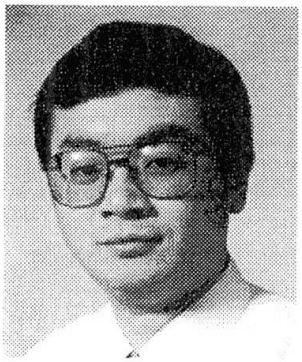

Naxin Zhang, born in 1968, received his B.Eng., M.Eng. & Ph.D. in Structural Engineering from Tsinghua Univ., Bejing, China. From 1997 to 1998, he was a research fellow in the Steel Structure Group of TU Delft.

Henk KOLSTEIN
Research Eng.
TU-Delft
Delft, The Netherlands

Henk Kolstein, born in 1952, joined Delft Univ. of Technology in 1971. Since 1978, he has been participating in ECSC research within the domain of bridge loading and fatigue of orthotropic steel bridge decks.

Summary

In the recent research of System Fatigue Durability Assessment for steel orthotropic bridge decks, the SRBA (Systematic Reliability Blocking Analysis) Technique is introduced and developed. This method is summarized as the procedure of *Structure Blocks Decomposition* plus *System Reliability Assembly*. So the structural redundancy and systematic scale are no longer the great worry of system reliability calculation, and the repairing effect becomes free to be involved. This paper gives an outline of the investigation. An example with on-site measured data is also presented for evaluating its system fatigue life and reliability.

1. Introduction

The steel orthotropic bridge deck is a welded structure comprising of the deck plates, deck stiffeners (or troughs), crossbeams, and main girders. The previous connection designs usually can not meet the fatigue durability demands. With the sponsor of ECSC (European Coal and Steel Community), a series of collaborative projects concerning such deck structures have been carried out in Europe. Topics covered the traffic loading, resulting stresses and detail fatigue strength, etc [1]. Nevertheless, the fatigue assessment is still stay at a componental or elemental level. That means the estimate life of a typical joint is taken as the deck integral service life.

During the componental fatigue S-N design or assessment, 95% is specified to be the confidence interval of reliability, which indicates that around 5 over (per) 100 joints might be failed during the service life. Normally there are several hundreds joints, with almost the same constructional detail and similar fatigue loading, inside the orthotropic bridge deck system. So, the elemental design, which is regularly believed safe enough for the individual elements, becomes unreliable for the whole deck system.

There are some difficulties in the systematic fatigue analysis for orthotropic decks, for instance, the very large quantity of similar joints, uncertain sequence and relationship among the damage of elements, and fuzzy criterion of the system failure, etc. Considering these characteristics, the Systems Reliability Blocking Analysis (SRBA) technique [3] was adopted to the deck system fatigue assessment. The integral structure is treated as a multi-leveled composition of chains of

serial/parallel blocks (subsystems). The individual welded joint is taken as the elemental block, whose reliability can be determined by the conventional method. By the assumed subsystem-assembling models, the system reliability could be derived from elemental ones level by level.

Because of the processing with subsystems, the structural redundancy is no longer a big trouble and the repairing influence becomes easy to discuss. Comparing with current system reliability methods, the computing amount of SRBA is much less, while the credibility of its result is not lost [4]. It has remarkable fitness to engineering applications, extremely for the structures which are comprised by lots of constructional-alike parts or elements.

2. System Fatigue Assessment Method for Orthotropic Decks

2.1 Subsystems decomposition

The System Blocking Procedure for orthotropic decks can be standardized to a three-leveled decompositions [4]. During every decomposition, the nascent system, ranked with the upper level, is divided into a series of blocks (or subsystems) taking up the next level.

1st-level subsystems: The bridge deck system visibly and functionally involves several traffic lanes. Different lanes normally expect similar constructional details, but different traffic loading. Sometimes the constructional style or details are segmental continuous along the bridge, for instance, the thickness of the deck plates are alternating. Each of the lanes or lane-segments could be taken as an individual 1st-level block, although there is some kind of coherence among their failure states. From the serviceability point of view, if anyone of the lanes or lane-segments suffers severe damage, the brige deck structure could be thought of failure and need repair. So, the 1st-level blocks are supposed cascade (or serial) to each other in the composition of integral system.

2nd-level subsystems: Every lane or lane-segment contains several *joint-groups* (the sets of joints with same type and constructional details) which might incur fatigue damage, such as the groups of (a) stiffener splice joints, (b) stiffener to deck joints, (c) stiffener to crossbeam joints, (d) deck plate splices, (e) crossbeam to deck joints, and (f) main girder to deck joints, etc. Sometimes one sort of joints consist of one or several joint-groups. Such joint-groups are taken as the 2nd-level blocks, and they are simply assumed serial to each other. A 2nd-level subsystem possesses a large number of joints with same typical construction and same simplified loading model.

3rd-level subsystems: Each joint-group holds only one *typical joint* as the representative, which is taken directly as the 3rd-level block. The fatigue behavior of typical joints, containing the details which propagate fatigue cracks, could be examined by the S-N tests.

2.2 System failure criterion and Bernoulli distribution assumption

For the fatigue of deck system, there is no clear definition of system failure.The common limit of no crack occur can be taken as a system safety index. Correspondingly the system reliability is represented by the *Probability of First Cracking* (PFC), which expects no more than one joint suffers fatigue damage. This index is very sensitive to the quantity of concerned joints. Normally it is not economic to keep every joint reliable during the whole service life.

From the deck serviceable and repairable demand, a few of joints damaged is allowed and does not affect the structural integrity. Therefore, the indexes of percentile joints failure are more suitable for the deck system. The system reliability can be represented by the *Probability of z% Joints Damage* (PJD- *z*%), which intends no more than *z*% of total joints are failed. Another benefit of such indexes is their insensitiveness to the system scale. It need more discussion and

experience to select a proper percentage as the system failure limit. PJD-0.5% and PJD-1% are recommended here as the failure limit of joint-groups of steel orthotropic decks.

The orthotropic deck system contains particularly a large number of elemental joints, most of them are working in several typical cases of consistent constructional details and similar stressing conditions. These joints act as the same functions and endure with roughly the same loading histories, wherever their locations are along the bridge deck. From the statistical point of view, it is reasonable to assume that the fatigue failure of a deck joint-group, which is taken as the damage occuring in a certain number of its joints, approximately follows the Bernoulli Distribution, and the reliability of a joint-group is then computable by the *Bernoulli Formula*.

2.3 System reliability calculation

The reliability assembling procedure, inverse to the sequence of system blocking, is carried out from lower level to upper level [4].

According to the schedule of fatigue S-N analysis and First-Order-Second-Moment probabilistic estimation, the elemental reliability can be derived [3,4] if the statistical data of S-N tests (for the resistance) and stress measurement (for the loading) are provided. Generally, the resistance and loading are assumed following the Log-normal Distribution.

With the hypothesis of Bernoulli Distribution of joint-groups failure, the 2nd-level reliability can be determined if the elemental reliability and joints quantity are known. Taking PJD-z% as the subsystem reliability of a joint-group, the 2nd-level reliability is formulated by

$$R_{1-2nd} = \sum_{x=0}^{m} C_n^x \cdot p_e^x \cdot (1-p_e)^{n-x} \quad \text{and} \quad C_n^k = n!/(n-k)!k! \tag{1}$$

where n is the joints quantity of the joint-group, excluding the eliminable portion; $m = [n_s \cdot z\%]$ is the limit number of failed joints; n_s is the sum of joints in the joint-group, including the eliminable portion; and p_e is the failure probability of the typical joint.

After getting the reliability of all 2nd-level subsystems, the 1st-level and the integral reliability can be determined in subsequence. Noting $\bar{\beta} = (\beta_1, \beta_2, \cdots, \beta_n)$ as the subsystems reliability index vector, the system reliability can be obtained in approximation [3,4]:

$$R_{\text{serial}} = \Phi_n(\bar{\beta}, \rho) \quad \text{and} \quad \Phi_n(\bar{\beta}, \rho) = \int_{-\infty}^{+\infty} \phi(t) \prod_{i=1}^{n} \left[\Phi\left(\frac{\beta_i - \sqrt{\rho}t}{\sqrt{1-\rho}} \right) \right] dt \tag{2}$$

where $\Phi_n(*,*)$ is the cumulative function of Standard N-dimensional Normal Distribution, $\phi(\cdot)$ and $\Phi(\cdot)$ are respective the density and cumulative function of Standard Normal Distribution. The correlation coefficient ρ describe the linear similarity and inclusiveness among the failure states of the blocks within same level. The equivalent average correlation coefficients for the SRBA of orthotropic decks are investigated and suggested in [4].

2.4 Repairing consideration

The reliability assembling process depends only on the systematic blocking diagram and its probabilistic model, so it is easy for the SRBA to access the repairing discussion. After a repair of some deck joints within same joint-group, a new joint-group composed of these repaired joints is added to the 2nd-level blocks. Sometimes the repaired joints cover different joint-groups, then several repaired joint-groups will arise. Every repaired joint-group belongs to its original 1st-level subsystem. The repaired joint-group has a individual calendar of servicing to calculate their elemental reliability of typical joint.

3. Example

3.1 Measured data

The example bridge [2] is shown in Fig.2, which was built in 1975. The truck intensity in the order of 2×10^6 per year in each direction is divided over three traffic lanes. The bridge deck consists of an orthotropic steel plate (of 10, 12 and 14mm varying in longitudinal direction) stiffened by the longitudinal trapezoidal troughs.

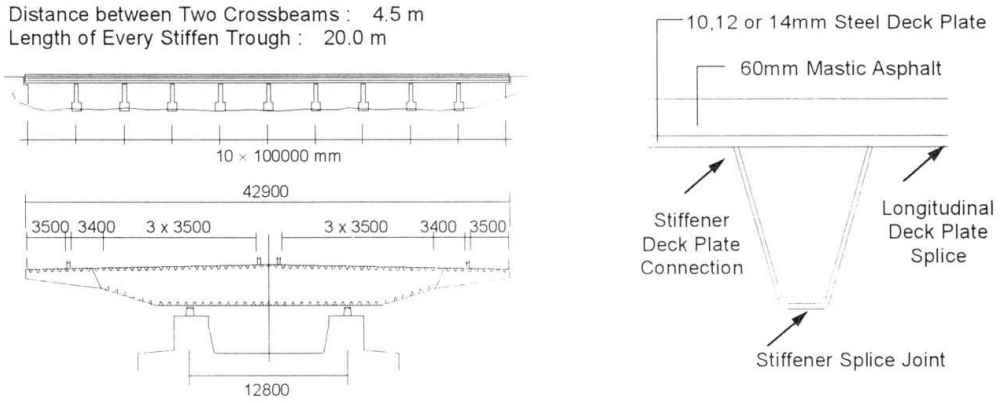

Fig. 1 *Example bridge and its orthotropic deck*

The stress spectra had been measured in three temperature conditions [2]. The equivalent stress-ranges with the corresponding fatigue detail classification are summarized in Table 1. The stress value of whole year takes an weighted average of [0.25(*Feb*)+0.5(*Nov*)+0.25(*Jul*)]. Table 2 shows the amount of several sorts of deck joints in evaluation. The non-uniformity in loading distribution and welding workmanship are regarded here, e.g. the *Elim. Factor* in Table 2.

Constructional Details		Load (from measurements)					Resistance (from tests)	
		Equivalent Stress Range				Stress Cycles	Detail Class	Deviation
		Feb(5°C)	Nov(15°C)	Jul(35°C)	Year	per Year	(Suggested)	of (logN)
Stiffener Splice Joints	deck plate 10mm	19.7	26.3	34.5	26.70	1.628 e6	71	0.2325
	deck plate 12mm	20.5	26.2	31.2	26.02			
	deck plate 14mm	19.0	26.8	29.9	25.62			
Stiffener to Deck Joints	deck plate 10mm	14.2	23.4	39.2	25.05	1.870 e6	56	0.3918
	deck plate 12mm	13.6	20.5	32.9	21.87			
	deck plate 14mm	10.8	18.8	29.0	19.35			
Longinal. Deck Plate Joints	deck plate 10mm	8	-	-	≈25.	1.450 e6	80 (or E in BS5400)	0.2510 (BS5400)
	deck plate 12mm	9	18	52	24.25			
	deck plate 14mm	9	20	44	23.25			

Table 1 *Results from on-site measurement and ECSC tests*

	Stiffener Splice Joints	Stiffener to Deck Joints	Stiffener to Crossbeam Joints	Longitud. Deck Plate Joints	Crossbeam to Deck Joints
n_s : Each Lane	200	1600	3200	200	1600
LaneSegment-10mm	40	320	640	40	320
LaneSegment-12mm	80	640	1280	80	640
LaneSegment-14mm	80	640	1280	80	640
n_s : Σ(6 lanes)	1200	9600	19200	1200	9600
Elim. Factor (1- n/n_s)	1/2	1/2	2/3	1/2	2/3

Table 2 *Amounts of deck joints in consideration*

3.2 Conventional fatigue assessment for typical joints

It is supposed by experience that the variation coefficients of the measured stresses on the details of Stiffener Splice Joints, Stiffener to Deck Joints and Longitudinal Deck Plate Joints are 0.050, 0.075 and 0.10 respectively. Table 3 shows the results of failure probability of typical joints at several intervals of bridge service time. From the elemental assessment, the fatigue life of the deck is about 68 years, governed by the Stiffener to Deck Joints with the 10mm thick deck plate.

Service time (years)		25	30	35	40	50	60	70	100
Stiffener Splice Joint	deck plate 10 mm	.00002	.00005	.00013	.00029	.00097	.0024	.0048	.0205
	deck plate 12 mm	.000007	.00002	.00006	.00014	.00049	.0013	.0027	.012
	deck plate 14 mm	.000004	.00001	.00004	.00009	.00032	.00085	.0018	.0092
Stiffener to Deck Joint	deck plate 10 mm	.0047	.0076	.0113	.0155	.0258	.0379	**.0514**	.0973
	deck plate 12 mm	.00061	.0011	.0018	.0026	.0049	.0079	.0117	.0270
	deck plate 14 mm	.00007	.00014	.00024	.00038	.00080	.0014	.0022	.0061
Longitud. Deck Plate Joint	deck plate 10 mm	.000005	.00001	.00002	.00004	.00010	.00022	.00040	.0014
	deck plate 12 mm	.000002	.000005	.00001	.00002	.00005	.00012	.00022	.00084
	deck plate 14 mm	.000001	.000002	.000004	.000008	.00002	.00005	.00009	.00039

Table 3 *The elemental fatigue failure probability of typical deck joints*

3.3 System fatigue assessment

For simplicity, suppose the 6 traffic lanes of the bridge carry a same traffic model. The thickness of deck plate is varied among 10, 12 and 14mm, consequently three lane-segments are identified (see Fig.5). Only three sorts of joints are measured and can be taken into evaluation, then there are altogether 9 joint-groups, which are regarded as the 2nd-level blocks (see Table 4). For more discussions, three system safety indexes for joint-groups, i.e. PFC, PJD-0.5% and PJD-1%, are selected in the reliability calculation. All the systematic analysis results are shown in Table 4 & 5.

Servicing time (years)		25	30	35	40	45	50	60	70	100
Stiffener Splice Joint-Group with Deck 10mm	PFC					1.	0.994	0.966	0.886	0.292
	PJD-0.5%					1.	0.994	0.966	**0.886**	0.292
	PJD-1%						1.	0.997	0.979	0.553
Stiffener Splice Joint-Group with Deck 12mm	PFC						1.	0.960	0.862	0.216
	PJD-0.5%						1.	0.996	0.972	**0.449**
	PJD-1%							1.	0.999	0.836
Stiffener Splice Joint-Group with Deck 14mm	PFC							1.	0.930	0.351
	PJD-0.5%							1.	0.990	**0.620**
	PJD-1%								1.	0.927
Stiffener to Deck Joint-Group with Deck 10mm	PFC	0.060								
	PJD-0.5%	0.983	**0.800**	0.356						
	PJD-1%		1.	0.992	0.883	0.507	0.140			
Stiffener to Deck Joint-Group with Deck 12mm	PFC	1.	0.376	0.140						
	PJD-0.5%					1.	0.998	**0.866**	0.272	
	PJD-1%							1.	0.999	0.026
Stiffener to Deck Joint-Group with Deck 14mm	PFC						1.	0.251	0.076	
	PJD-0.5%								1.	0.983
	PJD-1%									1.
Longi. Deck Plate Joint-Group with Deck 10mm	PFC								1.	0.987
	PJD-0.5%								1.	0.987
	PJD-1%								1.	0.999
Longi. Deck Plate Joint-Groups with Deck 12 &14 mm	PFC									1.
	PJD-0.5%									1.
	PJD-1%									1.

Table 4 *The system reliability of the 2nd-level blocks*

Servicing time (years)		25	30	35	40	45	50	60	70	100
Lane-Segement of Deck Plate Thickness 10mm	PFC	0.060								
	PJD-0.5%	0.983	**0.800**	0.356						
	PJD-1%		1.	0.992	0.883	0.507				
Lane-Segement of Deck Plate Thickness 12mm	PFC	1.	0.376							
	PJD-0.5%					1.	0.998	**0.886**	0.270	
	PJD-1%							1.	0.998	0.
Lane-Segement of Deck Plate Thickness 14mm	PFC						1.	0.251		
	PJD-0.5%							1.	0.990	**0.620**
	PJD-1%								1.	0.927
Deck Integral	PFC	0.060	-							
	PJD-0.5%	0.983	**0.800**	0.356	-					
	PJD-1%	1.	1.	0.992	0.883	0.507	-			

Table 5 *The system reliability of the 1st-level blocks and integral structure*

The estimated fatigue life of the integral deck system is around 28 years, providing PJD-0.5% as the safety index of joint-groups and 0.9 as the integral reliability criteria. The ratio of the service lives predicted by systematic assessment and elemental assessment is about 0.41. If take PJD-1% as the group safety index, the deck servicing years is computed to 39, which is nearly 1.4 times than the result under the selection of PJD-0.5%. The first fatigue crack might appear, most probably among the Stiffener to Deck Joints with 10mm deck plate, after 20~25 years in-service.

4. Conclusions

1) The SRBA is a system reliability approach to structural fatigue assessment. Its main parts are the system-blocking and reliability-assembling procedures, which are flexible to nearly all kinds of structures. The SRBA procedures need not a large amount of computation, and are capable to include the repairing consideration.

2) The failure of a deck joint-group is defined as the damaged joints reach to a certain percentage, and assumed following the Bernoulli Distribution.

3) The system reliability depends on not only its elemental standard, but also the system scale and composition. Systematic effect, here especially the statistical effect, is remarkable and could not be ignored in the fatigue assessment of orthotropic bridge decks. From the example, the system fatigue life is about 28 (or 39) years, while the elemental estimated life is about 68 years. The difference is more than 2 times. Due to the large quantity of joints within deck structures, the system reliability decrease much rapidly near the end of its service life.

References

[1] Kolstein, M.H. and Wardenier, J., etc. Fatigue Strength of Welded Joints in Orthotropic Steel Bridge Decks. *Proc. of the International Conference on Welded Structures in particular Welded Bridges, Budapest.* September 1996. pp179-189.

[2] Kolstein, M.H. and Wardenier, J. Stress Reduction due to Surfacing on Orthotropic Steel Decks. *IABSE Workshop, Lausanne.* March 1997. pp109-118.

[3] Zhang, Naxin and Li, Shaofu. Systems Study on Fatigue Durability of Steel Girder Bridges. *Proc. of IACSS'96, Hong Kong.* December 1996.

[4] Zhang, N. and Kolstein, M.H. Study on Systems Fatigue Assessment Method for Orthotropic Steel Decks. *Stevinlab Reseach Report, TU-Delft.* April 1997.

Computer-Aided Wind Engineering of Long-Span Bridges

Allan LARSEN
Dr Eng.
COWI AS
Lyngby, Denmark

Allan Larsen, born 1953, obtained his engineering degree in 1979, the von Karman Institute diploma in 1981 and a Ph.D. in flow induced vibrations in 1984. Mr Larsen joined COWI in 1989 working as a bridge engineer specialising in aeroelastic analyses, wind loads and structural dynamics.

Soren ESDAHL
Civil Eng.
COWI AS
Lyngby, Denmark

Soren Esdahl, born 1971, obtained his engineering degree in 1995 at the Technical University of Denmark. Mr. Esdahl is a bridge engineer working within Finite Element modelling analysis, structural dynamics, and aeroelasticity.

Summary

The design of long-span cable supported bridges often involves considerations of wind effects and aeroelastic stability. A new computational fluid dynamics code is combined with an existing in-house FEM code to form a computer-aided engineering system suitable for wind engineering analysis and assessment of bridges. This paper offers a brief discussion of two actual bridge designs analysed using this system. It is demonstrated how geometrical girder cross section details is significant to the aerodynamic performance of a long-span bridge.

1 Introduction

Wind engineering of long-span bridges most often focuses on the interaction of aerodynamic loads generated by the wind and the elastic response of the bridge structure. The related engineering discipline of aeroelasticity requires tools that will allow the engineering analyst to establish the effect of the over all structural lay-out as well as predict the influences of structural changes as they occur during the design process. Prior to the early 1970'ties most aerodynamic and structural dynamics analyses relied on physical model testing of the bridge in question. Needless to say, this approach was time consuming and did not allow for many design iterations. The advent of the computer based Finite Element Method rendered structural model testing superfluous and allowed the designer to explore the dynamics of a wide range of structural configurations, but aeroelastic analyses were still relying on experimental data obtained from wind tunnel testing. Recent advances in computer sciences have made numerical simulations of aerodynamic loads on bridge girder cross sections possible thus allowing the entire wind engineering process of long-span bridges to be aided by computers. This paper presents two examples of how computer-aided wind engineering analyses may influence the design and performance assessment of long-span bridges. Two design cases involving assessment of the critical wind speed for onset of flutter for cable-stayed bridges are discussed highlighting the influence of cross section geometry. The bridges discussed are a cable-stayed bicycle bridge to be build in Holland (Tuibrug in de Zuidtangent) and a cable-stayed motorway bridge (Sunningesund Bridge) now under construction in Sweden. Principal dimensions of the bridges discussed are shown in fig. 1.

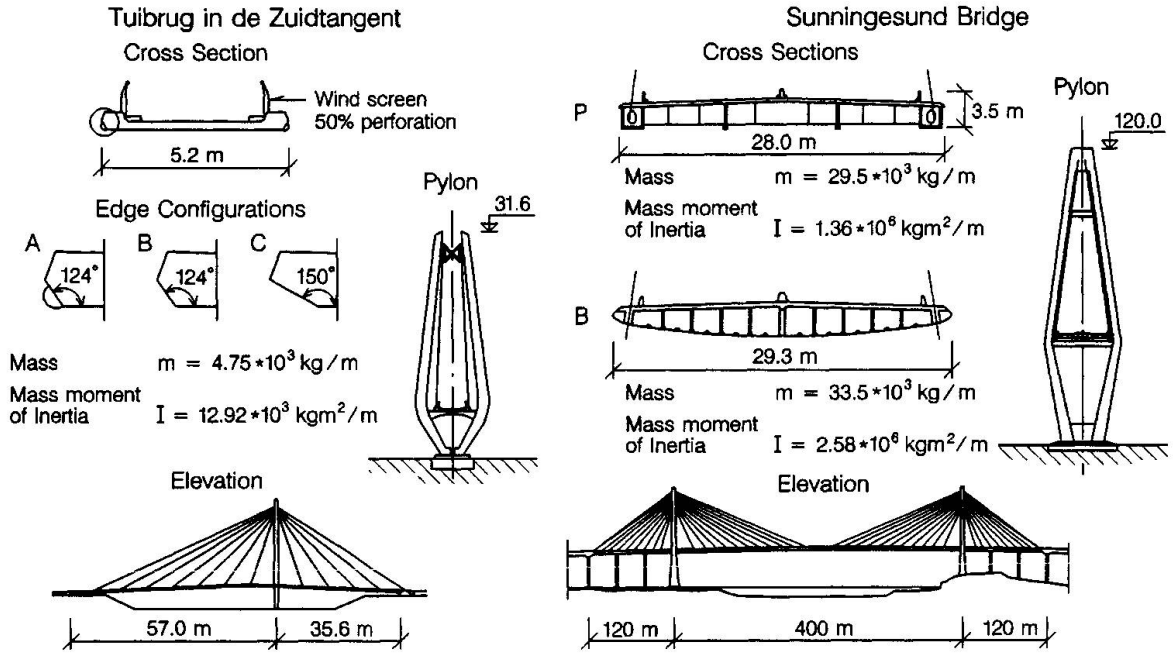

Fig. 1 Main particulars of cable-stayed bridges investigated

2 Computer-Aided Wind Engineering System

The aerodynamic back-bone of the computer-aided wind engineering system operated by COWI is the computer code DVMFLOW introduced to the IABSE community at the Copenhagen Congress 1996, Larsen and Walther [1]. The DVMFLOW code applies the discrete vortex method for simulation of aerodynamic loads on two-dimensional (2D) cross sections which are fixed or undergoing forced motion relative to the flow. Also the cross sections may be elastically suspended in the flow allowing simulation of non-linear flow induced response. Full three-dimensional (3D) dynamic analysis of a bridge structure is facilitated by the COWI CAE system IBDAS which makes a wide range of structural elements and a parametric representation of the turbulent wind available to the aeroelastic analyst, Sørensen, Andersen and Jacobsen [2]. Links between 2D simulations of the aerodynamic properties of the bridge girder and the dynamics of 3D pylon-cable-girder assemblies are provided by the modal analysis method developed by Scanlan [3] and co-workers. Specific details of the simulation and analysis procedures will not be detailed further. Interested readers are referred to Walther and Larsen [4], for a presentation of the discrete vortex method employed in DVMFLOW and to Larsen [5] for a general discussion of computer simulations of wind-structure interaction in bridge aerodynamics.

3 Cable-Stayed Bicycle Bridge

The infrastructure serving the Schiphol Airport, the Netherlands, is currently being expanded. One of the additions to the road system feeding the airport is a slender cable-stayed bicycle bridge designed by the Dutch engineers IBA / TauwMabeg. The bridge comprises a 92.6 m long and 5.2 m wide concrete girder carried by two fans of stay-cables anchored at the girder

edges and at the top of a single central steel pylon, fig. 1. Preliminary aeroelastic analysis based on a plane (2D) structural model and wind tunnel data compiled in the bridge design literature [6], yielded an unacceptable low critical wind speed for onset of flutter and further investigations were recommended. At the request of IBA / TauwMabeg, COWI was entrusted a computational aeroelastic analysis of the bridge involving a three-dimensional structural dynamics analysis and assessments of the influence of modifications of the bridge girder cross section geometry.

The IBDAS model developed for structural dynamic analysis of the bridge reproduced the full 3D geometry of the structure and included supports and fixations at the landfalls and pylon. Mass and stiffness properties of the individual elements were based on the material specifications and dimensions given in the design drawings. Particular attention was given to modelling of the cross beam at the top of the pylon as details in this region is known to have significant effect on the torsion frequency of the bridge. Fig. 2 shows the lowest vertical (h) and torsional (α) eigenmodes for which the bridge is likely to encounter flutter. Comparison of vertical eigenfrequencies f_h obtained from 2D and 3D analysis yields good agreement. Analysis of torsion modes is, by definition, not possible in 2D modelling as the torsion stiffness of the girder and twist of the pylon structure around a vertical axis is not accounted for. Torsion frequencies f_α are, however, sometimes inferred from the vertical modes by scaling the vertical frequencies with the ratio of the semi-distance (b) between the cable planes to the cross section radius of gyration (r): $f_\alpha = f_h \cdot b/r$. This simplification, which borrows from the analysis of suspension bridges with stiffening girders composed of open and thin walled cross sections, leads to serious underestimation of f_α in the present case.

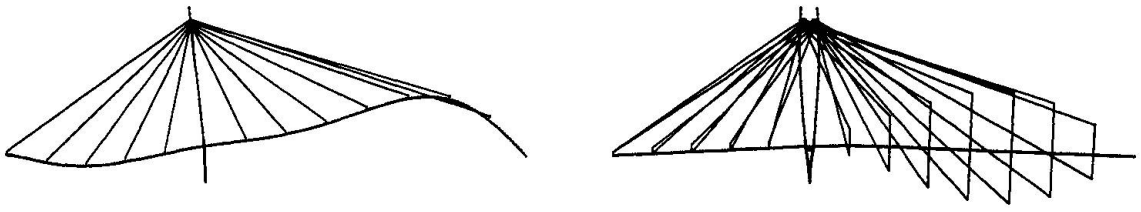

3D: f_h = 0.92 Hz 2D: f_h = 0.86 Hz 3D: f_α = 2.55 Hz 2D: f_α = 1.17 Hz

Fig. 2 Lowest vertical and torsion modes and frequencies obtained from 3D and 2D analysis

The main element of the DVMFLOW models developed for the three cross sections (A, B, C) investigated reproduced the external contour of the girders and featured approximately 200 vortex panels. The 50% perforated plate wind screens were modelled as assemblies of three equidistant spaced rectangles comprising 30 vortex panels each, covering a total of 50% of the frontal area of the wind screens. The circular hand rail was modelled by a ring assembly of 40 vortex panels. Aerodynamic derivatives computed for each of the cross sections by means of the forced oscillation technique, Larsen [5]. In case of cross sections A and B, the results revealed a change in sign (from - to +) of the A_2^* derivative at increasing non-dimensional wind speeds U/fB as shown in fig. 3. A behaviour indicating *one-degree-of-freedom* (1DOF) torsional flutter. The A_2^* and H_1^* derivatives of the C cross section displayed increasingly negative values at increasing non-dimensional wind speeds consistent with *two-degree-of-freedom* (2DOF) classical flutter.

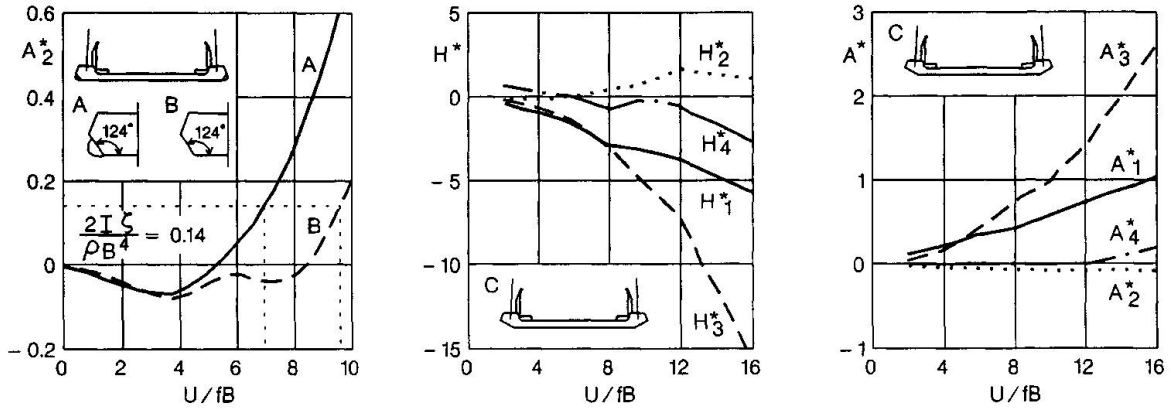

Fig. 3 Aerodynamic derivatives obtained from forced oscillation simulations of the flow about cross sections A, B and C.

Some insight into the flow conditions and cross section geometry responsible for the two flutter modes is offered in fig. 4. The flow about cross section A, which features a semi-circular edge profile, displays flow separation and formation of a vortex just downwind of the bottom plate / side panel joint. According to experience, Larsen [7], this type of vortex may create an aerodynamic moment which at a certain non-dimensional wind speed becomes in phase with structural twist of the girder thus amplifying the structural motion. This action is reflected in the change of sign of A_2^* at U/fB ≈ 5.2. In cross section B the semi-circular edge profile is removed securing a more smooth flow around the bottom plate / side panel joint. The separation vortex is still formed leading to a cross-over of A_2^*, but now at higher U/fB ≈ 9.5. The C cross section features a less steep bottom side panel as compared to cross section B. This detail prevents massive flow separation along the bottom plate and thus formation and drift of a large coherent vortex. The now "smooth" flow along the bottom plate is consistent with 2DOF flutter. Increase of the flutter wind speed is noted with increasing "streamlining" of the bottom portion of the cross section.

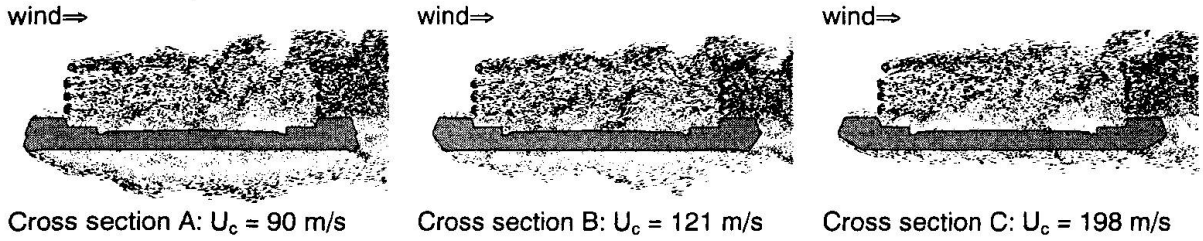

Fig. 4 Visualisation of the flow about cross sections A, B and C and corresponding wind speeds U_c for onset of flutter assuming a structural damping ζ = 0.5% re-to-crit.

3 Cable-Stayed Motorway Bridge

The E6 motorway running along the east coast of Sweden is expanded north of Gothenburg to connect the Øresund region to the Oslo region in Norway. At Uddevalla the E6 will be carried across the Sunningesund fjord by a 3 span cable-stayed bridge drafted by Vägverket, the Swedish National Road Administration. The bridge comprises a 400 m composite girder in the main span, flanked by two 120 m concrete side spans carried by four fans of stay-cables

anchored at the girder edges. Prior to tendering of the bridge COWI was entrusted with a computational aeroelastic analysis of two design alternatives involving plate (P) and closed box (B) section girders. The plate girder alternative incorporated two intermediate pier supports in the side spans (fig. 1) where as the box girder alternative featured three clear spans (no pier supports in the side spans) The analyses performed comprised a 3D structural analysis of the bridge and a 2D flow analysis for assessment of the influence of bridge girder cross section shape on the aeroelastic stability and buffeting response.

The structural dynamics effect of the girder / pier support configurations are demonstrated in fig. 5, which reproduces the lowest vertical and torsion mode shapes and eigenfrequencies of the bridge. It is noted that the torsion frequency of the box girder alternative is higher than the torsion frequency of the plate girder due to the increased torsion stiffness of the closed box compared to the open plate cross section. The vertical bending frequency of the box girder alternative is, however lower than the corresponding value of the plate girder bridge due to the absence of the intermediate piers in the side spans.

Fig. 5 Lowest vertical and torsion modes and frequencies obtained from 3D analysis of Plate girder (P) and box girder (B) alternatives. Modeshapes for Plate girder alternative shown.

The 2D aerodynamic analysis of the cross sections targeted the effect of cross section shape on the critical wind speed for onset of flutter U_c and the cross section drag coefficient C_D. In the case of the plate cross section P the results revealed a change of sign (from - to +) of the A_2^* derivative at increasing U/fB indicating 1DOF flutter. The A_2^* and H_1^* derivatives of the box cross section B displayed increasingly negative values at increasing U/fB, consistent with 2DOF classical flutter, fig. 6.

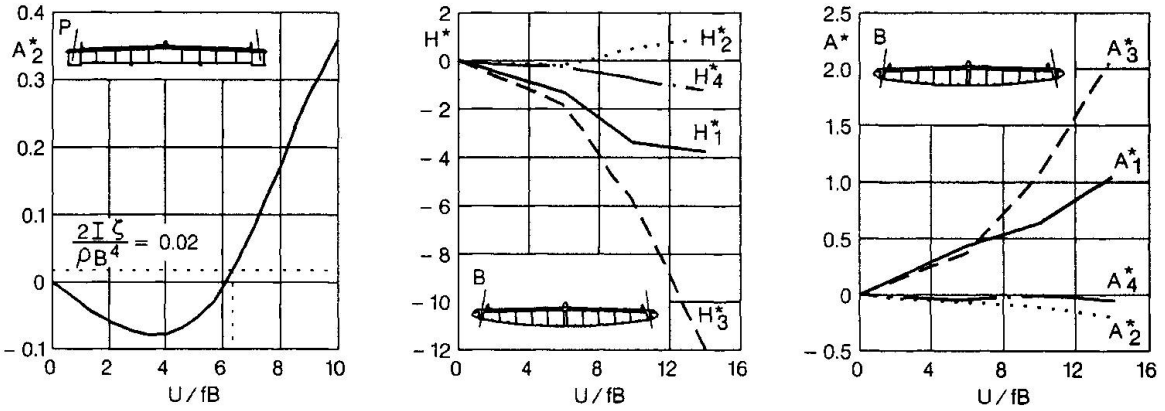

Fig. 6 Aerodynamic derivatives obtained from forced oscillation simulations of the flow about the plate and box cross sections alternatives for the Sunningesund bridge.

Fig. 7 offers a plot of the simulated flows and the predicted aerodynamic performance. The flow about the plate girder cross section forms large recirculating vortical structures below the

deck in the compartments between the edge girders and the longitudinals. In contrast the flow about the box girder cross section is smooth along the slightly curved bottom plate.

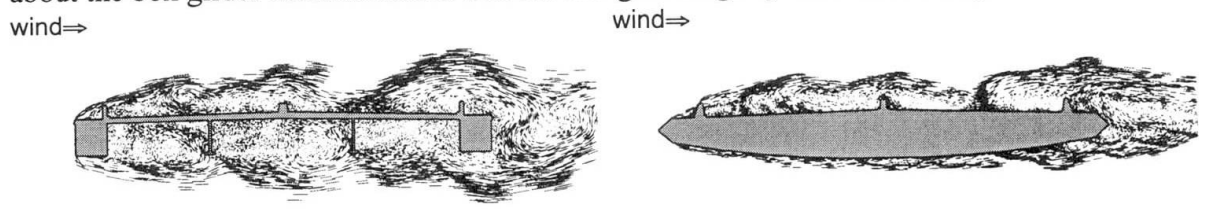

Cross section P: C_D = 0.12, U_c = 130 m/s Cross section B: C_D = 0.07, U_c = 210 m/s

Fig. 7 Visualisation of the flow about the plate and box cross sections. Drag coefficients C_D and flutter wind speeds U_c assuming a structural damping ζ = 0.5% rel-to-crit.

The differences in the respective flow fields carry over in the predicted aerodynamic properties. As in the previous example it is noted that increased "streamlining" of the cross section leads to better aerodynamic performance in terms a of higher flutter wind speed and a lower cross section drag coefficient. It should also be emphasised that the increased torsion stiffness of the box girder is beneficial for the aerodynamic stability.

4 Conclusion

A computer aided wind engineering system for analysis of long-span bridges is presented. This system allows the designer to explore the effect of cross section shape on aerodynamic performance of a given bridge structure without resorting to time consuming and costly wind tunnel tests. The cases discussed clearly demonstrate that the aerodynamic performance of a bridge may be significantly enhanced by "streamlining" of the bridge girder cross section. The importance of utilising a full three dimensional model for the structural dynamics input to aerodynamic analyses of long-span bridges is stressed.

5 References

[1] Larsen, A. and Walther, J.H.: A New Computational Method for Assessment of the Aeroelastic Stability of Long-Span Bridges, Proc. 15th IABSE Congress, Copenhagen, 1996

[2] Sørensen, K.A., Andersen, G.B and Jacobsen P.F.: Integrated Bridge Design and Analysis System. Proc. 13th IABSE Congress, Helsinki, 1988.

[3] Simiu, E. and Scanlan, R.H.: *Wind Effects on Structures*, 2. ed., Wiley Interscience, New York, 1986.

[4] Walther, J.H. and Larsen, A.: Two Dimensional Discrete Vortex Method for Application to Bluff Body Aerodynamics. Journal of Wind Engineering and Industrial Aerodynamics, vol. 67-68, pp 183-194, 1997.

[5] Larsen, A.: Computer Simulation of Wind-Structure Interaction in Bridge Aerodynamics, Structural Engineering International, Vol. 2, 1998.

[6] Walter, R., Houriet, B. et al. : *Ponts Haubané*, Presses Polytechniques Romandes, 1985.

[7] Larsen, A.: Aeroelastic Instability of an H-shaped Cross Section, Proc. ASCE Engineering Mechanics Conference, La Jolla, 1998.

Aerodynamic Instability of Long-Span Cable-Stayed Bridges

Domenico BRUNO
Prof.
Univ. of Calabria
Cosenza, Italy

Domenico Bruno, born 1949, received his Civil Eng. degree at the Univ. of Naples. Prof. of Structural Mechanics at Univ. of Calabria, presently carrying out research on mechanics of composite structures and problems in structural mechanics.

Angelo LEONARDI
Assoc. Prof.
Univ. Roma Tor Vergata
Roma, Italy

Angelo Leonardi, born 1945, received his chemical engineering degree at the Univ. of Naples. Associate Prof. of Structural Eng. at Univ. of Rome, presently carrying out research on computerised structural analysis.

Summary

In this paper an analysis of the aerodynamic behaviour of fan-shaped long span cable-stayed bridges under nonstationary aerodynamic loads is developed. A numerical analysis is carried out, based upon time integration of the motion equations of the discretized structure. The main structural nonlinearity arising from the elastic response of stay is accounted for together with the nonlinear effects related to the assumed nonstationary model of the aerodynamic loads. Moreover, a continuous model of the bridge based on the hypothesis of a small spacing between stays is developed, whose analytical results are usefully compared to numerical ones.

1. Introduction

As is well known the cable-stayed bridge scheme evoked great interest as a valid solution for long spans, particularly regarding the so-called fan-shaped scheme of the self-anchored type.
The structural behaviour of this scheme is marked by a dominant state of axial tensions in the stays and of axial compression in the girder, while less important is the bending stress as a result of the prevailing truss behaviour of the scheme.
Moreover, in long-span bridges the analysis of the dynamic behaviour is the most important one. The influence of moving loads, the precence of seismic forces and the influence of aerodynamic effects must be carefully examined; in fact, the more dangerous stresses and deformations are related to these kinds of external action. Therefore, the fan shaped cable-stayed bridge scheme, suitable for long spans, requires an accurate analysis of the aerodynamic instabilities.
In this paper an anlysis of the dynamic instability of long-span cable-stayed bridges under non stationary aeodynamic loads is developed by using both a discrete model of the bridge and a continuous one based on the assumption of small spacing between stays. The intrinsic nonlinearity arising from Dischinger constitutive equation is taken into account together with the nonlinear effects arising from the deformation dependent nonstationary aerodynamic forces.The analysis is developed at first by analyzing the flexural and torsional oscillations of the bridge. Then, the critical wind speed, both in the case of flutter and stall flutter is investigated.

2. The structural model of the bridge

The fan-shaped scheme of cable-stayed bridge of Fig.1 is considered, in which the girder is simply supported at its ends and is hung to the tops of H-shaped towers by means of two stays curtains.
It is assumed that the stays spacing Δ, the girder width 2c and the stay curtain interval 2b are small quantities compared to the central span length L_c. The aspect ratios $r_1=L_c/H$; $r_2=L_s/H$ of span legths to the tower height are usually obtained on the basis of economy and of the anchor cable stability condition.
The longitudinal vertical plane *yz* is assumed to be a symmetrical one; in addition, the bridge is also symmetrical with respect to the midspan cross plane.
According to the usual erection procedures, girder and towers are assumed to be free from bending under dead load g. Then, the cross sectional areas A_S and A_O of the couple of diffused stays and of the anchor stays, respectively, are given by

$$A_s = \frac{g\Delta}{\sigma_g \sin\alpha}; \qquad A_0 = \frac{gL_s}{2\sigma_{g_0}}[1+(\frac{L_s}{H})^2]^{1/2}[(\frac{L_c}{2L_s})^2 - 1] \tag{1}$$

where

$$\sigma_g = \sigma_a \frac{g}{p+g}; \qquad \sigma_{g_0} = \sigma_a \left\{1 + \frac{p}{g}[1-(\frac{2L_s}{L_c})^2]^{-1}\right\}^{-1} \tag{2}$$

and where σ_a is the allowable stress, α is the angle between a stay and its horizontal projection, and p denotes the live load.
We assume that towers and girder's axial elongations are negligible, and we apply the Euler-Bernoulli bending theory and the Saint-Venant torsion theory for the girder.
As far as the stays behaviour is concerned, the Dischinger modulus $E_s^*=E/(1+\gamma^2 l_0^2\, E/12\sigma_0^3)$ is used, where E is the Young modulus, γ is the specific weight, l_0 is the horizontal projection length of the stay and σ_0 is the initial tension. The tower is characterized by the flexural stiffness k_T.

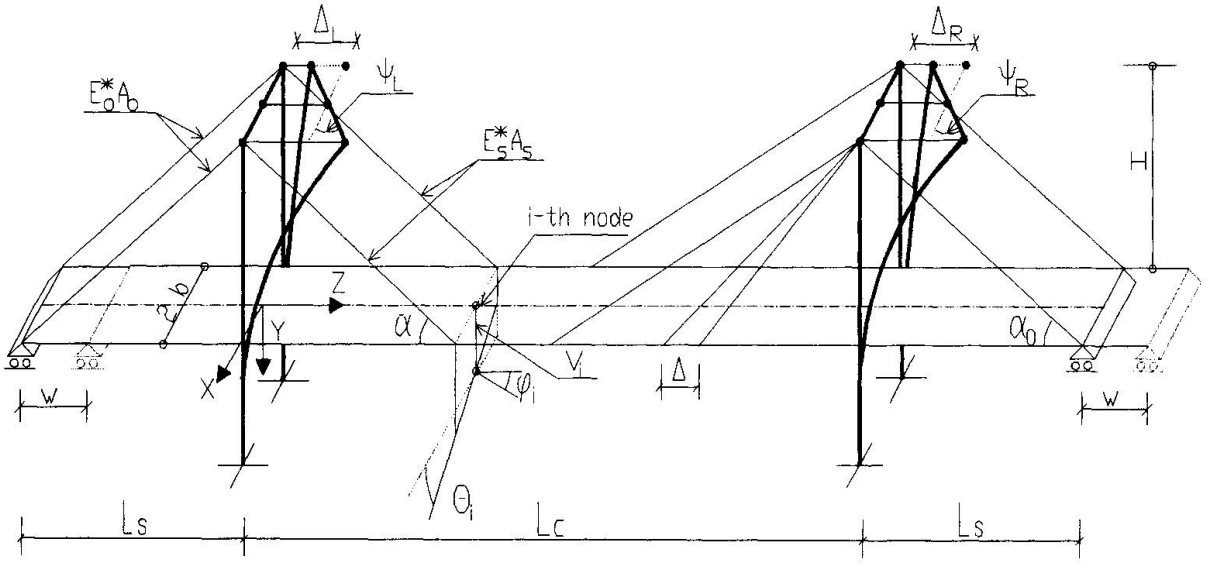

Fig.1. Cable stayed bridge scheme

At first we develop a discrete model of the bridge based on a finite element discretization of the girder by using hermitian cubic interpolation functions for transverse deflection and linear interpolation functions for torsional deformation.
Therefore, for the H-shaped towers scheme (Fig.1), the deformation of the bridge can be described by the following displacement parameters:
- the axial displacement w of the girder;
- the axial displacements Δ_L, Δ_R and the torsional rotations Ψ_L, Ψ_R around the vertical axis of the towers tops;- at each internal node i of the girder, where a couple of stays act on the girder:
  -the vertical deflection v_i;

-the torsional rotation θ_i;
-theflexural rotation φ_i around the x-axis.

Now the air forces acting on the bridge are considered. To give an accurate analysis of the aeroelastic behaviour of the bridge, a sound evaluation of the aerodynamic loads must be used.
It is widely accepted that the nonstationary formulation is the most adequate one for predicting the aeroelastic behaviour of the girder with good accuracy. Moreover, to obtain simple formulas we refer to the simple thin airfoil theory.
According to these assumptions the aerodynamic lift l and torque m per unit length acting on the cross section of the bridge in a laminar approaching flow with zero mean angle of attack can be expressed by:

$$l = \frac{1}{2}\rho V_0^2(2c)[kH_1^* \frac{\dot{v}}{V_0} + kH_2^* c\frac{\dot{\theta}}{V_0} + k^2 H_3^* \theta] \tag{3}$$

$$m = \frac{1}{2}\rho V_0^2(2c^2)[kA_1^* \frac{\dot{v}}{V_0} + kA_2^* c\frac{\dot{\theta}}{V_0} + k^2 A_3^* \theta] \tag{4}$$

where :
-V_0 is the approaching wind speed;
-ρ is the air density;
- $k = c\omega / v_0$ is the reduced frequency, where ω is the frequency of the oscillating bridge deck.
-H_i^*, A_i^* are the nondimensional Theodorsen aerodynamic coefficients, given in real notation, according to Scanlan, by:

$$\begin{cases} kH_1^* = -2\pi F \\ kH_2^* = -\pi(1 + F + \frac{2G}{k}) \\ k^2 H_3^* = -2\pi(F - \frac{kG}{2}) \end{cases} \qquad \begin{cases} kA_1^* = \pi F \\ kA_2^* = -\frac{\pi}{2}(1 - F - \frac{2G}{k}) \\ k^2 A_3^* = \pi(F - \frac{kG}{2}) \end{cases} \tag{5}$$

Then, the dynamical equilibrium equations of the discrete structure can be put in the following matrix form:

$$\mathbf{M}\ddot{\mathbf{s}} + \mathbf{K}(\mathbf{s})\mathbf{s} = \mathbf{F}(\mathbf{s},\dot{\mathbf{s}},t) \tag{6}$$

where **M** is the mass matrix, **s** is the displacement vector and **F** is the external load vector.
The above nonlinear problem was solved numerically by using the Newmark integration scheme. Moreover an algorithm based on the predictor-corrector method was used.
It must be observed that forces **F** depend on the reduced frequency k, that is on the deck oscillation ω. Due to the low sensitivity of the aerodynamic forces with respect to the variation of ω, k is updated only after one cycle of the midspan deflection (for the evaluation of l) or of the midspan torsional rotation (for the evaluation of m). The updated value of ω is then obtained from the wavelength of the corresponding oscillation. This procedure, when t tends to infinity, gives the flexural ω_v and torsional ω_θ frequencies converging to the unique critical value ω_c when V_o tends to its critical value V_c.
To determine the critical wind speed, integration stats with zero speed. Moreover, the initial conditions at time t=0 are choosen as the first flexural and the first torsional eigenmodes.
After some oscillation cycles, an increment is given to the wind speed, and integration stats up again assuming as initial conditions and as ω value, the final displacements, velocities, and ω values of the previous wind-speed step. The computation goes on step by step by means of wind-speed increments, and at each step w is updated as previously discussed and when ω convergence is reached, the motion character (damped or undamped) is estimated in order to determine the critical condition.
Now a continuous model of the bridge is employed to obtain simple formulas able to capture the main features of the bridge behaviour [1,2].This model is founded on the assumption that the spacing Δ is very small compared to the main span length L_c; this allows the development of a continuous structural model assuming a continuous distribution of stays along the deck. In this case, for

symmetrical motions with respect to midspan, the deformation of the girder is described by the flexural v(z) and torsional θ(z) displacement functions, respectively, together with the scalar displacement parameters $\Delta_L=-\Delta_R$, $\Psi=\Psi_L=-\Psi_R$ with w=0.
To give analytical developments, the following quantities are introduced:

$$\xi=\frac{z}{H};V(\xi,t)=\frac{v(z,t)}{H};U(t)=\frac{u(t)}{H};\varphi(\xi)=\frac{1}{(1+a\xi^2)(1+\xi^2)} \tag{7}$$

$$a=\frac{\gamma^2H^2E}{12\sigma_g^3};\frac{\varepsilon^4}{4}=\frac{I\sigma_g}{H^3g};\tau^2=\frac{C_t\sigma_g}{Eb^2H_g};M=\frac{\mu H\sigma_g}{Eg};J_0=\frac{I_0H\sigma_g}{b^2Eg} \tag{8}$$

$$\chi=\frac{k^T\sigma_g}{Eg};\chi_0=\frac{E_0^*A_0}{E}\frac{\sigma_g}{gH}\sin\alpha_0\cos^2\alpha_0;\rho=\int_L\frac{\cos^2\alpha}{1+a\xi^2}d\xi+\chi_0 \tag{9}$$

where:
- μ is the mass per unit length of the girder;
- I, I_o, C_t are the flexural inertia, the polar moment of inertia of mass and the torsional rigidity factor of the girder cross section

In practical cases the nondimensional flexural ε and torsional τ stiffness parameters are very small (ε≤0.3, τ≤0.1). This corresponds to a prevailing truss behaviour of the bridge in which girder's bending and torsion are of local nature, while axial forces and overall displacements are well defined on the truss bridge scheme(ε=τ=0). This enables terms in ε and τ to be disregarded with respect to others in the equilibrium equations.
With these assumptions the dynamic equilibrium equations for the continuous model are:

$$\begin{cases}\varphi V-\xi\varphi U=-M\ddot{V}+Q_1\theta+Q_2\dot{\theta}+Q_3\dot{V}\\ -(\rho+\chi)U+\int_L\xi\varphi V d\xi=0\\ -\varphi\theta+\xi\varphi\psi=J_0\ddot{\theta}-\mu_1\theta-\mu_2\dot{\theta}-\mu_3\dot{V}\\ \psi=\frac{1}{\rho+\chi}\int_L\xi\varphi\theta d\xi\end{cases} \tag{10}$$

with

$$\begin{cases}Q_1=\frac{1}{2}\rho V_0^2(2c)k^2H_3^*\frac{\sigma_g}{Eg}\\ Q_2=\frac{1}{2}\rho V_0^2(2c)kH_2^*\frac{c}{V_0}\frac{\sigma_g}{Eg}\\ Q_3=\frac{1}{2}\rho V_0^2(2c)kH_1^*\frac{1}{V_0}\frac{\sigma_gH}{Eg}\end{cases},\qquad \begin{cases}\mu_1=\frac{1}{2}\rho V_0^2(2c^2)k^2A_3^*\frac{H\sigma_g}{Egb^2}\\ \mu_2=\frac{1}{2}\rho V_0^2(2c^2)kA_2^*\frac{c}{V_0^2}\frac{H\sigma_g}{Egb^2}\\ \mu_3=\frac{1}{2}\rho V_0^2(2c^2)kA_1^*\frac{1}{V_0}\frac{H^2\sigma_g}{Egb^2}\end{cases} \tag{11}$$

The aerodynamic instability and the corresponding critical wind speed can be obtained by putting the solution of eqn (10) in the form:

$$V(\xi,t)=\bar{V}(\xi)e^{st};U(t)=\bar{U}e^{st};\theta(\xi,t)=\bar{\theta}(\xi)e^{st};\psi(t)=\bar{\psi}e^{st} \tag{12}$$

where a purely immaginary value of $s=\alpha+i\omega$ corresponds to flutter.
Substituting eqn (12) in (10) a linear homogeneous system in the time independent displacement variables introduced in (12) is obtained; putting its determinant equal to zero and disregarding less relevant terms, the following frequency equation is obtained:

$$\sigma^4+\sigma^3\beta\Omega\frac{\pi}{k}(2F+\gamma G_1)+\sigma^2(1+\varphi^2-\beta\gamma\Omega^2G_2+\beta^2\gamma\Omega^2G_3)+$$

$$\sigma\beta\Omega\frac{\pi}{k}(2\varphi^2 F+\gamma G_1)+(\varphi^2-\beta\gamma\Omega^2 G_2)=0 \tag{13}$$

with

$$\beta=\frac{\rho c^2}{\mu};\qquad \gamma=\frac{\mu c^2}{I_0};\qquad \varphi=\frac{\omega_{0\theta}}{\omega_{0v}};\qquad \Omega=\frac{\omega}{\omega_{0v}};\qquad \sigma=\frac{s}{\omega_{0v}} \tag{14}$$

$$G_1(k)=\frac{1}{2}(1-F-2\frac{G}{k})\qquad G_2(k)=\frac{\pi}{k^2}(F-\frac{kG}{2});\qquad G_3(k)=\frac{2\pi^2}{k^2}F; \tag{15}$$

where ω_{ov} and $\omega_{o\theta}$ denote the flexural and torsional free oscillation frequencies in still air [2].
The flutter condition is formulated by putting $s=i\Omega_c$ in eqn (13). We obtain the flutter condition:

$$\Omega_c^4(-G_1+2F\beta G_2-2F\beta^2 G_3)+\Omega_c^2(2G_1-2F\beta G_2)-G_1=0 \tag{16}$$

and

$$\varphi^2=\frac{\Omega_c^2(2F+\gamma G_1)-\gamma G_1}{2F}, \tag{17}$$

and the critical wind speed is given by the relation : $(V_c/c\omega_{ov})^2=(\Omega_c/k_c)^2$
Now, the single degree of freedom torsional mode of flutter of stalled airfoils is considered. In this case, according to the Ragget theory, the aerodynamic moment can be expressed by:

$$m=\frac{1}{2}\rho V_0^2(2c^2)[k\bar{A}_2^*c\frac{\dot{\theta}}{V_0}+k^2\bar{A}_3^*\theta] \tag{18}$$

with

$$k\bar{A}_2^*=-\frac{S_m}{2}(\frac{\pi}{S_m}-F_m-2\frac{G_m}{k})\qquad k\bar{A}_3^*=S_m(\frac{F_m}{k}-\frac{G_m}{2}) \tag{19}$$

$$F_m(k)=1+\frac{\frac{\pi}{S_m}-1}{1+\left(\frac{0.3}{k}\right)^2}-\frac{\frac{\pi}{S_m}}{1+\left(\frac{3}{k}\right)^2}\qquad G_m(k)=\frac{\frac{0.3}{k}(\frac{\pi}{S_m}-1)}{1+\left(\frac{0.3}{k}\right)^2}-\frac{\frac{3}{k}\frac{\pi}{S_m}}{1+\left(\frac{3}{k}\right)^2} \tag{20}$$

where S_m is the slope of the steady state moment versus angle of attack, approching π as the angle of attack vanishes. In this case dynamical equilibrium equations (10) can be rewritten accounting only for the torsional displacement and force parameters. After some algebra we get the following frequency equation for stall flutter:

$$\sigma^2+\Gamma_1\Omega\sigma+(1-\Gamma_2\Omega^2)=0 \tag{21}$$

where

$$\beta=\rho c^2,\ \gamma=\frac{c^2}{I_0},\ \Omega=\frac{\omega}{\omega_{0\theta}},\ \sigma=\frac{s}{\omega_{0\theta}},\quad \Gamma_1=\frac{\beta\gamma}{k}\frac{S_m}{2}(\frac{\pi}{S_m}-F_m-2\frac{G_m}{k});\ \Gamma_2=\frac{\beta\gamma}{k^2}S_m(F_m-k\frac{G_m}{2})$$

The flutter condition : $s=i\Omega_c$ in this case gives

$$\frac{\pi}{S_m}-F_m-2\frac{G_m}{k_c}=0;\qquad \Omega_C^2=\frac{1}{1+\frac{\beta\gamma}{k^2}S_m(F_m-\frac{k_cG_m}{2})} \tag{22}$$

and after some algebra

$$S_m=\pi\left\{1-\frac{3}{17}\frac{[1+(0.3/k_c)^2][(1+2/3(3/k_c)^2]}{[1+(3/k_c)^2][0.3/k_c]^2}\right\};\Omega_c^2=\left\{1+\frac{15}{17}\pi\frac{[(3/k_c)^2+3/2][(3/k_c)^2-2]}{[(3/k_c)^2+1][3/k_c]^2}\frac{\beta\gamma}{k_c^2}\right\}^{-1}$$

and the critical wind speed is given by the relation : $(V_c/c\omega_{o\theta})^2=(\Omega_c/k_c)^2$.

3. Numerical results and concluding remarks

Here we analyze a bridge scheme characterized by the following parameters:
r_1=5; r_2=5/3; L_c=750m; L_s=250m; H=150m; Δ=25m; b=c=17m; I=11.69m^4; I_0=918,378t_mm k_T=2350t/m; μ=4.8t_m/m; g=47t/m; p=28t/m; E=21x10^{6}t/m^2; σ_a=72x10^{3}t/m^2; ε=0.3; τ=0.2.

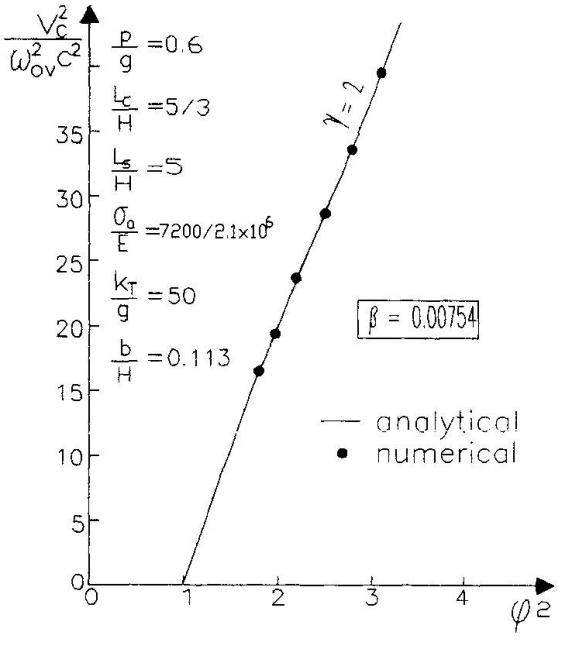

Fig.2: Critical wind speed versus frequency ratio φ.

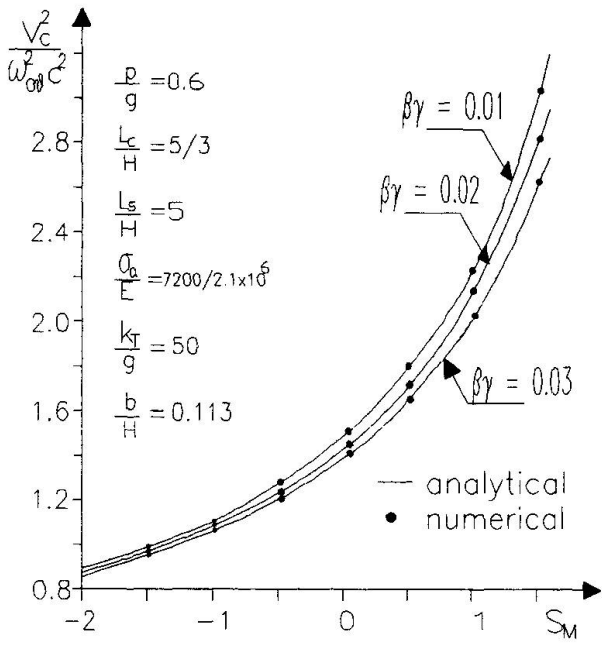

Fig.3: Critical wind speed versus slope S_M

In Fig.2 the flutter critical wind speed V_c is plotted versus the frequency ratio parameter φ; it can be observed that for φ=$\omega_{0v}/\omega_{0\theta}$=1, any wind speed is critical. In addition, a very high sensitivity of the bridge aerodynamic behaviour emerges with respect to variations of φ. In Fig.3 the torsional mode of flutter of a stalled airfoil is examined; in particular, the critical wind speed V_c is plotted versus the slope S_M of the steady state moment-angle of attack. It can be observed that the effect of the mass coefficients β and γ is very small and become practically negligible for negative values of S_M. Moreover, the numerical results obtained by the discrete model of the bridge well agree with the analytical ones obtained by the continuous model of the bridge.
In conclusion, the two models here established, that is the discrete model of the bridge and the continuous one, seem to work in a good agreement. Moreover, it can be observed that the discrete model allows us to analyze more complex situations, where the continuous theory is hard to apply, that is, for instance, non constant cross section of the girder, variable live loads, nonlinearities of stays. However, the continuous model seems to be capable of capturing the main features of the dynamical bridge behaviour,which is a useful tool to validate numerical results obtained by FEM computer codes.

References

1. Bruno D., Leonardi A., Maceri F., On the Nonlinear Dynamics of Cable-Stayed Bridges, *Cabridge 87*, Bangkok, 1987.
2. Bruno D., Leonardi A, Natural Periods of Long-Span Cable-Stayed Bridges, *Jou. of Bridge Engineering, ASCE*, Vol.2, N.3,1997.
3. Simiu E., Scanlan R.H., *Wind Effects on Structures*, John Wiley & Sons, N.Y., 1986.
4. J.D. Ragget, R.H. Scanlan, *ASCE Nat. Struct. Eng. Mtg.*, Baltimore, 1971
5. T. Theodorsen, General Theory of Aerodynamic instability and the Mechanism of Flutter, *NACA Techn. Rep.* N. 496, 1934.

Steel and Hybrid Stress-Ribbon Pedestrian Bridges

Takeshi YOSHIMURA
Prof. Dr
Kyushu Sangyo Univ.
Fukuoka, Japan

Won-Ho KANG
Prof. Dr
Dong-A Univ.
Pusan, Korea

Mitsuo OKADO
Chief Director
New Structural Eng., Inc.
Tokyo, Japan

Yoji MIZUTA
Prof. Dr
Kyushu Sangyo Univ.
Fukuoka, Japan

Hideo JO
Chief Director
Structural Eng. Center, Inc.
Fukuoka, Japan

Akiharu MIYAKE
Prof.
Ariake Nat. College of Techn.
Fukuoka, Japan

Summary

Not only the deck weight but also the sag ratio should be reduced in order that the type of stress-ribbon may be applicable to roadway bridges. The deck weight of the proposed steel stress-ribbon bridge could be reduced up to one-tenth of the conventional concrete stress-ribbon bridges. In another proposed hybrid structure, half of the inner cables inside this steel deck are stretched outside and lifted up over the decks close to the abutments and supported by low towers. The side decks are lifted up horizontally by introducing the pre-tension force in the hangers suspended by the outer cables. Thus, this 'stress-ribbon suspension bridge' type construction allows for a reduction in the deck sag as well an increase in the sag of about half of the cables remarkably yielding a remarkable reduction in the horizontal component of the tensile force in them.

1. Introduction

Many pre-stressed concrete stress-ribbon pedestrian bridges have been constructed since the 1980's mainly in the parks and the golf courses in Japan. Recently, one of the authors had a chance to conduct wind tunnel tests at Kyushu Sangyo Univ. (KSU) for examining the aerodynamic stability of concrete stress-ribbon pedestrian bridges with special reference to the Jomon Bridge shown in Fig. 1. It was found there that the half-circular cylindrical fairings and the similar edge modifications, Figs. 1(c)-1(e), are quite effective for increasing the stability, and the fairings have been attached to the actual bridge [1, 2]. Although the stress-ribbon concept in concrete has the advantage of utilizing the inner cables for pre-stressing the deck as well, there is no reason for the deck to be fabricated of heavy concrete as pointed out by Wheen & Wilson in the 1970's [3, 4]. The concrete deck could be replaced with much lighter steel construction.

To reduce the horizontal component of the extremely large tensile force in the cables, H_w, it is necessary to reduce the total deck weight, $W=wL$, as well as to 'increase' the sag ratio, f/L, as H_w is proportional to both W and the inverse of f/L. The previously proposed steel structure allows for a reduction in W up to one-fourth of that of conventional concrete stress-ribbon bridges [5]. However, f/L should also be 'reduced' in order that this type of structure, as the succeeding phases of this study, may be applicable to roadway bridges, since the bridge design code in Japan stipulates their maximum gradient should be 5 %, much smaller than that of 12 % for pedestrian bridges. Therefore, alternative structures should be invented for this application .

Based on these consideration, further study has been made to propose a new type of hybrid bridge together with an improved, much lighter steel stress-ribbon bridge with highly aerodynamic stability. The characteristics of non-linear cable sag change from the stage of cable erection throughout that after completion were also examined by a numerical analysis using a proposed method. The results obtained in a collaboration between Japan and Korea are reported below.

2. Pedestrian bridges treated as full scale models of roadway bridges

Hirai & Ito showed that the numerical values of non-dimensional parameter $C_{0L} = L\sqrt{H_w/(EI)}$ vs. L for various roadway suspension bridges are bounded by two lines: $C_{0L} = 0.011L$ and $C_{0L} = 0.019L$ (Eq. 2.1) [6], where EI is the bending stiffness. Substitution of C_{0L} =12 for the Nagashima Storage Dam Bridge [7], a steel suspension bridge for pedestrians with L = 160 m, into Eq. 2.1 gives L = 600 and 1100, and C_{0L} = 22 for the previously proposed steel stress-ribbon pedestrian bridge L = 1100 and 2000 m. These two examples suggest that the mechanical characteristics of pedestrian bridges with medium-span length are expected to be similar to those of roadway bridges with much longer-span length. Therefore, suspended pedestrian bridges could be treated as the full scale models for roadway bridges in a sense.

Roughly speaking, there is not too much difference between the reduced mass and the reduced mass moment of inertia of the bridge decks, μ and ν, for pedestrian and roadway bridges of suspended type. For example, $\mu \fallingdotseq 20$ and $\nu \fallingdotseq 3$ for suspension bridges of the Yunouchi Pedestrian (L = 69 m) and the Kanmon Roadway (L = 712 m); $\mu \fallingdotseq 200$ and $\nu \fallingdotseq 20$ for concrete cable-stayed bridges of the Naruse Pedestrian [8] and the Yobuko Roadway [9]. Since the logarithmic decrement, δ, is assumed to be 0.02 or 0.03 for both kinds of bridges in the wind resistant design in Japan, pedestrian bridges could be treated as the aeroelastic full scale models of corresponding roadway bridges in cases where *Re* (Reynolds number) effects on their response are not important.

The wind speed scale of a pedestrian bridge to the corresponding roadway bridge, $\lambda_V = V_P/V_R$, is rewritten as $\lambda_V = \lambda_L/\lambda_T = \lambda_L\lambda_F$ (Eq. 2.2), where suffices 'P' and 'R' pedestrian and roadway; λ_L, λ_T and λ_F denote the scales of the length, the time and the frequency, respectively. Since the lowest natural frequencies in both vertical bending and torsion of these bridges are nearly proportional to $1/L$, $\lambda_F \fallingdotseq 1/\lambda_L$ (Eq. 2.3) which differs from $\lambda_F = 1/\sqrt{\lambda_L}$ in the Frude number simulation. Substitution of Eq. 2.3 into Eq. 2.2 gives $\lambda_V \fallingdotseq 1$, which provides us very important knowledge: The critical wind speed of the aerodynamic instabilities of a pedestrian bridge, the aeroelastic full scale model for vehicles, is nearly equal to that for the full scale bridge itself!

3. Simulation of super-critical *Re* flow in wind tunnel model tests

The significant knowledge obtained in the Jomon Bridge model tests was: Greatly increase in the critical flutter speed V_F as well as suppressing vortex excitation for the deck with the fairing and the similar modified edge, Figs. 1(c)-1(e); Importance of *Re* effects on V_F for the round-shape decks, i.e., the importance of the simulation of the super-critical *Re* flow on the actual bridges in the model tests. *Re* at the design speed for the actual bridges is far above the critical *Re* where the boundary layer transition from laminar to turbulent flow should take place on the round-shape deck. It is expected that the separation bubbles may be hardly formed on the deck, Fig. 2(b), as the turbulent boundary layer separates from the cylinder surface at the angle of about 130°, Fig. 2(a). Also the super-critical *Re* flow on the smooth-surfaced modified edge on the actual bridges can be almost simulated in model tests in the range of *Re* of the order of 10^4 by attaching a pair of trip-wires, Fig. 2(d). Since the critical *Re* for a smooth-surfaced circular cylinder with the wires, Fig. 2(c), depends on their diameter and location, the optimum wires were used in the Jomon and the succeeding model tests referring the experimentally obtained *Re*-C_D curves shown in Fig. 3.

4. Previously proposed and improved, much lighter steel bridges

As described in section 3, the half-circular edge modification for concrete decks, Fig. 1(d), is quite effective for increasing their aerodynamic stability. Based on this study, similar cross-sectional configuration is formed for the previously proposed steel structure shown in Fig. 4(a). The bridge is composed of inner cables, a pair of circular steel pipes, cross beams, a concrete slab and a decoration panel. The most important idea of this proposal following the study by Wheen & Wilson is that the pipes are also pre-stressed by pre-tension force in themselves, and therefore, partially play an important role in suspending the deck weight and the loads.

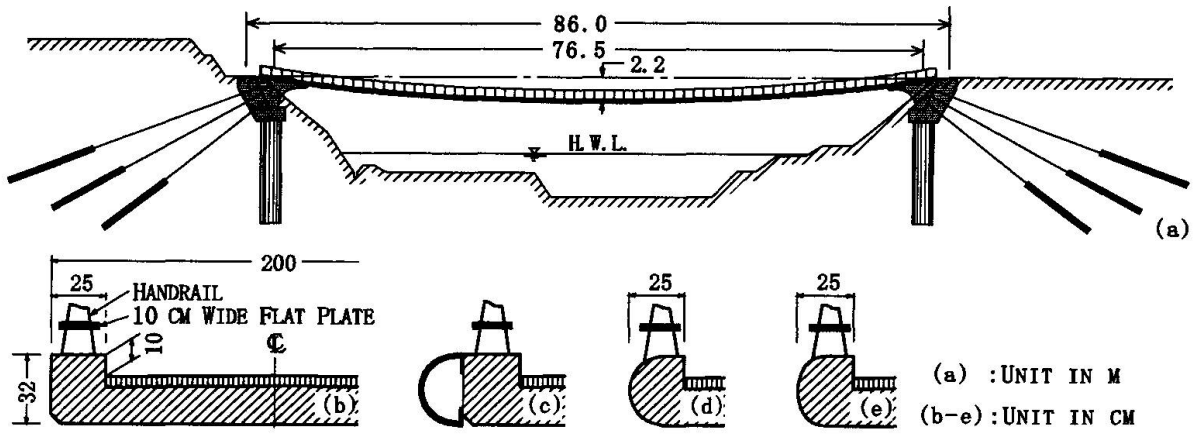

Fig.1 The Jomon Bridge. The elevation (a); the original cross-section with and without the half-circular fairings (b, c); the modified ones with the half-circular and the half-elliptic edges (d, e).

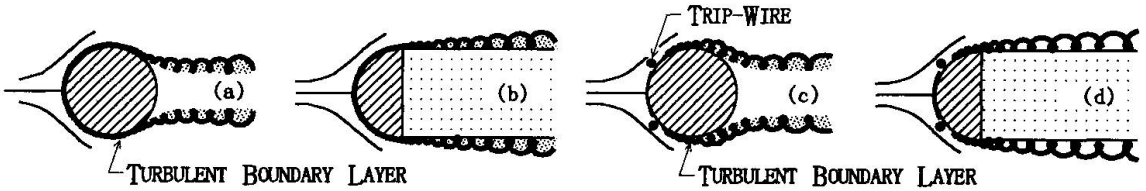

Fig.2 Super-critical *Re* flow on a circular cylinder and the modified edge on the full scale structures (a, b) and simulated flow on the wind tunnel models by attaching a pair of trip-wires (c, d).

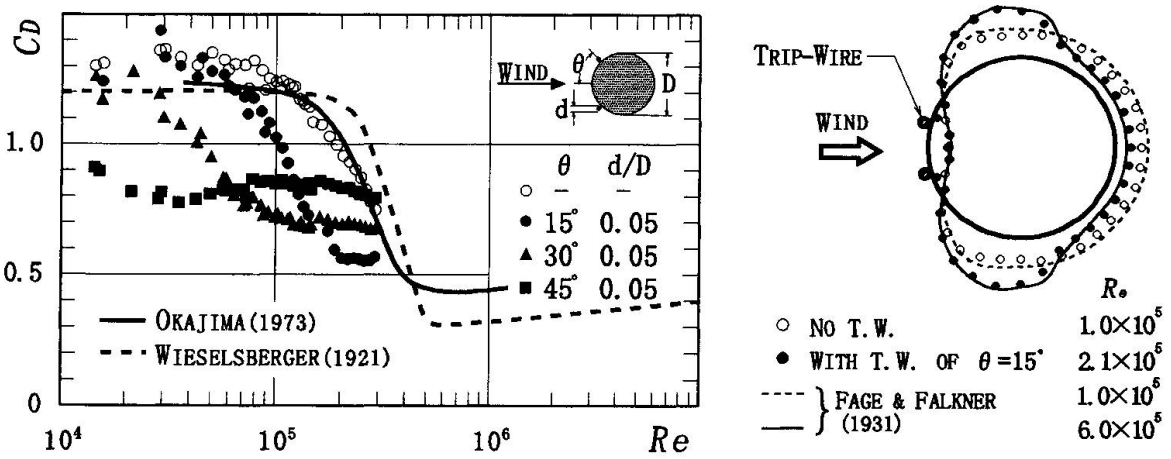

Fig.3 C_D vs. *Re* curves and the mean surface pressure distributions for a smooth-surfaced circular cylinder with and without a pair of trip-wires.

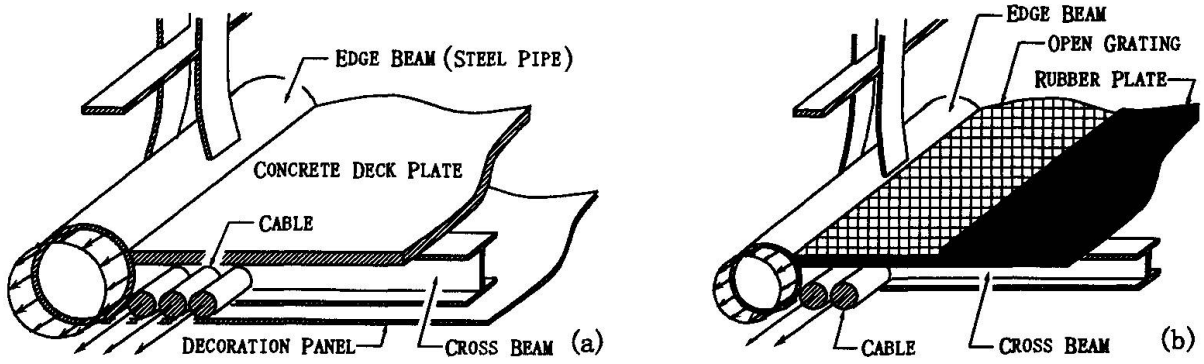

Fig.4 Cross-sections of the previously proposed steel structure (a), and the improved lighter steel one (b).

However, in the study of the Nagashima Storage Dam Bridge, which has a similar deck to that shown in Fig. 4(b), the deck was found to be quite aerodynamically stable. Although the stability depends on the width of the open gratings, its non-dimensional critical flutter speed is high enough, around 10, and the aerodynamic exciting force for vortex excitation is small, in the range of allowable value. This valuable experience is applied to the improved design presented in Fig. 4(b). The heavy concrete slab in Fig. 4(a) is replaced with a lighter steel open grating partially covered with a hard rubber plate. Moreover, the steel pipe diameter of 40 cm in Fig. 4(a) is reduced to 20 cm and the bottom decoration panel is removed. It can be easily understand that the deck weight of the improved structure could be reduced to about half of the previously proposed structure, i.e., up to about one-tenth of the conventional concrete structures.

5. Proposal of hybrid structures applicable to roadway bridges

As described in Section 1, not only the total deck weight W but also the sag ratio f/L should be reduced in order that the type of stress-ribbon may be applicable to roadway bridges. The alternative proposed hybrid structure shown in Fig. 5 provides a good solution for these problems. The original structure in Fig. 5(a) is a conventional concrete stress-ribbon bridge. However, the central portion of the deck is replaced with improved lighter steel stress-ribbon, Figs. 4(b) and 5(b). Moreover, about a half of the 'inner cables' inside the steel deck are stretched outside at the steel deck ends as shown in Fig. 6, and lifted up over the concrete decks close to the abutments. These 'outer cables' are supported by newly installed low concrete towers for increase in their sag remarkably yielding a remarkable reduction in H_W. The concrete decks are suspended by the outer cables and lifted up horizontally by introducing the pre-tension force in the hangers. Therefore, the partial introduction of the outer cable system with the low towers allows for a 'reduction' in the deck sag as well as an 'increase' in the sag of about half of the cables remarkably. In this 'stress-ribbon suspension bridge', the side concrete decks could be replaced with the same central steel deck, and another full-steel hybrid structure can be invented.

6. Non-linear cable deflection analyzed by proposed method

It is well-known that under the condition of $p \ll w$, the cable slope change $d\varphi$ in Fig. 7 and the contribution of the 4th-6th terms of the secondary order in Eq. 6.2 can be neglected,

$$\int_0^L d\zeta = 0 \qquad \text{....(6.1)}$$

$$d\zeta = \frac{(H_W + H_P)\sec(\phi + d\phi)}{(E_C A_C + EA)} \sec^2 \phi dx + \gamma t \sec^2 \phi dx - \frac{dy}{dx}\frac{d\eta}{dx} + \frac{1}{2}\left[\frac{(H_W + H_P)\sec(\phi + d\phi)}{(E_C A_C + EA)}\right]^2 \sec^2 \phi dx - \frac{1}{2}\left(\frac{d\eta}{dx}\right)^2 dx - \frac{1}{2}\left(\frac{d\zeta}{dx}\right)^2 dx \qquad \text{....(6.2)}$$

where p is live load. Because this conventional deflection theory provides good approximations for the cable deflection and the tensile force in the cable due to p. While, in the alternative method proposed here, $d\varphi$ and all the terms except the last one in Eq. 6.2 are taken into account in order that Eqs. 6.1 and 6.2 enable us to analyze the cable sag change from the stage of cable erection throughout that after completion [10]. EA of the girder in Eq. 6.2 and EI of the girder in the fundamental differential equation solved with Eq. 6.1 simultaneously should be zero in the analysis as the deck segments are not yet connected rigidly to each other on this stage.

Fig. 8(a) presents a sample result for comparing w-f curves of the cable for the actual concrete stress-ribbon bridge, the Jinya-no-Mori Bridge with L=123 m [5], analyzed by four methods: the proposed and the conventional methods, and the step-by-step method using the conventional theory together with the method using the popular bridge design formula. The significant features in the figure are: (1) Very large slope of each non-linear curve in the range of small w; (2) Over-estimation of f analyzed by the conventional theory denoted by a broken line; (3) Very good agreement between the other three. p-f curves, after connection of the deck segments to each other, for the Jinya-no-Mori Bridge and the previously proposed steel and the improved lighter steel bridges are denoted by dotted lines in Fig. 8(b). EA together with EI effects on the reduction of the deflection can be seen in the figure. More important is that the lighter structures give larger

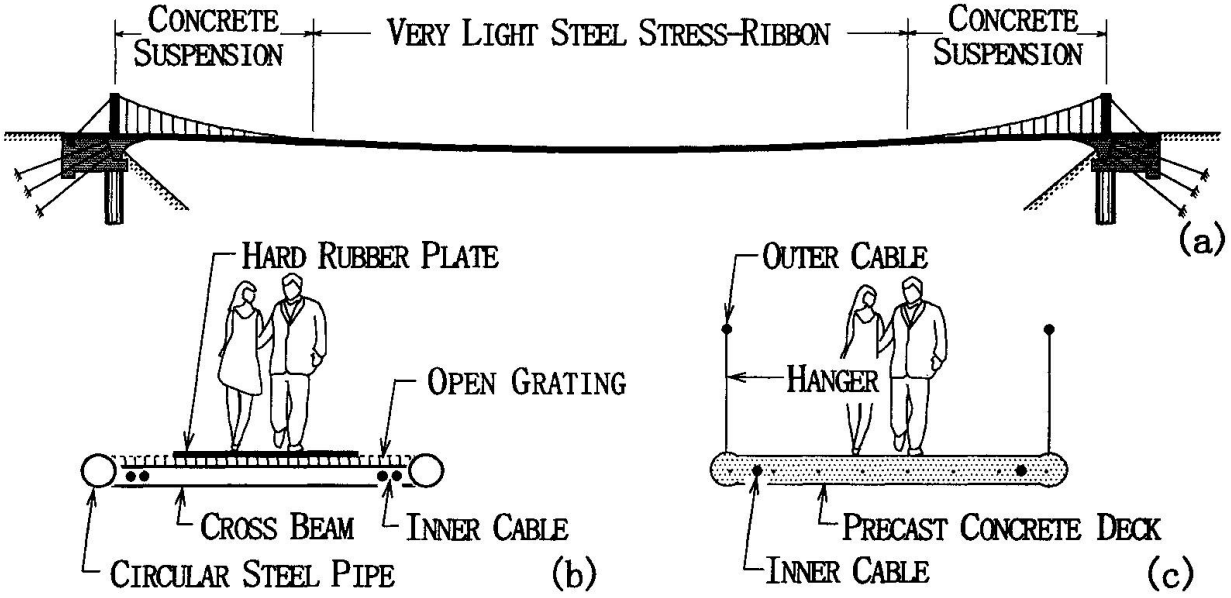

Fig.5 The proposed hybrid stress-ribbon pedestrian bridge. The elevation (a); the cross-section of the central portion of steel stress-ribbon deck (b); that of concrete suspension deck close to the abutment (c).

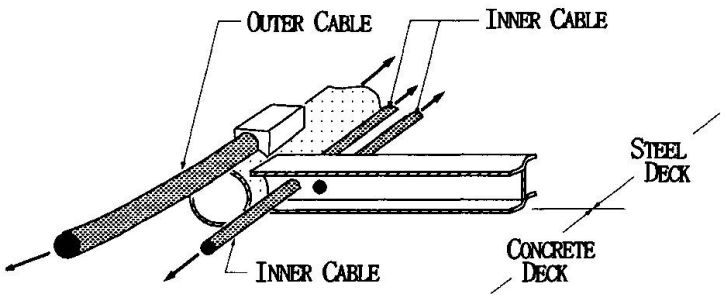

Fig.6 Inner and outer cables at the connection of steel and concrete decks.

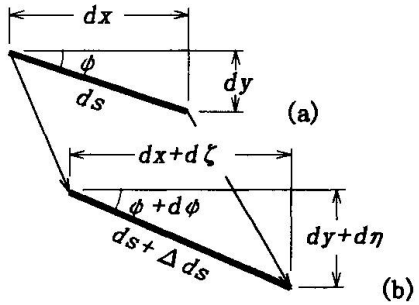

Fig.7 Deformation of cable segment.

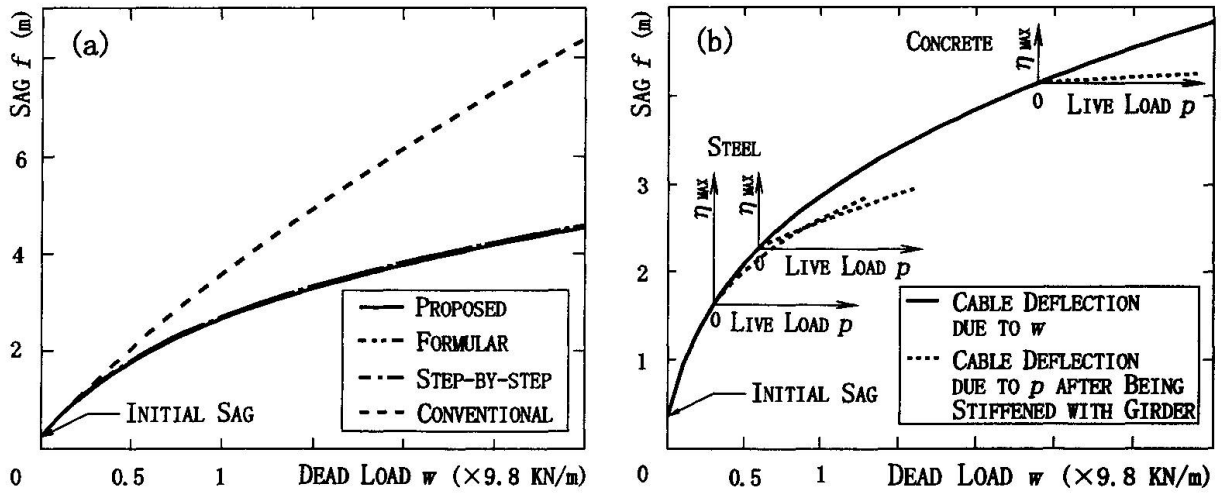

Fig.8 Cable sag change due to dead load (a), and deck sag change due to live load for bridges of conventional concrete, previously proposed steel and proposed lighter steel constructions (b).

deflection due to the same live load, i.e., the lighter structures are more flexible. Therefore, the hybrid bridge with concrete side decks may be better than the full-steel bridges as moderate stiffness is generally required for every structure in civil engineering.

7. Concluding remarks

A stress-ribbon bridge of very light steel construction and a hybrid bridge were proposed in this paper. These are for pedestrian use on the preceding phases but could be applicable to the bridges for vehicles on the succeeding phases. The characteristics of non-linear cable sag change at any stage including initial cable erection were also examined using a proposed method. The main results obtained are summarized as follows.
(1) The deck weight of the proposed steel stress-ribbon bridge could be reduced up to one-tenth of that of the conventional concrete stress-ribbon bridges.
(2) Another proposed hybrid structure, 'a stress-ribbon suspension bridge' type construction, allows for a reduction in deck sag as well as an increase in the sag of about half of the cables remarkably by partially introducing the outer cable system with the newly installed low towers.
(3) Highly aerodynamic stability is expected for these proposed bridges.
(4) The proposed method gives the exact values of the cable deflection due to dead and live loads, while the conventional cable equation gives over-estimated values.

The interests of the authors and the collaborative Korean researchers are focused on the following items and their examinations have been already partially started.
(1) How to apply the proposed pedestrian bridges to roadway bridges.
(2) Comparison of the static, dynamic and aerodynamic characteristics of the proposed steel and hybrid structures to those of the conventional concrete ones.
(3) How to connect the concrete and steel decks to each other as well as the outer cables to the steel edge girders shown in Fig. 6.
(4) Further studies on the earthquake resistant and the wind resistant designs of the bridges.
(5) The problems on contact and fatigue stress of the cable distributor in full-steel bridges.

Acknowledgments

The authors are grateful to Prof. K. CHOI of Don-A Univ., Dr. S Kwon of Korea Highway Corp., S. Tozuka of Kumamoto Prefecture Government Office and S. Ogata of Sumitomo Const. Inc. for their collaboration. They thank G. Liu, K. Akaza and Y. Yamada graduated from KSU, and Y. Kamei, T. Shirachi, T. Shinohara, K. Kojo and H. Minoda of KSU for their assistance.

References

[1] Yoshimura, T. et al., Aerodynamic stability of a concrete stress-ribbon pedestrian bridge, Proc. 6th Int. Conf. on Flow Induced Vibrations (1995) 601-610.
[2] Yoshimura, T. et al., Half-circular and half-elliptic edge modifications for increasing aerodynamic stability of stress-ribbon pedestrian bridges, J. Wind Eng. Ind. Aerodyn., Vol. 69-71, to be published.
[3] Wheen, R.J., Steel stress-ribbon concept - will it save money? -, Civil Engineering, ASCE, May (1976).
[4] Wheen, R.J. & A. J. Wilson, The stress-ribbon bridge concept in steel, The Structural Engineer, Vol. 55, No. 5 (1977) 223-229.
[5] Mizuta, Y. et al., Proposal of a steel stress-ribbon pedestrian bridge and its mechanical characteristics, J. Structural Eng., JSCE, Vol. 43A (1997) 1191-1196.
[6] Hirai, A. & M. Ito, Impact on long suspension bridges, Proc. Symp. on High-rise and long-span structures, JSCE & AIJ (1964).
[7] Yoshimura, T. et al., Aerodynamic stability of the Nagashima Storage Dam Suspension Bridge, Prep. JSCE Seibu Branch Annual Conf., to be published.
[8] Yoshimura, T. et al., Aerodynamic stability of the Naruse Cable-Stayed Bridge, Prep. JSCE Seibu Branch Annual Conf., to be published.
[9] Yoshimura, T., Aerodynamic stability of four medium-span bridges in Kyushu district, J. Wind Eng. Ind. Aerodyn, Vol. 41-44 (1992) 1203-1214.
[10] Mizuta, Y. et al., Proposal of methods for evaluating cable sag and estimation of construction cost for stress-ribbon pedestrian bridges, Bull. Faculty Eng. KSU, No. 36, to be published.

Damping Characteristics of Long-Span Suspension Bridges

Shigeki UNJOH
Head, Earthquake Eng. Div.
Ministry of Construction
Tsukuba, Japan

Yukio ADACHI
Senior Research Eng.
Ministry of Construction
Tsukuba, Japan

Summary

There is uncertainty in damping characteristics in seismic design of long-span bridges. In general, damping ratio of 2% has been employed in practical design. However, smaller damping ratios had been observed according to the results of vibration tests of suspension bridges[1]. A well-instrumented bridge, the Vincent-Thomas bridge, was hit by two major earthquakes, the 1987 Whittier earthquake and the 1994 Northridge earthquake, which generated the most comprehensive data on not only the seismic responses but also support excitations[2),3),4),5)]. Using these data, system identification study was conducted to identify damping characteristics from the half power method, the free vibration decay method, and earthquake response analyses to find out the damping ratio which gives better agreement with the measured data. As the result, identified damping ratios are generally around 2% or more. Smaller damping values were also found in some modes.

1. Vincent-Thomas Bridge and its Observed Data

The Vincent-Thomas suspension bridge was located southwest of Los-Angels, California. Fig. 1 shows the general feature of this bridge. The center, side, and total length of this bridge are 457m, 154m, and 766m respectively. The bridge was designed in 1959. The suspended structure consists of two stiffening trusses, floor trusses and lower chords and the deck was made from non-composite concrete slab. The each main steel tower was connected at 5 locations at mid height by lateral beams. 26 accelerometers were instrumented at the stiffening trusses, the towers, the tower bases, and the ground as shown in Fig. 2. This bridge had suffered two major earthquakes: the Whittier earthquake and the Northridge earthquake. Those acceleration data were very important and very precious to study the damping characteristics and seismic response behavior of long-span bridges. The measured peak displacements are shown in Table 1.

Table-1 Peak displacement amplitude observed during both earthquakes

Location	Whittier earthquake	Northridge earthquake
Center of center span (Transverse direction)	4.6cm (0.00010)*	4.5cm (0.00010)*
Center of center span (Vertical direction)	5.8cm (0.00013)*	17.7cm (0.00039)*
Center of side span (Transverse direction)	3.3cm (0.00007)*	4.7cm (0.00010)*
Center of side span (Vertical direction)	8.7cm (0.00019)*	20.6cm (0.00045)*
Top of tower (Longitudinal direction)	2.8cm (0.00006)*	4.8cm (0.00011)*
Top of tower (Transverse direction)	3.1cm (0.00007)*	4.4cm (0.00010)*

*: (Peak displacement) / (Center span length=457m)

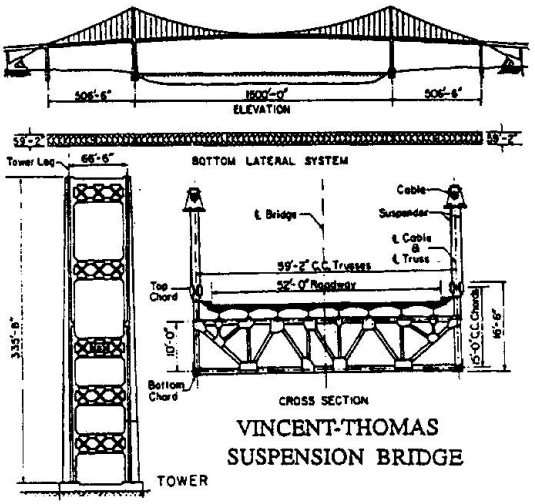

Fig. 1 Vincent-Thomas bridge[7]

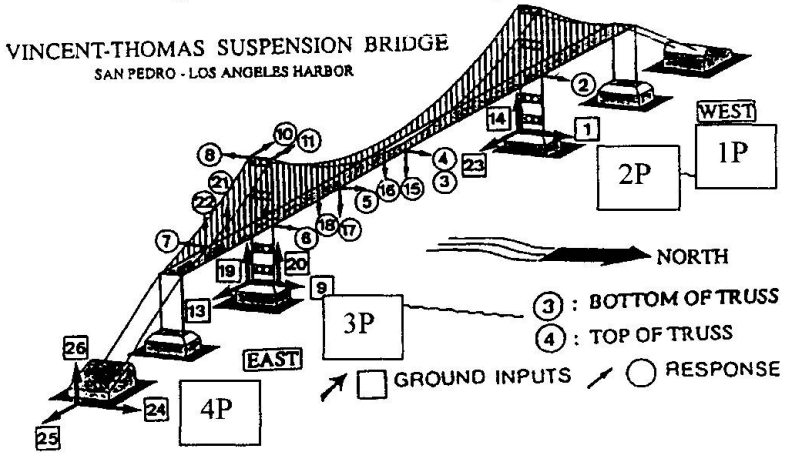

Fig. 2 Instrumentation of the Vincent-Thomas bridge [3]

2. Damping Characteristics Identification by the Half-Power Method and the Free Vibration Decay Method

The analytical methods to estimate the damping ratio have not been firmly established. The first try of identifying the damping ratio of each mode is employing the half power method and free vibration decay method applying to the measured acceleration data. When identifying the damping ratio by half power method, the transfer function and the power spectrum were employed in the frequency domain. The general idea of identifying the damping is shown in Fig. 3. No smoothing work was conducted to the observed data. Table 2 shows the average value of the each identified damping ratio calculated from the power spectrum and the transfer function with input data record of 2P or 3P tower base. According to the results from the transfer function of the Northridge earthquake, the damping ratios are identified as 1-3 % for the lower vertical vibration mode, 1-4% for the lateral vibration mode, and only 1% for the torsion mode of the girder. The estimated damping ratios using power spectrum from the Northridge earthquake data are 1-4% for the vertical and lateral vibration mode. According to the results from the both methods, the damping values estimated by power spectrum were estimated rather greater compared to the result using transfer function. The damping ratios identified for the Whittier earthquake are generally greater whereas the displacement amplitude of the earthquake were smaller. And also, in general, it seems that the damping values are estimated greater in the lower modes and smaller in the higher mode.

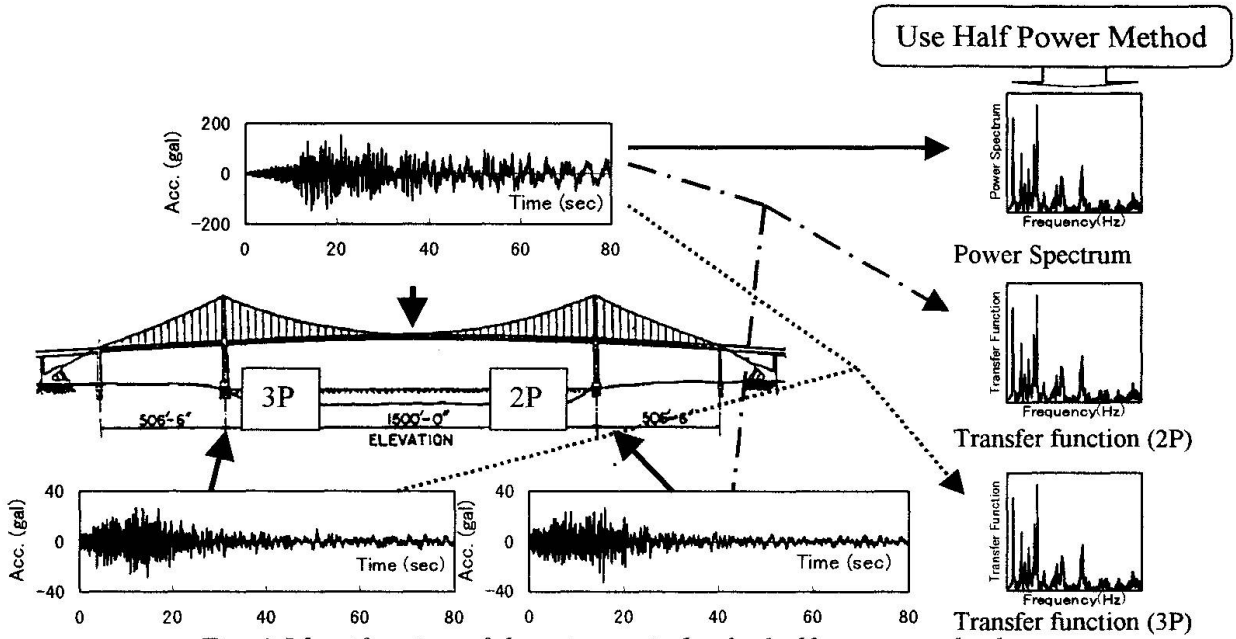

Fig. 3 Identification of damping ratio by the half power method

Table 2 Damping ratios estimated by the half power method

Vibration Mode	Power spectrum		Transfer function			
			Use 2P ground motion data		Use 3P ground motion data	
	Frequency (Hz)	Damping Ratio(%)	Frequency (Hz)	Damping Ratio(%)	Frequency (Hz)	Damping Ratio(%)
Whittier earthquake						
Vertical symmetric #1	0.226	5.3	0.226	2.3	0.232	2.1
Vertical symmetric #2	0.372	2.8	0.371	1.5	0.386	1.4
Vertical asymmetric #1	0.183	3.9	0.177	1.5	0.177	1.2
Lateral symmetric #1	0.134	7.9	0.134	5.4	0.140	3.5
Lateral asymmetric #1	0.427	2.1	0.421	0.8	0.421	0.9
Sway	0.232	4.3	-	-	0.232	4.8
Torsion #1	0.510	1.9	0.507	0.5	0.507	1.0
Northridge earthquake						
Vertical symmetric #1	0.226	2.0	0.226	2.5	0.226	1.3
Vertical symmetric #2	0.342	1.1	0.336	2.1	0.340	2.2
Vertical asymmetric #1	0.159	3.5	0.165	3.5	0.165	2.7
Lateral symmetric #1	0.134	5.8	0.140	4.1	0.110	4.5
Lateral asymmetric #1	0.419	1.7	0.421	0.7	0.417	1.9
Sway	0.244	5.9	-	-	0.238	4.0
Torsion #1	0.530	1.7	0.531	0.4	0.525	0.9

The measured data has long damped free vibration part after principal excitation so that damping ratio can be identified using the free vibration decay. Fig. 4(a) shows the lateral displacement time history at the center of the center span during the Northridge earthquake. According to this figure, it is recognized that the principal excitation was almost ceased 20 second or so but a long free vibration was followed and continued until 80-120 second. The identification work was carried out by extracting the target frequency component of the target vibration mode by band-pass filtering in the frequency domain and the damping ratio was identified the free vibration decay in the time domain using extracted data. The band pass filtering width was determined by trial and error basis. Fig. 4(b) shows the extracted displacement response of the lateral #1 mode of the main girder in the time domain. Table 5 shows the list of the identified damping ratios of each vibration mode. Star mark (*) was put if beating was not clearly removed when extracting the target frequency

component. According to the results of the Whittier earthquake, the damping ratio of lateral #1 vibration mode was identified as 5.5% but the rest shows smaller values. On the other hand, the larger damping ratio of vertical #1 and sway vibration mode were identified in case of the Northridge earthquake. The identified damping ratios using free vibration decays are relatively smaller compared to the result by the half power method.

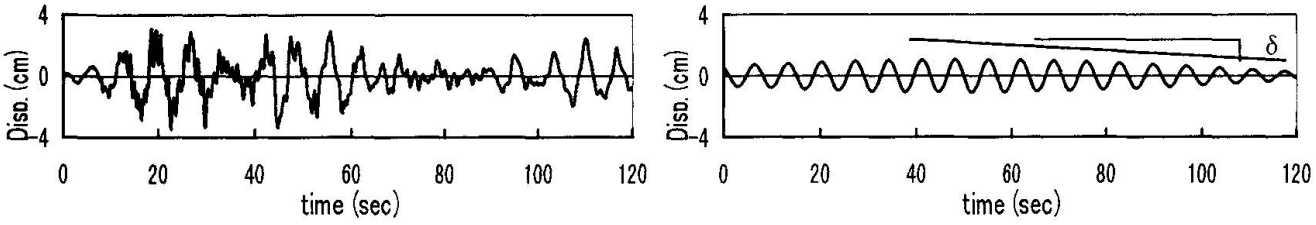

(a) Measured data *(b) Extracted data (Band width 0.20-0.25Hz)*

Fig. 4 Measured displacement history and extracted displacement time history of lateral #1 vibration mode at the center of the center span in the transverse direction (Northridge)

Table 5 Damping ratios identified from the free vibration decay

Vibration Mode	Location	Whittier earthquake(%)	Northridge earthquake(%)
Girder:			
Lateral symmetric #1	Center of the center span	5.5	2.6
Lateral asymmetric #1	1/3 point of the center span	1.4	1.4
Torsion #1	Center of the center span	0.8	0.9
Vertical asymmetric #1	1/3 point of the center span	1.4*	0.9
Vertical symmetric #1	Center of the center span	1.5*	2.9
Vertical symmetric #2	Center of the center span	2.0*	0.6
Sway	Tower point	1.7	3.4
Tower:			
Longitudinal direction	Top of the tower	0.7	1.6
Lateral direction	Top of the tower	0.3	0.6

*: Identification was carried out using beat waves

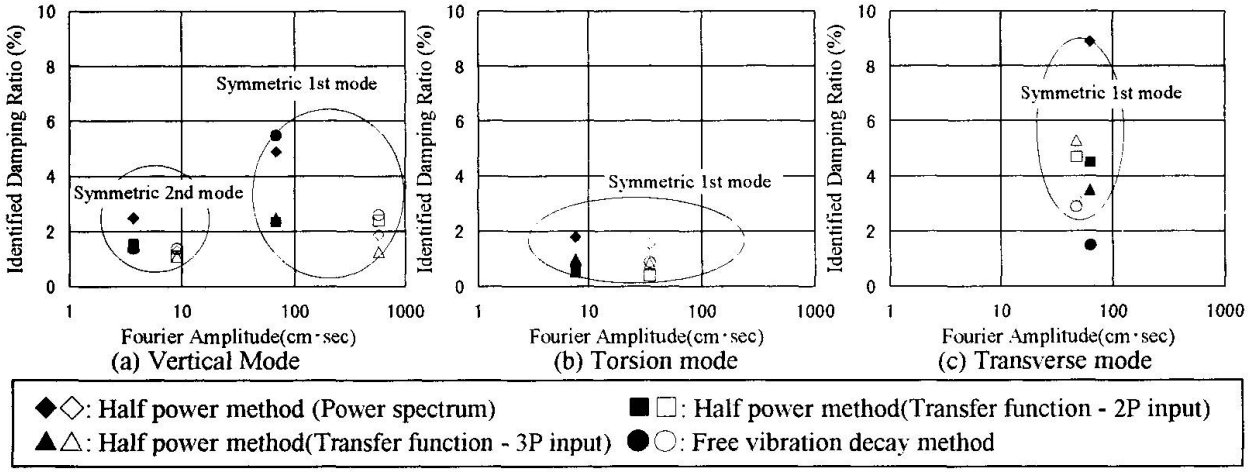

Fig. 5 Amplitude dependencies of damping ratio with Fourier displacement amplitude at the center of the center span

Fig. 5 shows the relation between the Fourier displacement amplitude and damping ratio of major modes identified by the half power method and the free vibration decay method in order to study the amplitude dependency of the damping ratio. The Fourier amplitude was focused at the center of the center span. Here the difference of the two earthquakes is expressed as the difference of the

Fourier amplitude. As for the vertical mode, the identified damping ratios are around 2%. When focusing the each mode, damping ratio decreases as the Fourier amplitude increases. The stiffness contribution of non-composite concrete deck or friction at the bearings may influence the damping characteristics of this bridge in the high Fourier amplitude region. As for the torsion mode of the girder, the damping ratios are around 1% and show no amplitude dependency. As for the lateral vibration mode of the girder, the damping ratios are relatively greater but the amplitude dependency could not be identified.

3. Damping Characteristics Identification by Earthquake Response Analyses

Another identification method of damping characteristics is to search the damping ratio that gives better agreement with measured peak acceleration or displacement data in the earthquake response analyses using a proper bridge model. In order to match the measured peak data and the analyzed data, proper modal damping ratio should be given. However, there is no theoretical and practical technique to set the best or the most proper modal damping ratio for each mode so that unique damping ratio, 0,1,2,3,5%, was set to each mode. The identification of the damping ratio was made by comparing the peak measured acceleration or displacement data the peak calculated data.

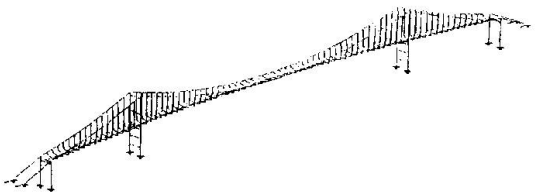

Fig. 6 Fish bone model of the bridge

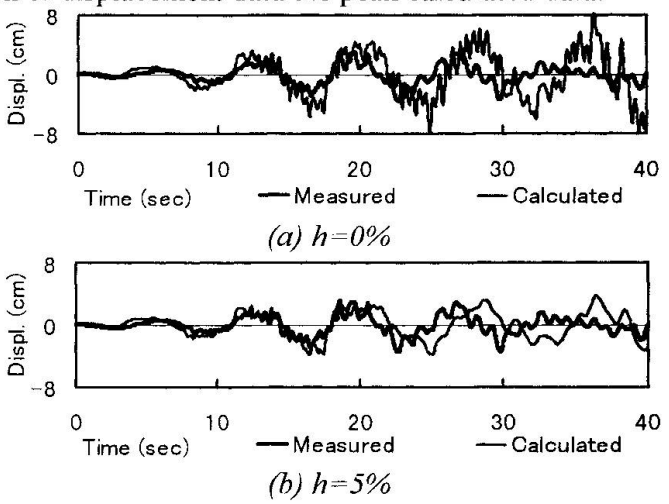

Fig. 7 Displacement time history data (Analytical and measured data, Northridge earthquake)

The super structure of the bridge was model by a fish bone model as shown in Fig. 6. The deck was non-composite concrete slab. It is assumed in this study that 40% of the stiffness contribution of the slab is expected for the lateral stiffness of the girder. The accuracy of the model had already been verified by comparing the measured dominant frequencies to the calculated ones obtained by the eigen analysis using this model. Using the verified model, a series of time history analyses were conducted by changing the modal damping ratio. The number of the modes that was considered in this study was 1st to 292nd modes. The total summed equivalent mass of those modes was 95%. Fig. 7 shows an example of an analytical result comparing the observed data. This figure shows the lateral displacement time history at the center of the center span during the Northridge earthquake and the analytical results by changing the damping ratios. According to this figure, the damping ratio can be identified 5% or more by comparing measured and calculated peak data. In this way, the damping ratios were identified if the maximum response of each data were agreed each other in terms of acceleration or displacement. Table 4 shows the identified damping ratios estimated using this method.

Table 4 Damping ratios identified by earthquake response analyses, which gives the same peak acceleration and displacement as the observed data

	Whittier earthquake		Northridge earthquake	
	Displ.	Acc.	Displ.	Acc.
Transverse Mode				
The center point of the center span	Greater than 5%	1%	Greater than 5%	3~5%
The 1/3 point of the center span	Greater than 5%	1%	Greater than 5%	2%
Vertical Mode				
The 1/3 point of the center span	Greater than 5%	1~2%	1~2%	3~5%
The center point of the center span	1~2%	1~2%	0~1%	Greater than 5%
The tower point of the center span	2%	0%	3~5%	0%
Tower				
Transverse, The top of the tower	2%	0~1%	Greater than 5%	Greater than 5%
Longitudinal, The top of the tower	Greater than 5%	5%	3%	Greater than 5%

According to the identification results, following damping ratios were generally identified: 0-2% for vertical direction of the center span of the girder and 2-5% for other vibration mode and the location. The identification results were different whether using acceleration data or displacement data. One possible reason is that some impulses were found in the measured data so that smaller damping ratio was needed when fitting the peak response. This assumption is also verified from the fact that the analytical peak displacements occurs almost at the same time as measured one whereas the analytical peak accelerations does not occur at the same time as measured one.

4. Conclusion

The identified damping ratio varies by estimation methods, modes, and earthquakes. In general, the damping ratio of around 2% is identified. This result shows that the damping ratio of 2% that is generally employed for seismic design of long-span bridges is reasonable enough. However, this result was obtained from the data on a suspension bridge with medium center span length. Therefore, further research is needed to study the damping characteristics of long or super long span suspension bridges.

Finally, the authors acknowledge Mr. M. Yashinsky, California Department of Transportation, and Mr. B. Darraugh, California Department of Conservation, to kindly help to obtain the strong-motion data of the Vincent-Thomas bridge.

References

1) Kawashima, Ohtsuka, and Unjoh: Dynamic behavior and damping characteristics of long-span bridge according to shaking tests of real bridges, Civil engineering journal, Vol.37, No.3, 1995.3

2) Abdel-Gaffar, et al: Seismic Performance Evaluation of Suspension Bridge, Proc. of 10th WCEE, Madrid, Spain, July, 1992

3) Abdel-Gaffar, et al: Seismic Behavior of Cable-Stayed and Suspension Bridges, Ponts Suspendus Et AHaubans, Cable-Stayed and Suspension Bridges, Deauville, France, 12-15 Oct. 1994

4) California Department of Conservation: CSMIP Strong-Motion Records from the Northridge, California Earthquake of 17 January 1994, Report No. OSMS94-07, Feb.18, 1994

5) California Department of Conservation: Processed CSMIP Strong-Motion Records for the Los Angels from the Whittier, California Earthquake of 1 October 1987: Vincent Thomas Bridge, Report No. OSMS-/NA, 3/30/1989

6) California Department of Conservation: Processed CSMIP Strong-Motion Records for the Los Angels from the Northridge Earthquake of 17 January1994: Vincent Thomas Bridge, Report No. OSMS 95-01S, 6/1/1995

7) Abdel-Gaffar, et al: An Analysis of the Dynamic Characteristics of a Suspension Bridge by Ambient Vibration Measurements, EERL Report, No.77-01 CALTECH, 1977

8) Abdel-Gaffar, et al: Ambient Vibration Tests of Suspension Bridge, J of the Engineering Mechanics Division, Proc. of ASCE, Vol.104, No.EM5, Oct. 1978

Corrosion Protection for the Main Cables of Suspension Bridges

Kazuhiko FURUYA
Mgr, First Constr. Div.
Honshu-Shikoku Bridge Authority
Kobe, Japan

Kazuhiko Furuya was born in 1956. He graduated from Civil Engineering Dept of Wakayama Tech. College in 1976.

Shoichi SAEKI
Executive Dir.
Honshu-Shikoku Bridge Authority
Kobe, Japan

Shoichi Saeki was born in 1938. He graduated from Civil Engineering Dept of Nagoya Institute of Techn. in 1962.

Haruki AKIYAMA
Gen. Mgr, Mukaijima Constr. Office
Honshu-Shikoku Bridge Authority
Kobe, Japan

Haruki Akiyama was born in 1949. He graduated from Civil Engineering Dept of Tokyo Univ. in 1972 and he received his Ph.D. in Engineering from Washington University in 1983.

Summary

Corrosion was found in investigative studies on the main cables of suspension bridges in service. These cables have mainly been protected from corrosion by a waterproof system composed of a surface paste on the wire surface, wrapping wires, and top coating. However, in the following studies, it has been clarified that the waterproofing would be gradually decreased due to the surface paste aging, and thermal cracks developing in the top coating. Therefore, various studies were carried out on the corrosion-proofing. As a result of these studies, it was concluded that some improvements should be made in the atmospheric environment inside the cable system. Eventually, further study was focused on development of a system which would dehumidfy the inside air by dried air injection. This paper introduces various findings on effectiveness and feasibility of this system.

1. Introduction

A study of more efficient method to protect suspension bridge cables against corrosion was started in 1988, being stimulated by an increase in cable wire strength (from 160 kgf/mm^2 to 180 kgf/mm^2) and a reduction in safety factor (from 2.5 to 2.2) in the design of the Akashi-Kaikyo Bridge.

Conventionally, bundled cables are protected from water ingress by overlaying them with a paste, wrapping the bundle in wire, and coating it with paint. However, this method was shown to offer inadequate protection in 1988, when a survey of the literature on suspension bridge cables in Japan and overseas, and visual checks of cables on Japanese bridges, was carried out. In 1989, an inspection of the interior of a cable bundle on the Innoshima Bridge, which entered service in 1983, demonstrated that water was present in the bundle and corrosion was found in the cable.

Following this finding, other suspension bridge cables were inspected. The cause of the corrosion was diagnosed, and tests aimed at improving the quality of sheathing materials and paints were implemented. The results of these efforts, however, demonstrated that a paste cannot adequately protect the cables if water is present within the cable bundle.

Given this proven difficulty in protecting a cable bundle from water ingress over the long term, it was decided that the corrosive environment within the bundle should be improved. Studies of

various methods led to adoption of a dry-air injection system, whereby the cable bundle is made airtight with a sheath and dry air is blown into the bundle.

This was not the first time that such a method was tried; a similar drying technique has been used to protect cable sprays in anchorages in Japan and in box girders abroad. However, this was the first attempt to dry an entire cable bundle consisting of 5-mm wires by injecting dry air. Thus it was necessary to demonstrate that protection against corrosion could be achieved as designed. A variety of tests were implemented to verify the effectiveness and feasibility of this method. This paper describes the results of these various investigations and tests.

2. Inspection of Existing Suspension Bridge Cables

2.1 Conditions Within Cable Bundles

Inspections of conditions within cable bundles on various Honshu-Shikoku Bridges, including the Innoshima, Onaruto, Oshima, and Seto Bridges, led to the conclusions below.

(i) Water was present inside the cable bundles.
(ii) The sides and bottoms of cables in a bundle were wet, but the upper area was dry.
(iii) The paste had deteriorated and was retaining water.
(iv) Corrosion had proceeded over the entire cable surface.
(v) Typical cable sections showed evidence of advancing corrosion and red rust was present to a depth of a few layers.
(vi) Band sections of the cable remained sound, with white corrosion present only on the bottom.
(vii) Corrosion began at an early stage.
(viii) The high corrosion-prevention paste protected only wires in direct contact with the paste, while inner wires were unprotected

2.2 Humidity Within a Cable Bundle

Temperature and humidity measurements within a cable bundle on the Onaruto Bridge revealed the conditions outlined below.

(i) In ordinary cable sections, the relative humidity within the bundle was high and was affected little by the outside air.
(ii) In band sections, the relative humidity within the bundle correlated with ambient humidity.

2.3 Mechanism of Cable Corrosion Within a Bundle

The inspections of suspension bridge cables revealed that water, possibly left within cable bundles during construction or permeating through cracked paint after entry into service, was present within cable bundles. This clarified that bundle interiors are subjected to repeated wetting as the water vaporizes when the temperature rises and then condenses as it cools. By carrying out a corrosion test on galvanized wire strands wrapped with wet gauze, it was demonstrated that strands corroded quickly and weakened under wet conditions. This does not only affect the surface layer; the inner layers of cables close to the surface also corrode.

Corrosion was severe on the sides of cable bundles, indicating that the surface layers on the sides had remained wet for a long time. Further, paste deterioration in which water was retained was supposed to be the cause of hastened corrosion.

3. New specifications to protect cables from corrosion

3.1 Study of New Specifications

To isolate the cause of the corrosion and study measures to protect cables, a series of tests was performed: tests of paste characteristics; accelerated tests using 29 scale-model specimens (20 mm in diameter; 70 cm in length; 1,270 strands) formed with conventional pastes (calcium plumbate, red lead, and high-polymer organic lead), improved pastes (aluminum phosphate, thiokol, sodium vanadate, and alkyl benzene sulfenic acid), and new sheathing materials (rubber, plastic, thermal-insulating materials, and S-shaped wires); and an exposure test using 52 small and 18 large (60 cm in diameter; 2 m in length; 11,557 strands) model cable specimens.

These tests led to the following understanding:
(i) None of the conventional pastes is able to fully protect cables against corrosion.
(ii) All of the modified pastes are better in protecting cables from corrosion.
(iii) No corrosion occurred when water was kept out of the cable bundle, but corrosion occurred within the bundle regardless of the paste type when water was already present within the bundle.

In practice, however, it proves impossible to protect the whole length of a cable from the entry of water by a cable sheathing method. For this reason, a study of the simple and highly feasible dry air injection method was initiated in 1993. A verification test using specimens on actual bridges began in 1994.

3.2 Study of Dry-air Injection System

To demonstrate the feasibility of using a dry-air injection system, several issues were investigated. The tested items, conditions, and the results follows.

1) Protection of cables from corrosion by injecting dry air

The system is based on the experimental result that steel hardly corrodes at all under dry conditions.[1] A test was conducted to ascertain whether such conditions can be realized by injecting dry air into a cable bundle. Attention focused on whether it would be possible to prevent the formation of the white corrosion found within cable bundles in the scale-model tests carried out during 1993. The test conditions were as outlined below.
(i) Test specimen: overlaid with a paste, wrapped with wire, and finished with paint (two specimens)
(ii) Test period: approx. 3 months
(iii) Temperature and humidity: 60°C and 85% RH for 12 hours + 20°C and 95% RH for 12 hours (with 1 hour/day under rainy conditions)
(iv) Wet conditions: 250 cc of water injected into specimen
(v) Dry air injection: injection of air (at about 20% RH and an air flow rate of 15 cm/min.).

Since it took about a month to dry out the specimen, white corrosion formed on the bottom where the water pooled. However, the original galvanized color was visible elsewhere, demonstrating the effectiveness of dry-air injection. Although other tests with volatile corrosion inhibitors and hollow pipe covers to facilitate the flow of air were carried out, they demonstrated no significant advantages. Further, no advantage was noted in tests with and without a paste, thus demonstrating that the use of paste would become unnecessary if the dry-air injection method were adopted.

2) Drying of cables by injecting dry air through one part of the cable bundle section

It was questionable whether dry air would flow across the entire section of a cable bundle. To check whether drying takes place in the sections through which the air does not actually flow during injection of dry air, a test was carried out using a 60 cm diameter by 2 m long model cable (11,557 strands of 5 mm diameter wire at a void ratio of 18%) with 2,500 cc of water added.

Dry air was injected through part of the cable bundle section. Dry-air injection removed all water after 300 hours.

3) Injection of air into a cable through the cable surface

One means of injecting air into the cable bundle on an actual bridge would be to force it into the bundle through the surface (with no wrapping material). To verify whether this is possible and whether injected air spreads through the cross-section, air was injected locally from the top face into a specimen with the same dimensions as in 2) above. This verified that air could be injected through a 13.5 cm by 5 cm opening at an air-flow rate of 0.19 m^3/min. at a low pressure of 90 mm aq. (0.009 atmospheric pressure). (It was later verified in tests for the Akashi-Kaikyo Bridge that it is possible to inject air through an opening of about one meter.) It was also verified that air injected through the side spread in the cross-sectional direction, although the flow rate was very small.

4) Critical humidity for the corrosion of galvanized steel strands

It is a known fact that galvanized steel strands hardly corrode when the relative humidity is below 60%.[1)] However, the effects of rust, paste, and salt buildup on corrosion are unclear. Accordingly, an investigation was carried out to determine the effects of various parameters on this value of critical humidity: the clearance between steel strands, the presence of white corrosion or red rust deposits or deteriorated paste, and the presence of trace amounts of salt that might be entrained by the injection of dried ambient air. In particular, the effects of trace quantities of salt were investigated quantitatively. The test was implemented by placing specimens in a desiccator, and adjusting the humidity by controlling the concentration of a sulfuric acid solution.

This test verified that galvanized steel strands rarely corroded below a relative humidity of 60% even in the presence of these buildups. Small amounts of white corrosion were found on steel strands where deteriorated phosphate paste had built up, whatever the humidity level. Although the degree of corrosion increased with salt buildup, galvanized steel rarely corroded when the relative humidity was below 60%.

5) Extent of dried area when dry air is injected into a cable bundle

A test was carried out on the Bisan Seto Bridge, whose cable diameter was 998 mm. After temporarily wrapping the bundle with rubber, dry air was injected at the saddle atop one of the towers. It was possible to lower the humidity within the bundle at distances of 140 m and 215 m from the tower to the same level as at the dry-air injection nozzle, i.e. to less than 30%, in about six months and one year, respectively. At the Innoshima Bridge (cable bundle diameter: 610 mm) a dry air injection test was carried out by fitting a dry-air injection cover over the bundle near the middle of the central span and injecting air into the bundle through a nozzle on the cover. As shown in Fig. 14, the humidity within the bundle at a distance of 230 m was fully reduced, while at a distance of 250 m it was continuing to fall.

6) Removal of salt from air before injection

To remove the salt from injecting air, a special system was developed using six different filters which removed 99.97% of salt particles over 0.3 μm in diameter. (Salt particles range mostly from 0.5 μm to 30 μm in diameter.)

4. Corrosion Protection System for the Akashi-Kaikyo Bridge Cables

After studying the results of the tests, it was decided to adopt a dry-air injection system as described below for the protection of the Akashi-Kaikyo Bridge cables.

(1) Cable sheathing system

To enhance air tightness and protection against water permeation, the conventional wire wrap is enhanced by wrapping with rubber. For the reasons given earlier, the paste is eliminated. To seal the cable band sections, the cable bundle is covered with butyl rubber on the bottom and with modified silicone on the top surface to increase air tightness and durability (Fig. 1).

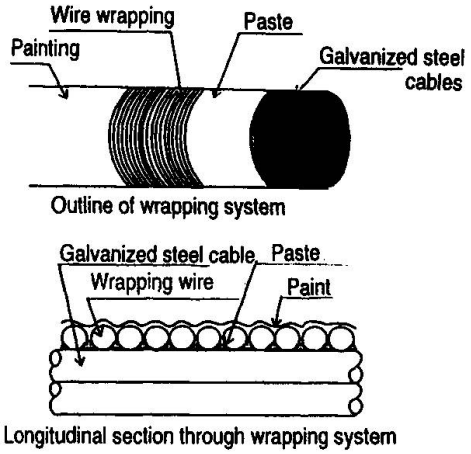

Fig. 1 Conventional cable protection system

(2) Dry air injection system

The basic design policy adopted for the dry-air injection system is as follows.

(i) Air is injected through cable covers placed at intervals of about 140 m.
(ii) The dry-air flow rate at each cover is 3 m^3/min. and the pressure within the cable bundle is kept below 300 mm aq. (0.03 atmospheres), taking into account the rupture pressure of seals and sheathing materials.
(iii) Dry-air injection covers are located as close to cable bands as possible.

Figures 2 and 3, and Photo 1, show the arrangement of pipes, a schematic drawing, and a dry-air injection (exhaust) cover, respectively.

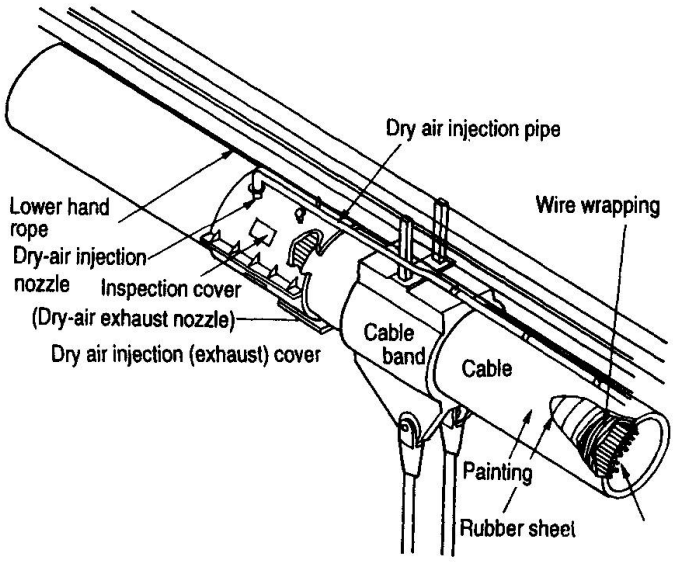

Fig. 2 Dry Air injection system (arrangement of pipes)

(3) Maintenance plan

(i) It is important to take particular care in inspecting dryers, blowers, and salt filters.
(ii) Dry-air injection pipes and cable sheathing materials must be well maintained.
(iii) Cable bundles are checked visually through inspection covers on the dry-air injection/exhaust covers.
(iv) Temperature and humidity within the dry-air injection/exhaust covers are measured periodically.

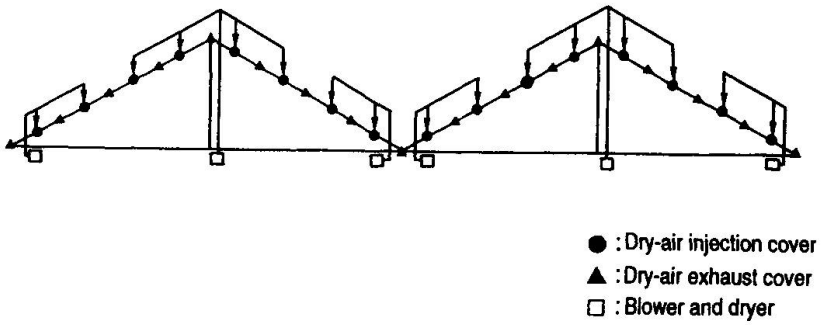

Fig. 3 Schematic drawing of dry-air injection system

(v) Cable bundles interiors are inspected after a few years of operation.

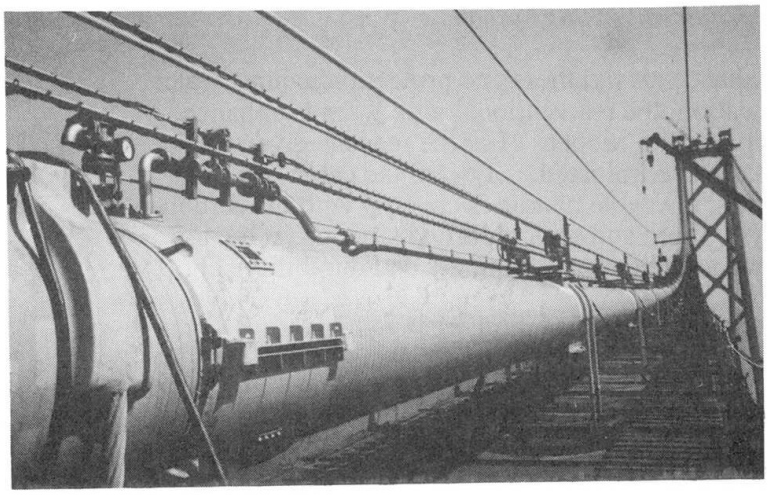

Photo 1 Dry air injection (exhaust) cover

Conclusions

This is the first-ever attempt to use a dry-air injection to protect suspension bridge cables. Further studies will be necessary to make the system more effective.

The cable sheathing on the Akashi-Kaikyo Bridge consists of wrapping the bundle with conventional wires and then rubber. A wire with an S-shaped cross section was developed to improve air tightness; after being tested in practical use on the Hakucho Bridge, it is now being tested by the Authority to verify its usability. A two-liquid very-fast-hardening urethane sheathing sprayed on in the field as a thick, flexible film is also being tested. Further, the interval between air-injection covers is being increased. Taking these changes into account, further studies will lead to a plan for protecting the cables of the Kurushima Bridge against corrosion. At the same time, policies will be developed for improving conventional corrosion protection systems already in use for suspension bridges.

The authors are greatly indebted to Prof. Asakura and the members of the Working Group on Corrosion Protection of Suspension Bridge Cables for their guidance during the course of this study.

References

1) H. H. Ulick and R. W. Levy, "Corrosion Reaction and Control: Third Edition," December 20, 1989
2) Shoichi Saeki and Kazuhiko Furuya, "Corrosion Protection of Suspension Bridge Cables," Construction of Civil Engineering Structures, Vol. 38, No. 7, July, 1997
3) Kazuhiko Furuya, "Dry Air Injection Test for Corrosion Protection of Suspension Bridge Cables," Honshu Technical Report, Vol. 21, No. 84, November, 1997

Computer-Aided Bridge Design and Selection of Construction Methods Using Fuzzy Logic

Moisés RAMIREZ-MARQUEZ
Researcher Assist.
School of Civil Eng.
Barcelona, Spain

Moisés Ramirez Marquez, born in 1967, got his civil engineer degree form the Iberoamerian Univ. (UIA) in 1991. Since 1995 he has been a doctoral student at the Techn. Univ. of Catalonia (UPC). His research field is application of the fuzzy-set theory in bridge projects.

Juan R. CASAS
Assoc. Prof.
School of Civil Eng.
Barcelona, Spain

Juan R. Casa, born in 1960, received his Civil Eng. degree form the Techn. Univ. of Catalonia (UPC) in 1984 where he completed his doctorate in 1988. Since then, he has been professor of bridge engineering at UPC. His research includes dynamics analysis and testing of bridges as well as bridge reliability.

Summary

The paper develops a multi-criteria decision model for selecting the best bridge design from the technical and economical points of view. The model considers the current "state of art" in bridge engineering, organizes hierarchically the different construction alternatives and determines the ranking of the best structural design and construction method using fuzzy logic. The fuzzy combined programming method has been developed according to the fuzzy sets theory, which has been thoroughly proven in the resolution of engineering problems where uncertain information with multiple solutions exist. The multi-objective programming method considers the fuzzy information provided by specialists as well as a data base of 495 bridges built in Spain during the last 25 years.

1. Introduction

Due to the different design criteria, the election of the structural configuration and the construction method are the most important decisions of a bridge project. Depending on the specialist's experience, the decisions can vary in function of the project constraints such as the geographical conditions, execution term, service life, cost, etc., therefore such decision can vary depending on each case and the specific requirements of the client.

Traditionally during the selection of a bridge design, the construction cost is one of the most important factors. However, a proposal with a high cost can result from a high degree of technical quality, while a proposal with lower cost may not provide the minimum technical requirements. Therefore the minimization is in conflict with maximizing the technical factors and a long service life. This study outlines a solution through analysis of uncertain variables with the application of the fuzzy-set theory. The method is applied to the resolution of an explanatory example.

2. Concept of Fuzzy Logic

The central concept of fuzzy logic is the membership function $\mu(x)$, which represents numerically the degree in which an element belongs or not to an specified set. The membership function can range from 0 to 1, therefore the transition between member and non-member of a set appears by gradual way. When the membership function of an element has only values of 0 or 1, the fuzzy set theory is reduced to the classical set theory. The fundamental characteristic of the fuzzy sets is the possibility to quantify vagueness of the human thinking as the common sense, experience, or language ambiguities such as "more and less" or "tall men", which are not possible to quantify in classic logic. Therefore it is feasible to imitate the human reasoning and to take decisions based on fuzzy data [1,2,3].

3. Fuzzy-combined methodology

Many objectives in bridge design are difficult to arrange since their values contain a high degree of uncertainty and subjectivity. The fuzzy-combined model here proposed defines the basic criteria of bridge design, groups the values of each criterion hierarchically, evaluates the possible solutions and finally ranks the options obtaining the most adequate solution. The method combines the fuzzy sets theory with the analytic hierarchy process (AHP) and with the built bridges data and is fully explained in [4]. Highway prestressed concrete and composite bridges are considered for the analysis of each construction choice. The model divides the bridges in deck, piers and abutments. This possibility was outlined in order to obtain independent results from each structural element in case of having some constraints.
The first step of the model consists on the identification of the most representative variables involved in bridge design and construction (Table 2). Once defined the elements of the basic criteria, they are joined by sets (Fig. 1). The 82 variables that form the first level represent the basic criteria (33 for the deck, 28 for the piers and 21 for abutments). They are grouped to form the second level. For example, the elements of the first level for bridge deck (slenderness , span, adequacy to longitudinal slope and curvature) can be grouped into geometry in longitudinal section, which is an element of the subset of second level (see Table 2). By this way, the variables that integrate the second level as geometry in longitudinal section, construction method, etc. are grouped into technical valuation (third level). Finally, the solution (fourth level) is formed by technical valuation, service life and cost. Analogous diagrams have been made for piers and abutments.

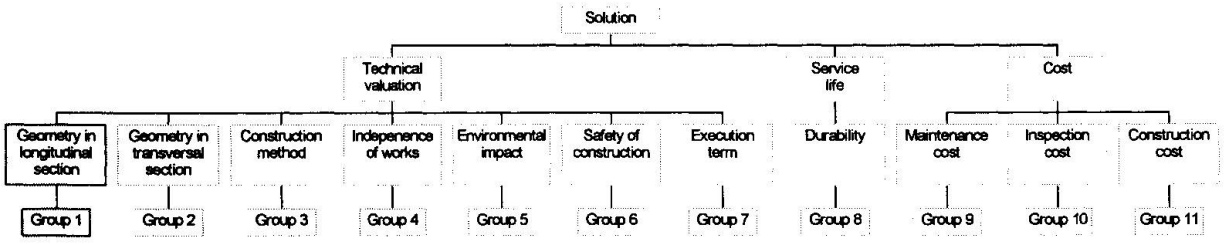

Fig. 1 Diagram of deck bridge basic criteria (see Table 2)

3.1 Quantification of fuzzy values

To obtain the fuzzy values and the membership function of the basic criteria and their relative importance, a survey was developed among a group of Spanish experts in design and bridge construction. The purpose was to establish the recommendation in the use of construction systems for specific situations such as prevention of alignment mistakes, adaptability to technical problems, environmental constraints, etc. which are the level 1 of basic criteria. The specialists answered the questions according to linguistic scales. In the same way, regarding safety and relative importance a different scale was adopted (Table 1). The values given by the experts have been completed with the existing data base of bridges built in Spain in the last 25 years. The data base contains a summary of the "state of the art" of bridge design and construction in Spain.

Intensity of recommendation	Definition	Intensity of security	Definition	Intensity of importance	Definition
1	Not recommendable	1	Unsafe	1	Equal importance
2	Low recommendable	2	Not much secure	3	Weak importance
3	Recommendable	3	More and less secure	5	Strong importance
4	Very recommendable	4	Secure	7	Demonstrate importance
5	Absolutely recommendable	5	Very secure	9	Absolute importance
				2,4,6,8	Intermediate values

Table 1 Linguistic measures

3.2 Analysis of fuzzy values

The values of the basic criteria are fuzzy numbers represented by $\mu(x)$, where x is a discreet element of the set. Be $Z_i(x)$ a fuzzy value for the ith basic criterion, and its membership function $\mu[Z_i(x)]$ a trapezoid (Fig. 2) [5].

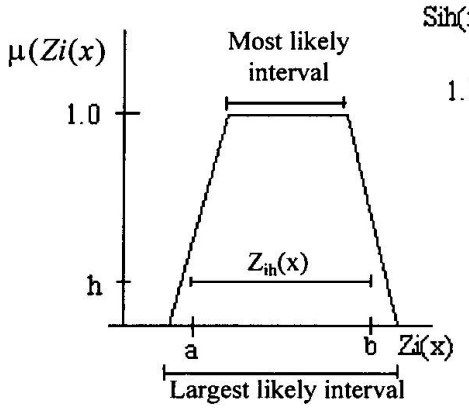

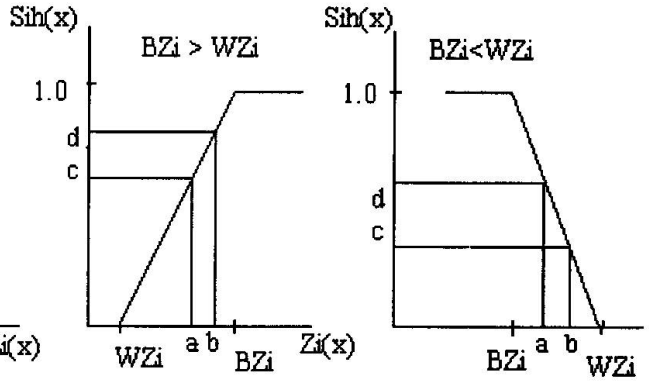

Fig. 2 Fuzzy calculation of basic criteria *Fig. 3 Tranfering value* $Z_{ih}(x)$ into $S_{ih}(x)$

Because of the units of the basic criteria are different, since for some the best value is the highest while for other is the opposite (the best price is the lowest and the best constructive yield the highest), the value of each basic criterion $[Z_{i,h}(x)]$ in Fig. 2 is transformed into a index $S_{i,h}(x)$ in the following way [6]:

If $BZ_i > WZ_i$, then $S_{i,h}(x) =$

$$\begin{bmatrix} 1, & Z_{i,h}(x) \geq BZ_i \\ [Z_{i,h}(x) - WZ_i]/(BZ_i - WZ_i) & WZ_i < Z_{i,h}(x) < BZ_i \\ 0, & Z_{i,h}(x) \geq WZ_i \end{bmatrix} \quad (1)$$

If $BZ_i < WZ_i$, then $S_{i,h}(x) =$

$$\begin{bmatrix} 1, & Z_{i,h}(x) \geq BZ_i \\ [Z_{i,h}(x) - WZ_i]/(BZ_i - Z_i) & WZ_i < Z_{i,h}(x) < BZ_i \\ 0, & Z_{i,h}(x) \geq WZ_i \end{bmatrix} \quad (2)$$

$Z_{i,h}(x)$ is an interval with lower bound a and upper bound b, therefore the index value $S_{i,h}(x)$ ranges between bounds c and d (Fig. 3). BZ_i and WZ_i, are the best and worst values of Z_i.
To calculate the following levels of the basic criteria, the expressions (3), (4) and (5) are used:

$$\text{Second Level: } L_{j,h}(x) = \left\{ \sum_{i=1}^{nj} W_{i,j}[S_{i,h,j}(x)]b_j \right\}^{1/bj} \quad \text{.....(3)}$$

$$\text{Third Level: } L_{k,h}(x) = \left\{ \sum_{i=1}^{nk} W_{j,k}[L_{j,h,k}(x)]b_k \right\}^{1/bk} \quad \text{.....(4)}$$

$$\text{Fourth Level: } L_h(x) = \left\{ W_1\,[L_{1,h}(x)]b + W_2\,[L_{2,h}(x)]b + W_3\,[L_{3,h}(x)]b \right\}^{1/b} \quad \text{.....(5)}$$

Where n_j, n_k = number of elements in the "xth" level-group. $S_{i,h}$,= index value for the ith basic criterion in the second level-group j. $L_{j,h,k}$ = index value for the second level group j in the third level group k. W = weight coefficient representing the relative importance of the four levels of the basic criteria. $L_{1,h}(x)$, $L_{2,h}(x)$, $L_{3,h}(x)$ = index values of technical valuation, service life and cost. b = balancing factors for the level groups [7], representing the variability between the values of the different levels ($b \geq 1$). The larger the value, the greater the variability.

3.3 Determination of Weights

The values of W represent the judgement of the surveyed group of experts and are obtained applying AHP which compares each criterion of the different groups [7]. The comparison between criterion i and criterion j gives the value a_{ij} of matrix A. If $a_{ij} = \delta$, then $a_{ji} = 1/\delta$, where $\delta \neq 0$ and $i \neq j$; if $i=j$, then $a_{ij} = a_{ji} = 1$. For example, regarding group 4 and according to table 1, if the importance of *interference of local transit* (IT) for a construction method is *strong* ("5") compared to *provision of materials to the construction site* PM, then IT/PM = 5 and PM/CI = 1/5.

$$\mathbf{A} = \begin{array}{c} \\ \text{IT} \\ \text{PM} \\ \text{CA} \end{array} \begin{array}{c} \begin{array}{ccc} \text{IT} & \text{PM} & \text{CA} \end{array} \\ \begin{bmatrix} 1 & 5 & 1 \\ 1/5 & 1 & 1/3 \\ 1 & 3 & 1 \end{bmatrix} \end{array} \begin{array}{l} \\ \text{IT interference of local transit} \\ \text{PM provision of materials to the construction site} \\ \text{CA compatibility with other construction activities} \end{array}$$

Starting from the eigenvalue of matrix **A**, the desired weights are obtained [7]. For the case of group 4 (independece of works) an according to the expert's opinion the weights coefficients are: W = 0.481, 0.114, 0.405 for IT, PM and CA respectively.

4 Ranking of the possible solutions

Once obtained the fourth level (5), let $L(x)$ be the fuzzy number representing the final composite indicator of alternative x, $L_{h=1}(x)$, $L_{h=0}(x)$ = index value. The membership function of the fuzzy number $L(x)$, is calculated in the following way:

$$\mu[L(x)] = \begin{bmatrix} 1, & r_{min} \leq L(x) \leq r_{max} \\ (L(x)-R_{min})/(r_{min}-R_{min}) & R_{min} \leq L(x) < r_{min} \\ (L(x)-R_{max})/(r_{max}-R_{max}) & r_{max} < L(x) \leq R_{max} \\ 0 & \text{otherwise} \end{bmatrix} \quad \text{...(7)}$$

where r_{min} and r_{max} = lower and upper bounds of $L_{h=1}(x)$ of the final indicator obtained by using $Z_{i,h=1}(x)$. R_{min} and R_{max} = lower and upper bounds respectively of $L_{h=0}(x)$ of the final indicator calculated by using $Z_{i,h=0}(x)$. The fuzzy numbers L(x) will be limited according to (7). The ranking of all the possible solutions are calculated maximizing and minimizing sets [8].

5 Example

The multi-criteria model evaluates the most suitable structural configuration (cable stayed, arch, frame and continuous beam) with more than 20 possible construction systems that have been applied for deck, piers and abutments. As an example, suppose that a consulting firm have to evaluate four projects for the construction of a deck bridge with the following characteristics: 300 m of total length, 15 m deck width and crossing a precipice of 100 m. The alternatives are: long span arch built by the cantilever method with temporary stays (A), incrementally launched continuous beam (B), cable-stayed bridge using formwork supported on the ground (C) and isostatic spans cast in situ using a self-supported movile formwork. (D). As shown in table 2, the span-length varies as function of the construction system (from 25 to 250 m for proposal A, from 40 to 80 m for proposal B, etc.). The largest likely interval is the range between the minimum and maximum values of the alternatives and the most likely interval is the range of the most common values of the alternative. The intervals represent the uncertainty in each criterion and establish the membership function $\mu[Z_i(x)]$. When the values of the variables are single numbers such as slenderness (group1), or deck width (group 3), are analyzed as non-fuzzy numbers.

Group	Basic Criteria	Proposal 1		Proposal 2		Proposal 3		Proposal 4	
		Least likely	Most likely	Least likely	Most likely	Least likely	Most likely	Least likely	Most likely
1	Slenderness l/h	16.7-16.7	16.7-16.7	6.67-6.67	6.67-6.67	16.67-16.67	16.67-16.67	3.33-3.33	3.33-3.33
1	Span	25.0-250.0	25.0-250.0	25.00-100.00	40.0-80.0	40.0-80.0	25.00-250.00	25.00-50.00	25.00-50.00
1	Adequacy to longitudinal slope	1.0-3.0	2.04-2.86	3.00-5.00	3.82-4.72	3.00-5.00	3.82-4.72	3.00-5.00	3.82-4.72
1	Adequacy to curvature in plant	1.0-1.0	1.00-1.00	1.00-1.00	1.00-1.00	1.00-1.00	1.00-1.00	1.00-1.00	1.00-1.00
2	Adequacy to functional platform	2.0-3.0	2.11-2.62	3.00-5.00	3.82-4.72	3.00-5.00	3.82-4.72	3.00-5.00	3.82-4.72
2	Width/Span ratio	15.0-21.0	15.0-21.0	15.0-21.0	15.0-21.0	18.0-25.0	18.0-25.0	18.0-25.0	18.0-25.0
2	Adjustment to variable cross-section	2.00-3.00	2.14-2.66	4.00-5.00	4.24-4.76	4.00-5.00	4.24-4.76	4.00-5.00	4.24-4.76
3	Adequacy to horizontal layout	2.00-3.00	2.11-2.62	3.00-5.00	3.82-4.72	3.00-5.00	3.82-4.72	3.00-5.00	3.82-4.72
3	Adequacy to cross-section geometry	1.00-3.00	2.04-2.86	3.00-5.00	3.82-4.72	3.00-5.00	3.82-4.72	3.00-5.00	3.82-4.7
3	Adequacy to cross-section depth	2.00-3.00	2.14-2.66	4.00-5.00	4.24-4.76	4.00-5.00	4.24-4.76	4.00-5.00	4.24-4.76
3	Adequacy to different span lengths	1.00-4.00	1.89-3.02	3.00-5.00	3.81-4.56	3.00-5.00	3.81-4.56	3.00-5.00	3.81-4.56
3	Adequacy to variable cross-section	1.00-2.00	1.11-1.62	4.00-5.00	4.49-4.96	3.00-5.00	4.04-4.86	4.00-5.00	4.49-4.96
3	Deck width	15.0-15.0	15.0-15.0	15.0-15.0	15.0-15.0	15.0-15.0	15.0-15.0	15.0-15.0	15.0-15.0
3	Prevention of alignment mistakes	3.00-5.00	3.89-4.71	3.00-5.00	3.88-4.67	2.00-4.00	2.74-3.66	2.00-4.00	2.66-3.54
4	Interference on local transit	4.00-5.00	4.59-5.00	4.00-5.00	4.74-5.00	1.00-3.00	1.89-2.71	3.00-5.00	3.65-4.58
4	Provision of materials to const.site	3.00-4.00	3.52-3.98	4.00-5.00	4.56-5.00	3.00-5.00	3.29-4.11	3.00-4.00	3.23-3.77
4	Compatib. with other const. activities	3.00-5.00	3.55-4.45	3.00-5.00	3.90-4.77	2.00-4.00	2.48-3.12	3.00-5.00	3.29-4.11
5	Aesthetics	3.00-5.00	3.55-4.45	3.00-5.00	3.81-4.56	3.00-5.00	3.44-4.19	3.00-5.00	3.44-4.19
5	Conceptual design of the bridge	8.00-9.00	8.00-9.00	8.00-9.5	8.00-9.50	7.00-8.50	7.00-8.50	8.50-9.00	8.50-9.00
5	Adequacy to landscape	3.00-5.00	3.89-4.71	4.00-5.00	4.46-4.94	1.00-4.00	2.18-3.28	3.00-5.00	3.66-4.54
5	Adaptability to the enviroment	8.50-9.00	8.50-9.00	8.50-9.50	8.50-9.50	7.50-8.50	7.50-8.50	7.50-8.00	7.50-8.00
5	Slenderness	31.7-37.7	31.7-37.7	20.3-26.3	20.3-26.3	34.7-41.7	34.7-41.7	21.3-28.3	21.3-28.3
6	Safety of the construction system	3.00-5.00	3.44-4.19	4.00-5.00	4.38-4.89	3.00-4.00	3.70-4.05	3.00-5.00	3.56-4.26
6	Safety of specific works	2.67-4.78	3.35-4.24	3.20-4.60	3.61-4.22	2.60-5.00	3.33-4.31	3.00-5.00	3.77-4.51
7	Adaptability to unexpected problems	2.00-3.00	2.72-3.06	2.00-4.00	2.41-3.19	3.00-5.00	3.46-4.34	2.00-4.00	3.67-2.88
7	Yield of construction system	14.0-18.0	14.0-18.0	35.0-40.0	35.0-40.0	15.0-20.0	15.0-20.0	55.0-60.0	55.0-60.0
8	Durability of structure	1.00-5.00	1.00-5.00	5.00-9.00	5.00-9.00	5.00-9.00	5.00-9.00	5.00-9.00	5.00-9.00
8	Inspection facility	7.00-7.50	7.00-7.50	9.00-10.00	9.00-10.00	9.00-10.00	9.00-10.00	8.50-9.00	8.50-9.00
8	Aesthetics	9.00-9.00	9.00-9.00	10.00-10.00	10.00-10.00	8.50-8.50	8.50-8.50	8.00-8.00	8.00-8.00
8	Simplicity of design	4.00-4.50	4.00-4.50	6.00-6.50	6.00-6.50	6.50-6.50	6.50-6.50	7.50-8.50	7.50-8.50
9	Inspection cost	150-164	150-164	133-144	133-144	138-156	138-156	110-130	110-130
10	Maintenance cost	225-246	225-246	199-216	199-216	227-234	227-234	170-200	170-200
11	Construction cost	750-820	750-820	665-720	665-720	690-780	690-780	700-730	700-730

Table 2 Deck bridge basic criterion values

The final result of the classification is in table 3, showing that the most appropriate in this case is the launching alternative (B).

Ranking	Construction alternatives	Final value
1	"B"	0.561
2	"D"	0.462
3	"C"	0.409
4	"A"	0.389

Table 3 Ranking of design and construction alternatives

6 Conclusions

1. The paper presents the most important features of the proposed fuzzy combined programming method. The method can be applied to determine the most feasible structural system and construction technique to be used in highway prestressed and composite bridges as a function of the input-values (design constraints) for each specific case.
2. The model can be applied separately (deck, piers and abutment) or in a complete way, according to the design constraints of the location.
3. It can be used as a tool to evaluate construction options, since permits to change the values of the basic criteria and adjust the importance W to specific constraints.

7 Acknowledgements

The research has been financially supported by the Spanish Ministry of Education (*Dirección General de Enseñanza Superior*) through Research Project PB95-0769.

8 References

[1] Zadeh, Lofti Asker (1965) "Fuzzy Sets" *Information and Control* 8, 338-353.
[2] Zadeh, Lotfi A. (1975) "Fuzzy Sets" *Encyclopedia of Computer Science and Technology* 325-363.
[3] Terano, T./Asai, K./Sugeno, M. (1992) "Fuzzy Systems Theory and Its Applications" *Academic Press.*
[4] Ramírez M., "Decision making in design and construction of bridges using fuzzy logic" *Doctoral Thesis. Technical University of Catalonia* (in progress)
[5] Dong, Wimin/Sha, Haresh C. (1987) "Vertex Method for Computing Functions of Fuzzy Variables" *Fuzzy Sets and Systems* 24, 65-78.
[6] Paek, J.H./Lee, Y.W./Napier, T.R. (1992) "Selection of Design/Build Proposal Using Fuzzy-Logic System" *Journal of Construction Engineering and Management*, ASCE,118(2), 303-317.
[7] Saaty, T.L. (1996) "The Analytical Hierarchy Process", University of Pittsburgh.
[8] Chen, Shan-Huo (1985) "Ranking Fuzzy Numbers with Maximizing Set and Minimizing Set" *Fuzzy Sets and Systems*, 17, 113-129.

A Proposal in Steel Arch Bridge Design: The Stayed Lonely Arch-Rib

Francesco CAFARELLA
Full Prof.
Dept of Structural Eng.
Pisa, Italy

Walter SALVATORE
Res. Eng.
Dept of Structural Eng.
Pisa, Italy

Francesco Cafarella, born in 1936, is Prof. of Theory of Structures since 1980. He is involved in several researches regarding long span bridges, safety and reliability of civil structures.

Walter Salvatore, born in 1966, got PhD degree in 1997. He is involved in several researches regarding bridges, fatigues, safety of civil structures, damage in reinforced concrete structures, vibration control.

Summary

In the paper we suggest a new way to secure the arch-ribs of bridges of the Langer-girder type against transversal wind and spatial buckling. In analogy with the stayed-column design concept, the load capacity of curved slender rods subjected to high compressive stresses can be increased by equipping them of an assemblage of prestressed stays and rigidly connected crossarm members. We present many possible patterns of stay and crossarm arrangement. A representative arch-bridge structure with single central stayed arch-rib is analysed up to the collapse by a nonlinear elasto-plastic finite element method.

1. Introduction

The deck-stiffened tied arch, in its through-type version, is an attractive and efficient device for highway and railway bridges, in the medium-span range up to the bottom of the large-span range (about 300 m). It is particularly suitable and may offer the best engineering solution if the site is wide-sweeping and the subsoil conditions are rather difficult and could be preferred in terms of costs, ease of erection, short construction time and minimised environmental impact. Many impressive realisations in the last decades and recent years (e.g. [1], [2], [3], [4]) confirm the validity of the solution in satisfying, with different configurations, the requirements of strength, feasibility, aesthetics and economy.

The continuing success of the tied-arch bridge in the modern engineering is strongly influenced by aesthetic purposes: the intrinsic beauty of the elegant sweep of the arches, the spatial arrangement of the slender suspenders, the clean-lined appearance of the thin girders have a great potential to lead to striking pieces of structural Architecture.

However, the pronounced trend toward lighter bridges, with more slender arches, and the increasing traffic demands, both of number of traffic lanes and size of traffic loads, make the problems of the overall stability of such bridges more acute.

Since the in-plane stability of the arches is not usually of concern, the main challenge for the designers lies in creating a lateral bracing system rational, reliable and not overwhelming. Really, the least satisfactory aspect of the trough-type arch bridges is sometimes the boring impact of the overhead structural mass visible from the deck, a tunnel-effect unattractive as well as unsafe for

drivers.
The aim of this paper is to suggest a new type of wind-bracing of the arches: cross-arms cantilevering from the arch-core and taut, high strength, cables generate a their own spatial truss, *the cable-stayed arch*, a new structural form that express lightness.
Our proposal is for a synthesis of a tied arch, carrying the vertical load, and of a cable stayed system, for the horizontal stabilisation of the arch-rib, with a natural visual elegance.
The innovative system could also be used to upgrade many existing bridges to deal with increased vehicular loading following changes in road transport.
We will give a first insight into the behaviour of the proposed lateral bracing system, attempting to clarify its true role through an elasto-plastic spatial analysis, considering the influence of finite deflections and inevitable structural imperfections.

2. The Stayed Arch Bridge

The earliest form of the "Langer girder" [5] has been subjected to several refinements, with primary concern in finding handsome solutions for the stiffening of the arch ribs against wind and buckling.
A determinant improvement of competitiveness has been attained by the adoption of self-standing arches, located in the central strip of the bridge or laterally to the deck. The arches obtain the necessary transverse stiffness through stocky cross section, either flat rectangular or tubular twinned, and the result is an awkward visual impact at the bridge access ([2], [3]).
A new impetus, mostly centred in Japan, took place in the last years with bridges of "basket-handle" type [4]. A number of long span "Nielsen-Lohse" bridges have been constructed, in which the deck is carried by a lattice of crossed hangers and the twin lateral arches are inclined inwardly and connected by few – or just one or two – bracing struts near the crown. In spite of the obvious advantages of the solution, the appearance of the bridge is rather cumbersome.
Seeking to find new paths for the lateral bracing of arches rising above the deck, we propose an innovative conception of the arch itself, which is planned as *self-braced.*
It has been shown that the strength of a centrally loaded slender column may be increased many times by reinforcing it with three or four identical planar stay frames, evenly spaced around and rigidly connected to the core by simple radial spokes or bipods ([6], [7]).
Arch bridge ribs are spatially curved slender rods subjected to high compressive stresses: hence their load capacity can be enhanced, in analogy with the columns, by equipping them of an assemblage of prestressed stays and rigidly connected crossarms members (stayed column concept towards stayed-arch concept). The preloaded stays, placed side by side to the arch, integrate its transversal and torsional stiffness.
Many patterns of stay and crossarm arrangement are possible, for a variety of structural forms.

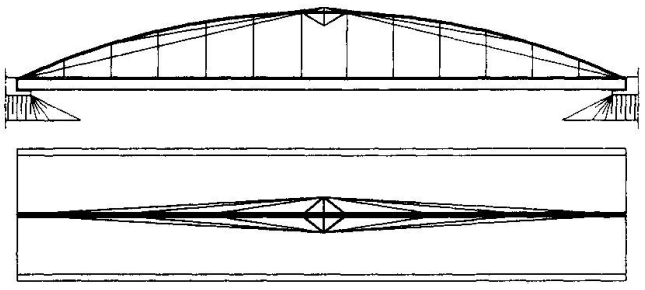

Fig. 1

The simplest but effective staying system presents a double three-dimensional arrangement of the stays fanning from "tripods" (spatial trusses) cantilevering from the crown of the arch (fig. 1). Also with a width-to-span ratio as low as 1:20, by the connection of the top of the arch with the ends of the stiffening girder at bearings, the out of plane rigidity is considerably increased and the propension of the

arch to buckle out-of-plane is contained by the torsional restraint of the mid cross-section.
If the crossarms provide intermediate supports to the stays in many sections along the central line of the arch (fig. 2), we achieve a good lateral supporting with little bending in the arch and the tie in consequence of the tensioning of the cables.
A totally innovative unusual shape – structurally quite plausible – presents arches tilting from the vertical outwardly while crossarms inclines inwardly (fig. 3) so that visual flight lines are balanced.

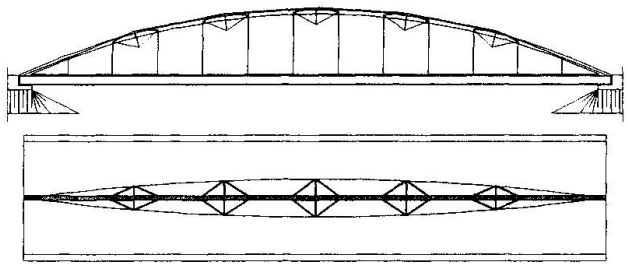

Fig. 2

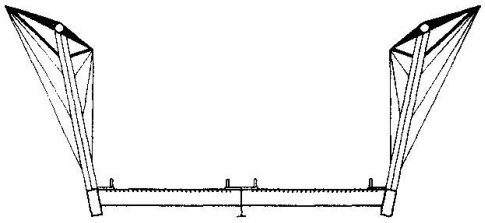

Fig. 3

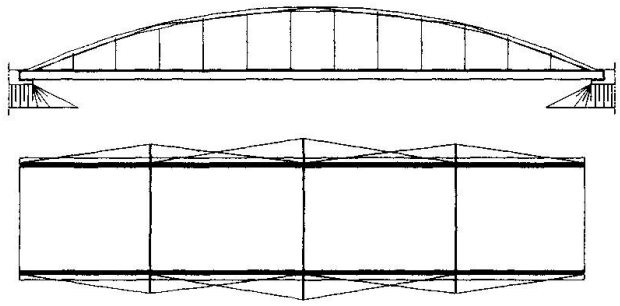

Fig. 4

For twin ribs, upper lateral bracing of Vierendeel type becomes very light when integrated by lateral staying (fig. 4), leading to a better acceptance of structural members above the carriageway.
In the basket-handle type bridges, the outward concavity of the horizontal projection of the arch ribs naturally receives the stay bracing (fig. 5) for an optimum location and rigidity of wind bracing.
It is noteworthy to point out that a peculiar characteristic of the tied-arch bridges is the possibility to adjust, during the erection, the axial forces in hangers, in order to control the bending moment diagrams [2]. Since the staying of the arches increases the internal statical indetermination of the structure, it is apparent that the cable-force adjustment calls into play further degrees of freedom for the load balancing operations.

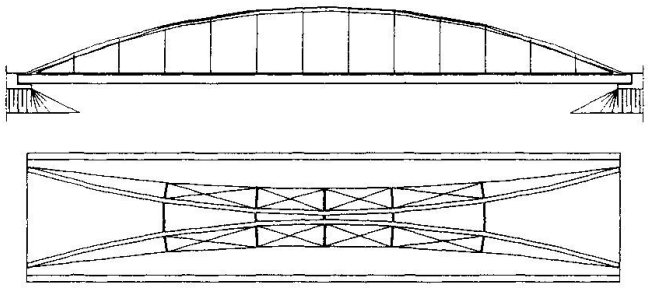

Fig. 5

3. Case Studies

We present in some detail two expressive examples of staying to horizontal straightening of tied arches: bridges studied are representative of typical arch structures actually constructed.
To visualise a comparison between the existing bridges and their proposed enhancement, we created computer renderings with almost photographic level of realism.

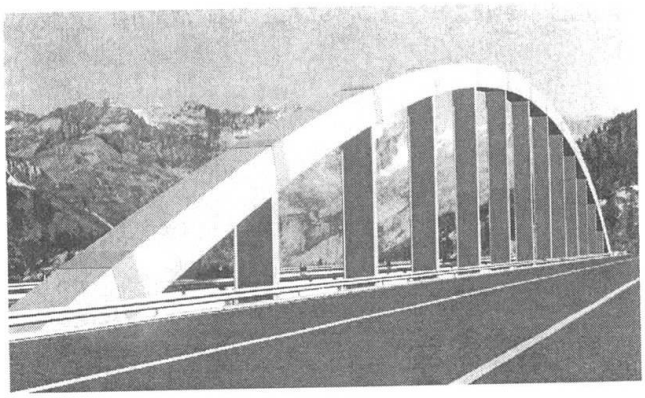

Fig. 6

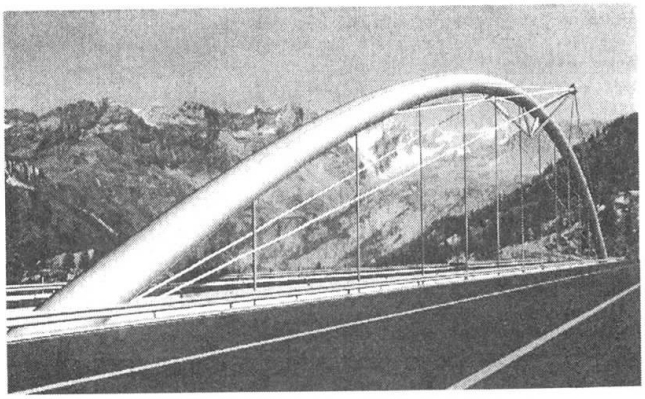

Fig. 7

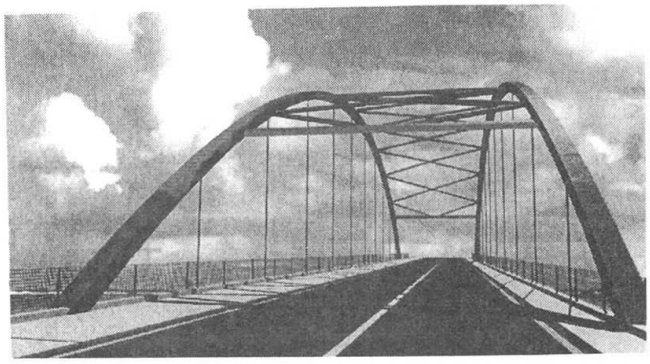

Fig. 8

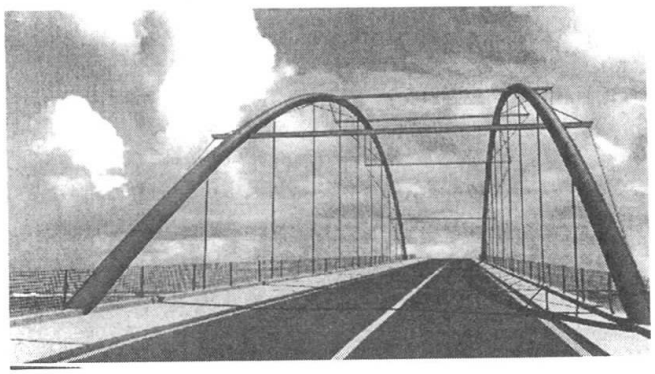

Fig. 9

The first case focuses on a highway bridge of the central-arch-girder type [8]. The heavy requirements for eight lanes of traffic resulted in a relevant beam depth and stocky cross-section of the arch-rib (fig. 6). Broad steel plate hangers seemed necessary to ensure the out-of-plane stability of the arch: looking at the structure while crossing the bridge shows little of anything but masses of columns.

Main features of the suggested variant are (fig. 7): a more slender tubular arch-rib – with slower drag coefficient for wind load -, thin high-strength hangers made of parallel wire strands and a "diamond shaped" crown lattice that supports the spatial fan of stays, of the type of fig. 1, for the lateral bracing of the arch. The total effect is obviously much more handsome.

Fig. 8 shows a beautiful town-arch-bridge carrying four lanes and walkways [9]. An upper lateral bracing of the twin arches of the double Warren truss type were adopted, with flat box sections for the end-portal-frame and tubular sections for the diagonals.

Although the upper truss appears a refined solution, it is busy with its diagonal members extending over most of the span. The modified design (fig. 9) adopts a transparent wind bracing without diagonal members, high lateral stiffness being provided by the side stays. The mainly aesthetic choice leads to a dynamic spatial structure.

4. Ultimate Strength of Stayed Arches

The strength of unbraced or traditionally braced steel arches is an intricate problem to which only recently several important researches have been devoted with almost exhaustive conclusions. In particular, the Japanese school of arch-bridges designers developed comprehensive numerical studies and parametric analysis on the load carrying capacity of actual arch-bridges by an

accurate F. E. approach ([10], [11], [12]). Design recommendations and formulas have been proposed for the prediction of the ultimate strength of through-type steel arches that fail by lateral instability.

The mayor findings that are brought out by such numerical analysis, with respect to the general behaviour of stiffened arch-bridges loaded to the ultimate state, can be summarised as follows:

i. Bifurcation approach to the out-of-plane stability is inadequate: linearized buckling load appears almost as a purely mathematical concept;
ii. The only possible accurate approach to the safety assessment against ultimate load is an elasto-plastic and finite displacement analysis of a three-dimensional model, taking account of initial out-of-plane imperfections, residual stresses, tilting loads of the hangers, horizontal loads. With it, the behaviour of the system may be traced from the erection stage until the maximum load capacity, determinate by deflection divergence, in a complex interaction of in-plane and out-of-plane instability.

Nearly unexplored is the field of the design concepts of prestressed load-bearings curved bars in compression, in which hogging frames and tension ties introduce at several points along the length of the central core restraints against lateral translations and rotations.

A lot of problems still remain unsolved also for the simplest case of stayed columns. From a literature review ([6], [7]), again it appears that an elastic stability analysis, linear or nonlinear, produces uncertain results, while the large displacements nonlinear elasto-plastic analysis (considering the initial core crookedness, errors in stay prestressing, the possibility of stay slackening, residual stresses and lateral loads) is an indispensable tool.

On the ground of these considerations, it seems obvious to infer that the load carrying capacity of arch-ribs stiffened by stay frames can only be understood and accurately determined by finite element analysis, including geometrical-mechanical changes in the structure until the collapse.

We present here an example of such ultimate strength analysis, applied to the central-arch girder bridges of figures 6 and 7. With the aim of a comparison of the performances of the existing bridge and of the proposed stayed-arch variant, we used the standard finite element package ADINA [13], containing all the features needed to manage an efficient nonlinear frame analysis.

The bridges are idealised as three-dimensional framed structures (fig. 10); in the simulation, the

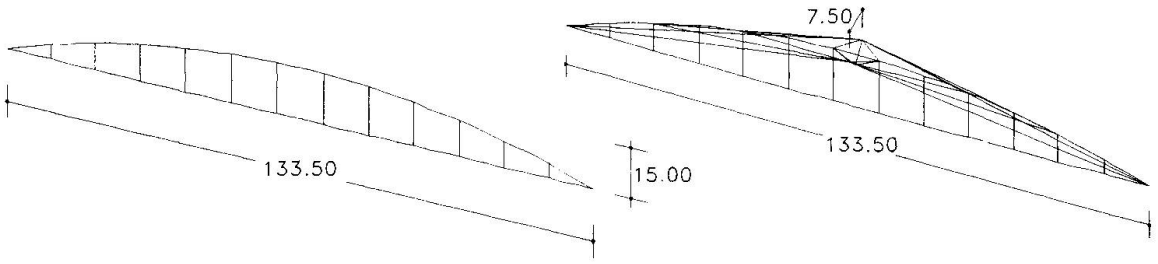

Fig. 10

arch ribs and the I-shaped hangers have been modelled by beam-elements in which elasto-plastic and large displacements behaviour can be taken in consideration, the stiffening girder by large displacement elastic beam elements ([12]) and the cables as truss nonlinear elastic elements supporting tensile but not compressive loading.

The arch members of the actual bridge have been modelled with thin walled circular cross section having about the same cross-sectional properties as the original ones; the cross section of the arch rib and the central "diamond shaped" spoke in the variant have been designed with pipe sections. The characteristics of the various members are summarised in table 1.

The material properties were represented by steel stress-strain curves from EC3, part 2: Steel Bridges (for the girder and the arch ribs Steel Grade S 355 H).

Imperfections in initial geometry of the arch ribs similar to the first buckling mode, derived from

a linearized buckling analysis, has been introduced, with a value of the horizontal eccentricity at the crown of 1/1000 of the span. Moreover, an initial configuration with very reduced bending moments in the upper and lower chords of the bridge has been heuristically realised in the numerical models, subjected to dead load and prestress forces introduced in the hangers and the stays, by the ADINA "initial strain" option: from this configuration began the incremental nonlinear analysis under increasing live loads.

	Arch rib	*Girder*	*Hangers*	*Stays*
Actual bridge	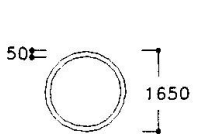	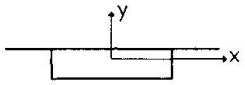 $J_x = 1.2254\ m^4$	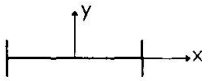 $J_x = 0.00037\ m^4$ $J_y = 0.01771\ m^4$	
Proposed bridge	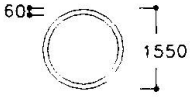	$J_y = 68.1990\ m^4$ $J_t = 0.4159\ m^4$	PWS 163 ϕ 7.11	PWS 121 ϕ 7.11

Table 1

Traffic loads on bridges were assumed in agreement to Eurocode 1, Part 3, as in fig. 11 (eight notional lanes on the carriageway, load model 1 over the full span, each tandem system having an axle at midspan).

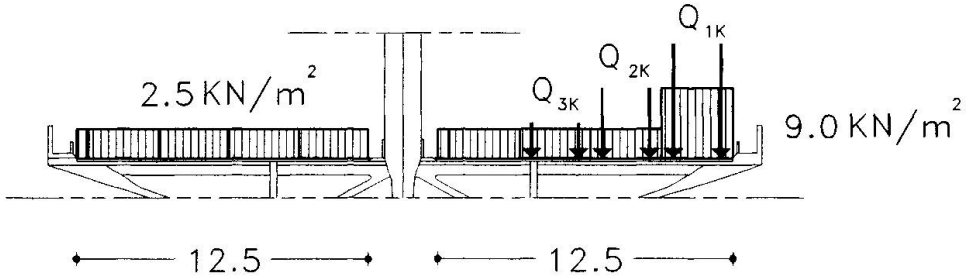

Fig. 11

The structure is examined subjected to both vertical and horizontal loads: the service wind load is 1.0 kN/m^2 on exposed surfaces. Two loading paths are investigated in checking for ultimate limit state: 1) dead load, increasing road traffic load proportionally to a load parameter, wind load; 2) dead load, increasing wind load proportionally to a load factor.

The calculated load parameter versus deflections curves at the crown of the arch-rib in the two cases are shown in figures 12 and 13.

At the ultimate state, extended plastic zones are present, spreading from the springing of the arch-rib; diagrams confirm the remarkable effect of the stays on the ultimate strength of the stayed arch.

The stay-stresses and load-factor relationship is shown in fig. 14 for load combination 1): it is noteworthy that to the evanescent tension in some stays does not correspond the maximum load carrying capacity; it is evident, also, the complex and unpredictable spatial interaction of the various members of the structure.

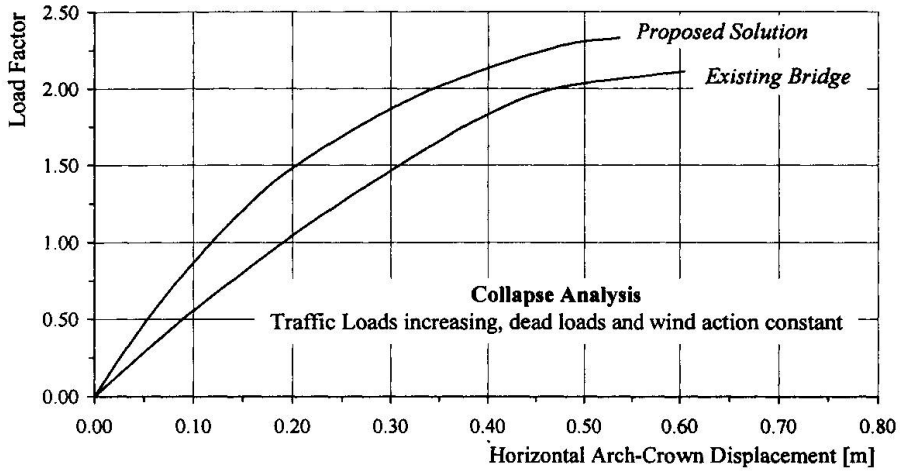

Fig. 12

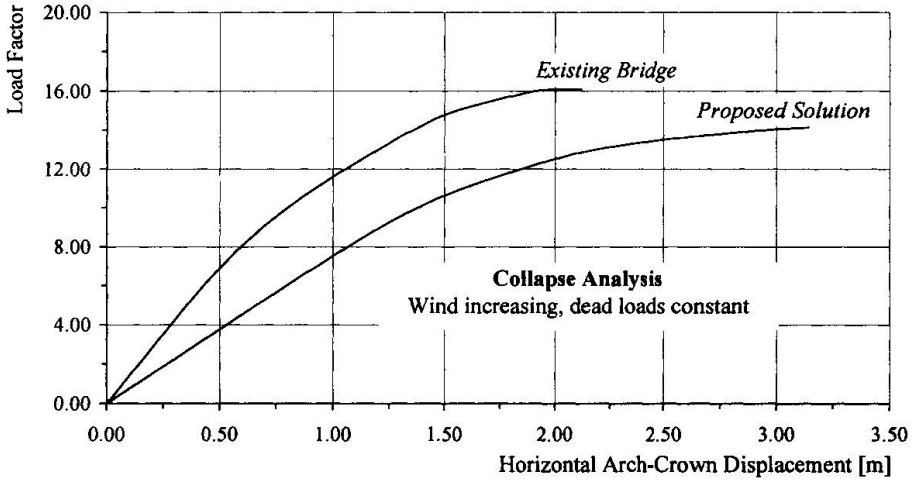

Fig. 13

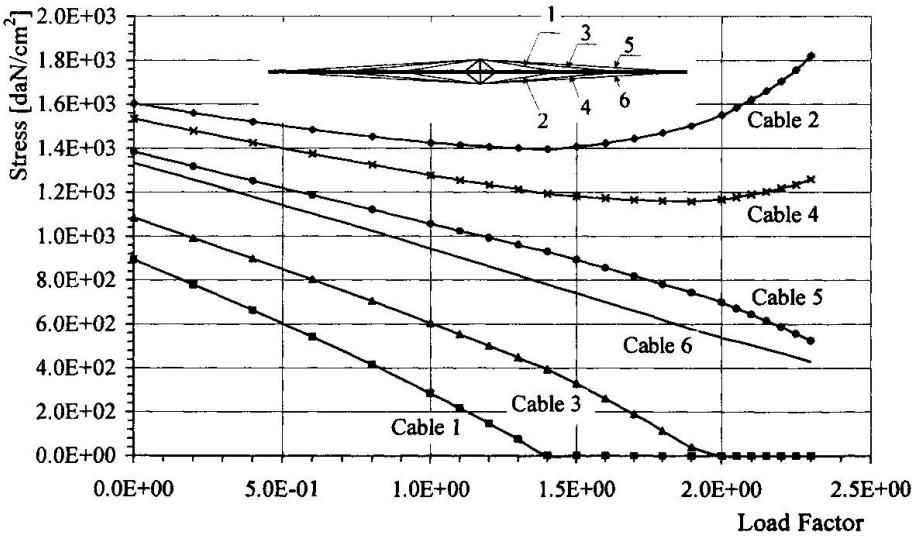

Fig. 14

5. Conclusions

The proposed stayed-arch is a composite structure in which a curved slender beam-column (the arch-rib) is stiffened against overall out-of-plane buckling by high strength prestressed stays, supported by crossarms cantilevering from the core.
Technically, such combination of elemental components results in a good design concepts; aesthetically, in a through-type arch-bridge this arrangement, which substitutes the cluttering traditional wind-bracing, leads potentially to an elegant appearance.
The ultimate load-carrying capacity of a representative example of stayed central-arch-bridge has been studied: the development of the structural idea needs obviously deeper researches and field verifications.

References

[1] Hartwig, H., J.: Die Kaiserleibrücke, *Der Stahlbau*, 4, 1965
[2] Stein, P., Wild, H.: Das Bogentragwerk der Fehmarnsundbrücke, *Der Stahlbau*, 6, 1965
[3] Carl, J., Hilbers, F., J., Meyer, H., Wiechert, G.: Die Donaubrücke Regensburg-Schwabelweis, *Der Stahlbau*, 1, 1982
[4] Yoshikawa, O., Sugiyama, I., Kurimoto, H., Aketa, H.: Construction of the Shinhamadera Bridge, *Der Stahlbau*, 5, 1993
[5] Leonhardt, F.: *Bridge. Aesthetics and Design*, The Architectural Press, London, 1982
[6] Temple, M., C., Prakash, M., V., Ellis, J., S.: Failure Criteria for Stayed Columns, *Journ. of Struct. Eng.*, vol. 110, n. 11, november, 1984
[7] Jemah, A., K., Williams, F., W.: Parametric Experiments on Stayed Columns with Slender Bipods, *Int. J. Mech. Sci.*, vol 32, n.2, 1990
[8] Beer, H., Müller, Th.: Eine Mittelträger-Stabbogenbrücke über die Salzach, *Der Stahlbau*, 11, 1970
[9] Wiechert, G., Boch, R.: Die Franz-Josef-Strauss-Brücke in Passau, *Der Stahlbau*, 7, 1989
[10] Yabuki, T., Vinnakota, S.: Stability of Steel Arch-Bridges. A State of the art Report, *S.M. Archives*, 9, 1984
[11] Sakimoto, T., Sakata, T.: The Out-of-plane Buckling Strength of the Through-type Arch Bridges, *J. Construct. Steel Research*, 16, 1990
[12] Nakai, H., Kitada, T., Kunihiro, M., Kitazawa, M., Hasino, F.: Proposition of Methods for Checking the Ultimate Strength of Arch Ribs in Steel Nielsen-Lohse Bridges, *Der Stahlbau*, 5, 1995
[13] ADINA, *Theory and Modeling Guide*, ADINA R & D, Inc., Watertown, MA 02172 USA, 1995

A Large Arch Bridge Using Concrete Filled Steel Tubular

Li TAO
Vice-Chief Eng.
Ministry of Railway
Lanzhjou, China

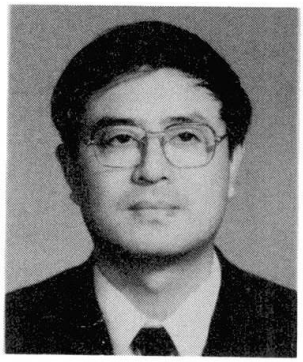

Li Tao, born 1957, received his civil eng. degree from the South-Western Jiaotong Univ. in 1982. H is currently senior eng. (prof.) and vice-chief eng. of Bridge and Tunnel Dept.

Summary

A large highway arch bridge with its one span of 160 meters,across the Huangbai River was built on the main road leading to the Yangtze Three Gorges Project in 1996.
The arch rib of this bridge was built on concrete filled steel tubular (CFST) along the river bank, then turning with a balance weight to locate on the bridge site. It is the longest-span bridge of this kind constructed by new method in China today.
This paper not only introduces the static and dynamic analysis of this highway arch bridge, but also discusses the new constructional method of arch ribs turning with a balance weight.
Several structure models have been tested in the laboratory to testify the safety of the bridge. It proved that the construction method and CFST are more suitable and more efficient for the arch bridge.

1. Introduction of the Bridge and Main Technical Standards

The Huangbai River Bridge lies in Hubei province of China and it crosses the Huangbai River, the main sub-stream of the Yangtze River. It belongs to one of the most important water conservancy junction engineering items on the transportation highway of the Yangtze Three Gorges Project in China. Its surface width of water is 150m, the design volume is 500 m^3/s, its depth is 15m and the geological character of the river is arenaceous limestone.
The surface of the bridge is 18.5m wide. The design loading is the automobile team 36-grade standard of China, 4 tracks every row, the weighe of every automobile is 56t, and the checking loading is 200 tons every trailer.
The type of the whole bridge is 4 × 20m PC beam bridge + 160m arch bridge + 20m PC beam bridge and the bridge foundation is on the arenaceous limestone(see fig.1).
The construction of the bridge was set about in 1994 and completed to have traffic in 1996. This bridge plays an important role in the construction of the Yangtze Three Gorges Project(fig.2).

2. The Structure Feature of the Arch Bridge

The CFST was used in the arch bridge. It is the longest-span bridge of the concrete filled steel tubular in China and its arch span is 160m, arch rise is 32m and arch axis coefficient ***m*** is 1.543.
The steel tube diameter ***d*** of arch rib is 1000mm, the wall thickness of the steel tube at arch springer is 12mm and the thickness of other parts is 10mm. The steel tube, whose diameter ***d*** is between 100 and 600mm is used in the connecting constructional elements between the ribs(Fig.3).
The steel tube,whose diameter ***d*** is between 600mm and 800mm is used in the arch column. The wall thickness of steel tube is 12mm and the largest heighe of columns is 27m.
The 16 Mn steel plate was rolled to make the steel tube and 50-grade concrete was filled in the steel tube. Thus the steel-concrete combination structure was formed.
The arch seat foundation was designed into the upper and the lower two parts. The diameter of the middle rotational hinge was 2.2m, the lowe part foundation was reinforced concrete structure and the upper part was prestressed concrete structure.
The bollow pier was designed above the foundation in particular in order to have the balance weight. While constructing, water was filled inside the hollow pier so that the balance system was formed. The plate beam structure of 13m and 14m span was used in the arch beam.

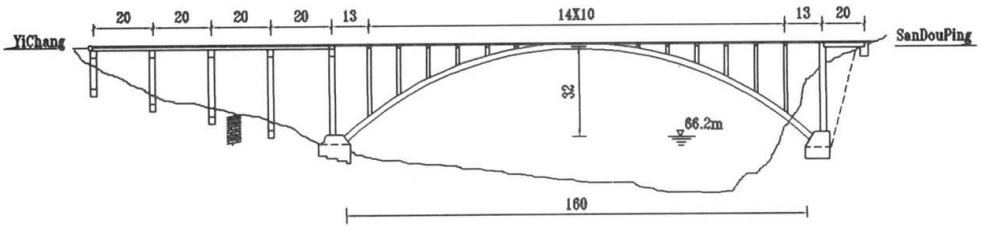

Fig.1 The whole sketch of the Huangbai River Bridge
(Unit:m)

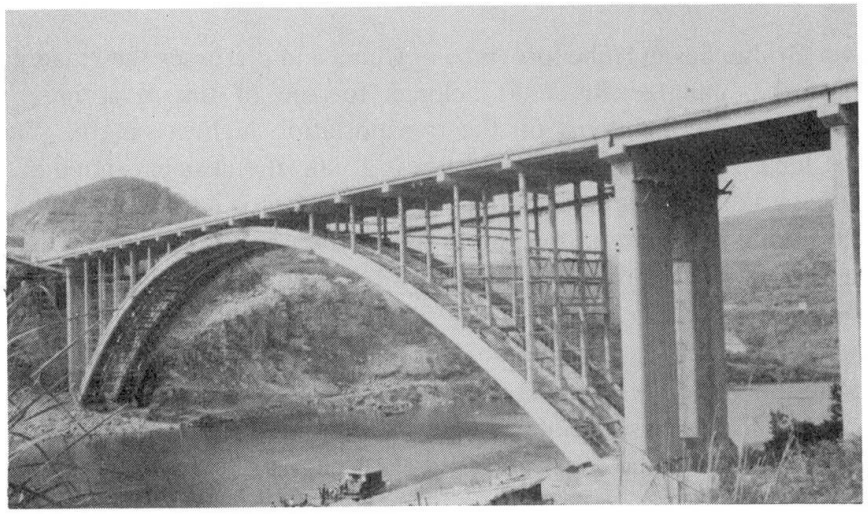

Fig.2 The Huangbai River Bridge

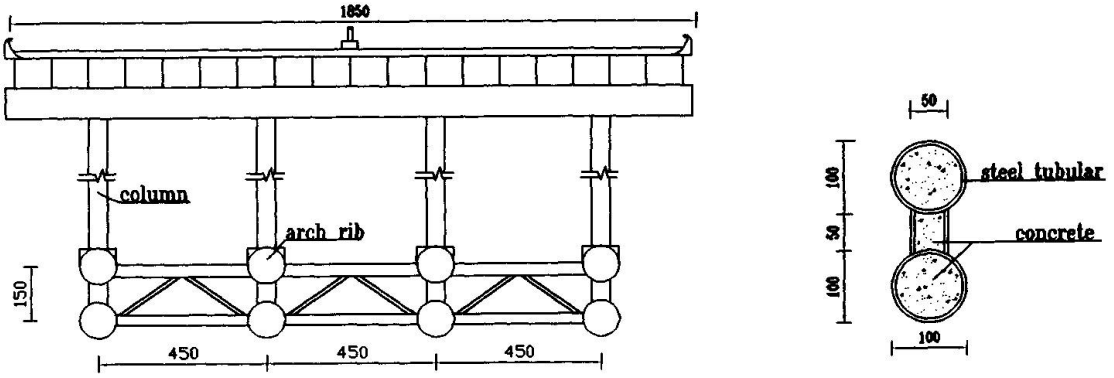

Fig.3 Arch bridge structure cross section
(Unit:cm)

3. The Calculating Method of the Arch Bridge and Its Main Results

3.1 Structural Load-bearing Capacity

The Finite Element Method is used to perform spatial mechanics analysis and the structural internal forces are gotten under 24 kinds of loading condition. The structural design load-bearing capacity is judged according to China's "Specification for Design and Construction of Concrete-filled Steel Tubular Structures" (CESE 28:90)while designing.
The formula of design load-bearing capacity for the elements is:

$$N_u = \phi_1 \phi_2 N_0 \tag{1}$$

where, N_u=design value of bearing capacity for CFST member;
N_0=design value of bearing capacity for short column the axial compression;
ϕ_1=the reduced coefficient considering the influence of slenderness ratio;
ϕ_2=the influence of axial eccentricity.
The load-bearing capacity should meet the following:

$$N \leqslant N_u \tag{2}$$

Where, N is the design value of axial compression force.

3.2 Structural Non-linear Influence

The combination of the Increment Method and Newton-Raphson Method is used in the non-linear calculation of structural analysis. The calculation results are very close to that of the linearity and the error is among 2-3%.

3.3 Seismic Checking

The seismic force of bridge structures is calculated according to 7 earthquake intensity degree.
The first three natural vibration periods of the arch bridge structure are as follows:

T_1 (S)	T_2 (S)	T_3 (S)
0.979	0.822	0.607

The arch rib footing is the most dangerous part of the structure when earthquakes occur and its axial force N is 64KN, bending moment M is 154KN-m , which is much smaller than the internal force induced by automobile loading. It indicates that such kind of structure has good seismic capacity.

4. The Construction Erection Method of the Arch Bridge

In order to avoid the assignments such as instalment and welding of steel structure in the air and to take advantage of the geographical position of the bridge site as well as the features of the lighter weight of hollow steel tube and its higher strength, the flat surface swing method was used in the construction of the arch bridge. The weight of swing body is 3600 tons, which is the heaviest bridge swing body in China. The construction sequence is as follows:

(1)The steel tubes of about 2 meters long were manufactured in the factory, then were welded into 10 meters long members and sent to the bridge site. They were erected on the built supporting framework and the mountain body in opposite direction.
(2)Held fast the prestressed "tie". Filled water in the hollow pier so that the balance system was formed and was able to rotate on the flat surface; rotated 180 degrees and 105 degrees, and the bridge members were thus linked into a whole body (Fig. 4, Fig. 5).

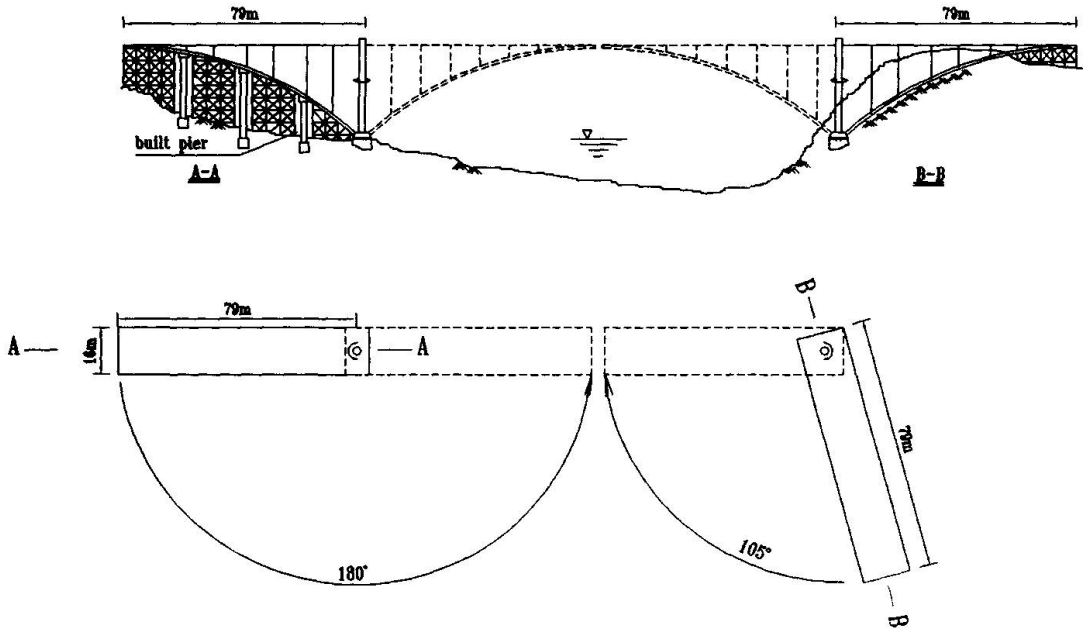

Fig.4 To rotate the arch rib

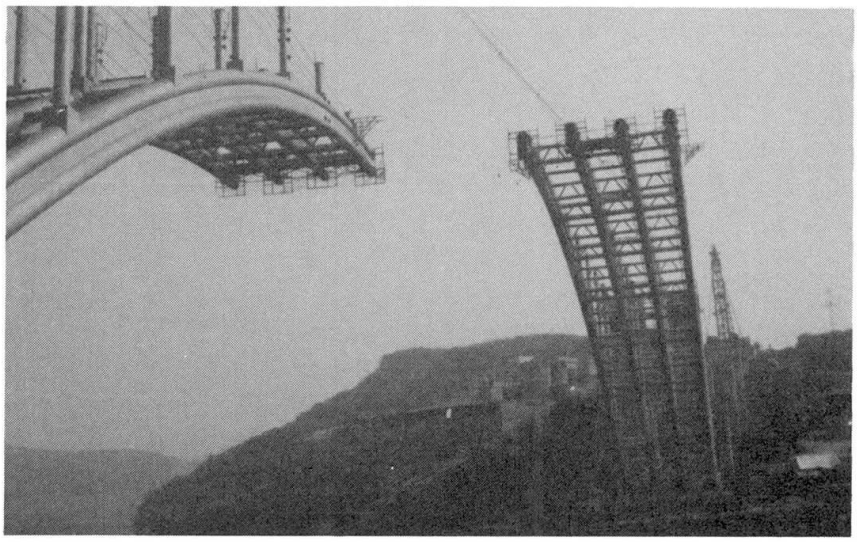

Fig.5 The arch rib turning

(3)Pour concrete so that the arch springer is fixed. Fill concrete to the steel tubular structure. After the strength of concrete was gained, the slab beam on the arch was erected and the floor system was laid and installed.

5. Structral Experiment in the laboratory

5.1 Comparative Model Test of Bearing Capacity of The Arch Rib Cross-section

The aim of the test is to study the mechanical influence of the mid-hollow concrete between the arch rib on the whole structure. The breaking tests of A-type and B-type member were carried out (Fig.6). The similar ratio between the model and the actual members is 1:5. The results of the test indicated that under the same loading, the deformation of B-type members is the same as that of the A-type, but the shear force of the steel plate is double. A-type was used to insure the safety in practical construction.

5.2 Stability Model Test of The Compressive Member of CFST Arch Columns

The ratio of length and the diameter of the CFST arch column λ is L/d=34. In order to keep the stability of the column under the axial loading, the breaking test of the model under the axil centre compression was performed. The results indicated that under the biggest design loading the safety coefficient of the column K was 1.9, which is in correspondence with the calculating results of the actual bridge in design.

5.3 The Fatigue Test for The Surface Protection Course of The Steel Tube

The spray aluminiurm protection layer was used on the surface of the steel tube and the model fatigue test was performed. The results indicate that the performance of the protection course on the surface of the steel tube will be in good condition within 20 years.

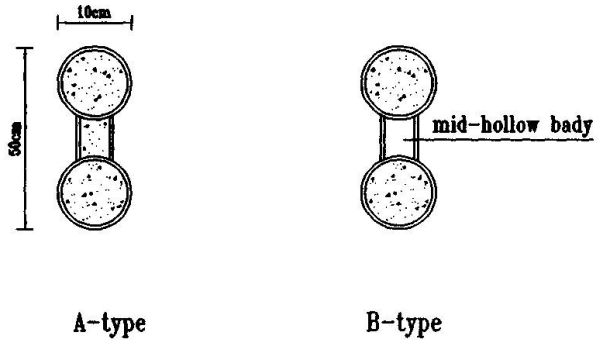

Fig.6 The section of arch rib model

6. Conclusions

It has turned out that there are some excellent advantages of using CFST in the bridge engineering. From the year of 1990, this kind of structure has been used, or is being constructed or is being designed in 37 bridges. The completion of the Huangbai River Bridge makes the study of the CFST develop a lot in the fields of the bridge engineering.

Reference

1."Specification for Design and Construction of Concrete-filled Steel Tubular Structures" (CECS 28:90)(in Chinese), The Planning Publishing House of China. 1992.

2.Shangtong Zhong. "Concrete Filled Steel Tubular"(in Chinese), Scientific and Technological Publishing House of Hei Long Jiang, 1994.

Study of Cable-Stayed Bridges for Pipelines

Deena NATH
Dr Eng.
College Gorakhpur
Gorakhpur, India

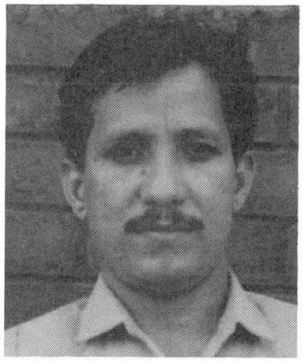

Deena Nath Mishra , born 1958 received his civil Eng. degree from K.N.I.T. Sultanpur and obtained his masters and doctoral degree from Univ. of Roorkee (India). He is a senior faculty member and reputated structural Engineer of Civil Engineering Dept. M.M.M. Engineering College Gorakhpur.

Summary

Cable-stayed pipeline bridges have very high vertical stiffness but due to their small width and the probability of coinciding there resonant frequency with the peak of horizontal gust spectra, they are vulnerable to wind gust loading. In this work a special emphasis has been laid to investigate the effect of horizontal stiffening system arrangements using cable and cable trusses of different configurations along with aerodynamic and seismic analysis.

1. Introduction:

Cable Stayed pipeline bridges (CSP-Bridges) are generally narrow needing additional stiffening in the horizontal plane. They are vulnerable to wind gust loading due to their small width and the fact that their resonant frequencies coincide with peaks in the horizontal gust spectra. As in any cable stayed bridge, it has inclined stays emanating from one or more points in the pylons and holding the deck of the bridge at intermediate locations between the main supports, thus imparting a high degree of vertical stiffness to the bridge.Since a few studies (5,6,7,8,9,10,11) are only available on the CSP- bridges the designer has little guidelines available for selecting the geometry of the bridge and the sectional properties of its elements. keeping in view the size of the pipeline and access required for repair and maintenance gangs, the width of the bridge has been considered between 2.5m and 7.5m, yielding main span to width ratio in the range of 25 to 35.

2. Bridge Types

Two types of bridges have been taken for the study as shown in Fig. 1.
Type-A: Single span with towers at the ends, as used in the hills and,
Type-B: Three span with towers in between,as commonly used in the plains.
In Type-B Bridges two cases have been studied:

i. Without any horizontal "offsets" at the towers for supporting the stiffening cables and

ii. with an "offset" projecting horizontally at right angles on both sides of the bridge axis at the tower locations and supporting the stiffening cables.

A bridge span range of 50m to 400m total span (main span 50m to 200m for Type-A and 55m to 220m for Type-B) has been considered, which is close to the reported economical span range of 90m to 270m for cable stayed bridges (8,9).

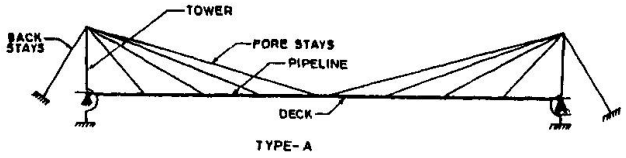

TYPE-A

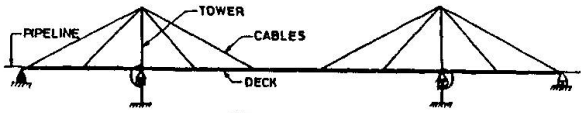

TYPE-B

FIG.1 ELEVATION OF CSP-BRIDGES

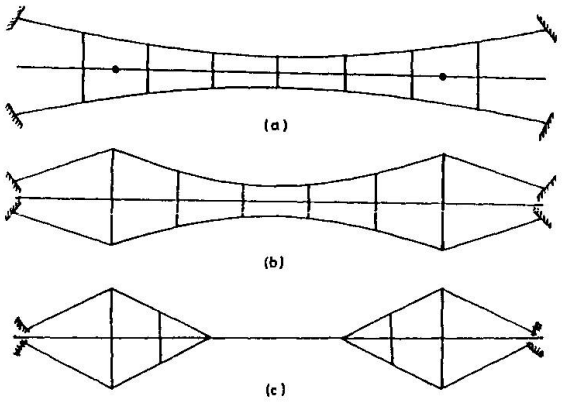

(A) VARIOUS FORMS OF STIFFENING CABLE TRUSSES

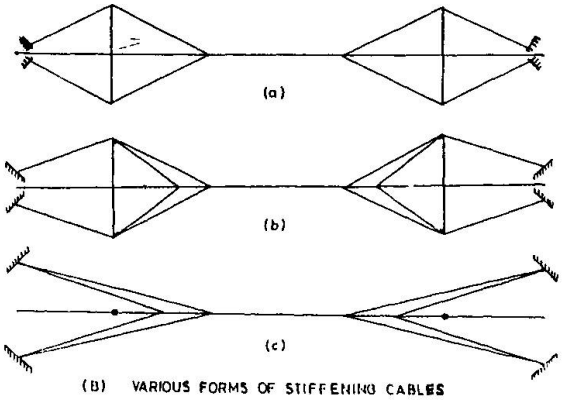

(B) VARIOUS FORMS OF STIFFENING CABLES

FIG. 2 VARIOUS HORIZONTAL STIFFENING ARRANGEMENT

3. Lateral Stiffening Arrangements

Special emphasis in this work has been laid to systematically investigate the effect of horizontal stiffening arrangements as shown in Fig.2 needed to stabilize the bridge against lateral loads since the narrow bridges have a high degree of susceptibility to wind/earthquake oscillations. The stiffening arrangements studied are cables and cable-trusses of different configurations in the horizontal plane. Firstly,the most effective location for the cable connection with the deck was investigated and the same has been used for the various cases. The criteria adopted for the design of the deck for the lateral stiffness is that its deflection under the lateral loads should not exceed about 1/180 of the span.

4. Static and Dynamic Analysis

Static analysis for various loading cases has been carried out by

(1) considering the structure to be linearly elastic, and

(2) including the effect of cable nonlinearity.

The stiffness matrix method has been used for both static and dynamic analysis. Dynamic analysis study includes the dynamic behavior of CSP-Bridges under wind as well as earthquake loads. To carry out the dynamic analysis the mode shapes and natural frequencies of vibration have been determined by three dimensional free vibration analysis which uses the inverse iteration technique coupled with Strum sequence property of the characteristic polynomials of the eigen value problem (1). In all, 15 modes of vibration have been considered in the analysis and the dynamic response is computed for a specified base motion. However, the dominant modes are only 2 to 5. The maximum seismic displacement responses (SRSS-values) for the six bridges have been evaluated using the average response spectra specified in the IS: code (IS:1893-1984) for 2% damping.

The wind loading on the CSP-bridges is considered in two parts; the static wind loads due to the steady component of wind and the fluctuating wind loads due to the horizontal gustiness of the wind. The response to the fluctuating load is determined using statistical concepts of stationary time series. Pertinent data on CSP-bridges is evaluated (modes and natural frequencies) to estimate the displacement responses. The vertical vibrations (cross-wind) caused by the action of vertical component of wind turbulence would be insignificant due to the use of highly perforated decks in pipeline bridges coupled with the large vertical stiffness available in the bridge system.

The dynamic analysis for wind loads has been carried out using Davenport's formulation (2,3,4). Some modifications, however had to be made for the cable stayed bridges. The method was also tested for an example illustrated by Davenport (2). Both the bridge configurations could be analyzed using the same procedure.

5. Results of the Analysis

The main findings of the study are as follows:

(a) Static vertical load analysis:

For the linear static analysis the maximum deflection/span ratio in Type-A bridges is found under vertical loading for 50m, 100m and 200m bridges as 1/335, 1/397.5 and 1/230 respectively; whereas; when the nonlinearity of cables is considered the deflection to span ratios are 1/334, 1/397 and 1/229 respectively. It is thus seen that there is little cable non-linearity effect. This is on account of the small LL/DL ratio.

For the linear static analysis the maximum deflection/span ratio in Type-B bridges is found under the vertical loading as 1/328.2, 1/462.0 and 1/229.65 for 100m, 200m, and 400m span bridges respectively. When the nonlinearity of cables is considered the deflection to span ratios are 1/327.6, 1/460 and 1/229 respectively. The nonlinear analysis takes 2 to 5 iterations for convergence. The cable non-linearity in Type - B bridges is found in significant.

(b) Mean wind load analysis:

The maximum lateral deflection to main span ratio under the basic wind speed of 44 m/sec for Type-A and Type-B bridges is given in Table 1.

TABLE 1
Deflection to Span Ratio for Mean Wind Load

Bridge Type	Main Span (m)	Width (m)	Lateral Deflection to Main-span Ratio (Δ/L) Without Lateral Stiffening	With Horizontal Stiffening Cable: Linear	With Horizontal Stiffening Cable: Nonlinear
Type A	50	2.5	1/323	1/3587	1/3509
	100	3.0	1/146	1/2523	1/2260
	200	7.5	1/170	1/1053	1/985
Type B	55 (100)	2.5	1/1366	1/4136	1/3892
	110 (200)	3.0	1/410	1/2904	1/2208
	220 (400)	7.5	1/477	1/1400	1/911

Note: Figures n( ) indicate the total span.

It can be seen from Table 1 that the Type- A bridges are far more wind susceptible than the Type-B bridges. However, with the stiffening cables the lateral deflections get greatly reduced. The deflection response of both type of bridges can be effectively controlled by use of the horizontal cables.

(c) Effectiveness of the lateral stiffening systems

In all, three cable truss systems and three horizontal cable systems have been investigated for providing the necessary lateral stiffness to the bridge, as shown in Fig. 2. In order to compare the various stiffening systems used, analysis has been carried out on the 100m span Type-B bridge (main span 55m) for the mean wind load. The results for mid-span lateral deflection to span ratios are given in Table 2.

TABLE 2.
Lateral Deflection to Main-span (55.0m) Ratios for Type-B 100m Span Bridge With Various Horizontal Stiffening Arrangments.

Form	Cable Trusses: Linear	Cable Trusses: Non Linear	Horizental stiffening Cables: Linear	Horizental stiffening Cables: Nonlinear
a	1/179 (without offsets)	1/179	1/186	1/186
b	1/183	1/183	1/222	1/222
c	1/186	1/186	1/215 (without offsets)	1/214

Note: Forms a,b & c are as shown in Fig. 2.

It can be seen from the results summarised in Table 2 that the horizontal deflection of CSP bridges can be more effectively controlled by the use of horizontal stiffening cables. Also the effectiveness of the "offsets" provided at the base of the towers to hold these cables is

found to depend upon the cable arrangement. It is also seen from Table 2 that the stiffening cable systems are more effective compared to the cable trusses. The most effective system has been considered to be the one that yields the minimum value of the deflection to span ratio.

(d) Dynamic analysis :-

(i) Modal analysis

When the pipeline loads including the mass of fluids it carries, are considered, the lowest mode of vibration is the vertical mode. However, when only the self weight of the bridge without the pipeline is considered, the first mode of vibration shifts to the horizontal plane.

(ii) Earthquake response

Under the design earthquake loading, the dynamic deflection response of Type-A and Type-B cable-stayed pipeline bridges are given in Table-3. The responses have been obtained by taking S.R.S.S. of the responses in the significant modes of vibration.

The contribution of the second and higher modes were found to be generally less than 2 % .

TABLE 3.
Deflection of Cable Stayed Pipeline Bridges for Design Earthquake Loads

Bridge Type	Main Span	Without Horizontal Stiffening		With Horizontal Stiffening	
	(m)	Lateral (mm)	Vertical (mm)	Lateral (mm)	Vertical (mm)
Type A	50	28.70	17.70	10.60	25.20
	100	14.60	43.90	30.00	43.80
	200	40.20	61.20	29.30	56.90
Type B	55 (100)	20.70	22.20	10.60	22.10
	110 (200)	50.40	37.20	37.60	38.60
	220 (400)	50.20	82.50	36.90	70.40

Note: Figures in ( ) indicate the total span

(iii) Buffeting wind response

The buffeting wind response of the Type-A bridges for spans 50m, 100m, 200m for basic wind speed 44m/sec is found to be 112.5mm, 734.0mm and 178.0mm without the stiffening cables. With stiffening cables the buffeting response values are found to be 27.0mm, 148.9mm and 75.9mm respectively.For Type-B bridges of main spans 55m 110m and 220m the buffeting response is found as 46.9mm, 323mm, and 150.4mm respectively without the stiffening cables and 35.4mm, 233.0mm and 101.5mm respectively with the stiffening cables.

6. Conclusions:

Following are the main conclusions of the study.

(i) It is found that the stiffening cables are more effective than the cable trusses to control the lateral deflections of the deck.

(ii) The effectiveness of offsets used in Type-B bridges to reduced the lateral deflections is found to depend upon the cable configuration.

(iii) Unlike the traffic bridges the geometric non-linearity due to cable sag has been found negligible for the vertical load being less than 1 % .

(iv) The dynamic response for design earthquake loads is found to be significant for the cable stayed pipeline bridges

(v) Although the effective pressures across the entire span due to gusts are in themselves small, they excite large amplitude vibrations and, thereby, induce large inertia loads, which may have an effect as great as or greater than that of the mean wind.

(vi) The susceptibility of cable stayed bridges for pipelines to gusts is due to their flexibility compared to the highway traffic bridges and to the fact that their resonant frequencies concide with broad peak of the horizontal gust spectra.

(vii) Type-A bridges are found to be more buffeting prone than the Type-B bridges.

(viii) The lateral deflection of cable stayed pipeline bridges can be controlled by the use of lateral stiffening arrangements.

References

1. Bathe, K.J., Finite element procedures in Engineering Analysis, Prentice-Hall, Int. Englewood cliffs, New Jersey 1982.

2. Davenport, A.G., "Buffeting of A Suspension Bridge by Storm Wind" J. Str. Engrg. Div., ASCE Vol. 88, 1962.

3. Davenport, A.G., "The Response of Standard Linelike Structure to a Gusty Wind" J. Str. Engrg. Div., ASCE, Vol. 23, 1967.

4. Davenport, A.G., "Gust Loading Factor" J. Str. Engrg. Div., ASCE Vol. 93, June 1967.

5. Dusseau, R.A., El-Achkar R. Haddad, M. "Pipeline geometry and pipeline bridges wind oscillations" Proc. Conf. on pipeline infrastructures, ASCE Massachusetts, June 6-7 1988.

6. Krishna, P, Kumar, K., Design Report on Cable Stayed Bridge Across the Ganga Canal at Roorkee, Uttar Pradesh Irrigation Department., India, 1983.

7. Kumar, K., Cable Stayed Pedestrain Bridge Across the Ganga Canal at Roorkee- A case study, Specialist course No. 403-SPL on cable stayed bridges, continuing Education Department, University Of Roorkee, Roorkee Nov. 1983.

8. Podolny W. Jr., and Scalzi, J.B., Construction and design of cable stayed bridges, John Wiley & Sons, 1976,

9. Troitsky, M.S., Cable-Stayed Bridges- Theory and Design, Second edition, BSP Professional Books, 1988.

10. Troitsky, M.S., Prestress Steel Bridges-Theory and Design, Bridge Series, Van Nostrand Reinhold Company, New York, 1992.

11. Walther, R. et.al, Cable Stayed Bridges, Thomos Telford, London, 1988.

Repair and Strengthening of Slabs Using Bonded Concrete Overlays

Samih JADA
Assist. Prof.
Nirzeit Univ.
Birzeit, West Bank, Palestine

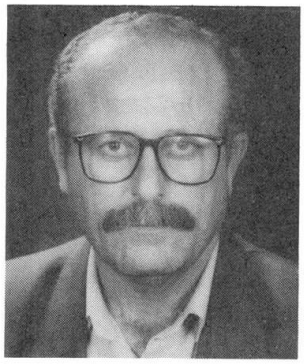

Samih Jada, born 1952, received his civil engineering degree from Kashmir Univ.,India in 1976, MSc from Rookee Univ.,India in 1981 and PhD from Birmingham Univ.,UK in 1986. He is currently assistant professor of Civil engineering at Birzeit University.

Mohamed ZIARA
Assist. Prof.
Nirzeit Univ.
Birzeit, West Bank, Palestine

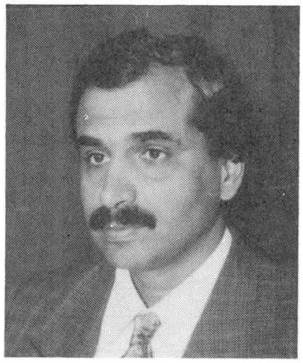

Mohamed Ziara, born 1956, received his civil engineering degree from Alexandria Univ., Egypt in 1980, MSc from Georgia Tech, USA in 1982 and PhD from Heriot-Watt Univ.,UK in 1993. He is currently assistant professor of structural engineering at Birzeit University.

Summary

Strengthening of slabs has been achieved by casting a new concrete overlay on top of original slabs. The inter-laminar shear failure has been prevented using expansion screws which provided positive anchorage between the two concrete parts. The test results on six slab types have indicated the adequacy of the proposed strengthening technique. The strengthened slabs have reached their full flexural behavior and acted as one unit. The strengthened slabs have achieved an increase in the load carrying capacity up to 310% compared to their original strength.

1. Introduction

Cracks may develop in concrete slabs of bridge decks because of the development of internal tensile stresses due to volumetric changes, applied loading conditions, and environmental effects. Large cracks may also develop in slabs due to incorrect design and detailing, or poor construction practice. Cracking has an important influence on deflection of slabs. In particular, long-term deflection may be large when compared to initial deflection as cracking progress with time. These adverse effects may reduce the load carrying capacity, and increase deflection of the cracked slabs. Such slabs need strengthening to enhance their load carrying capacity, to minimize their long-term deflection, and to enhance their durability.

2. Strengthening technique and test results

The proposed strengthening technique is based on the composite action between the original slab and a newly cast concrete overlay. The inter-laminar shear failure is prevented by using expansion screws which provide positive anchorage between the two concrete parts. The concrete overlay will protect against corrosion of reinforcement steel, reduce the long-term deflection and will result in the improvement of the serviceability and strength of the slabs. The concrete overlay may also be used to provide drainage slopes thus resulting in improving the durability of structures.

The test program has included six types of one-way slabs. The slabs were tested under single loading applied at mid-span up to failure. All slabs had an overall length of 1400 mm, effective span of 1300 mm and width of 400 mm. The original slabs Type O had a thickness of 60 mm, and effective depth of 48 mm. Slabs Type S were strengthened by casting a concrete overlay of thickness of 40 mm on top of the original slabs. The concrete compressive strength f_{cu} was 25 MPa. The reinforcement steel yielding strength f_y was 412 MPa. Expansion screws of 80 mm

MPa. The reinforcement steel yielding strength f_y was 412 MPa. Expansion screws of 80 mm length and 8 mm diameter were used for anchorage. The screws were tightened inside a 50 mm length hole drilled in the upper part of the original slab. The remaining lengths of the screws were embedded in the concrete overlay. The head of the screw was intended to act as an end plate to ensure the required anchorage. Each strengthened slab was provided with a total of 10 screws which were uniformly distributed in pairs along the length of the slabs. The test program also included nominally identical control slabs Type C. These slabs had the same overall dimensions and reinforcement as those used in the strengthened slabs and were included for comparison purposes. Two identical slabs were cast for each strengthened slab Type S. The details of the test program are shown in Table 1.

Table 1: Test details and results

Slab Type	Cross Section (mm X mm)			a/d*	A_s (mm^2)	ρ	P (kN)
	Original	Overlay	Overall				
O1	60 X 400	-	60 X 400	13.5	4 ϕ8	0.0105	12.9
C1	100 X 400	-	100 X 400	7.4	4 ϕ8	0.0055	34.0
S1	60 X 400	40 X 400	100 X 400	7.4	4 ϕ8	0.0055	31.3
O2	60 X 400	-	60 X 400	13.5	8 ϕ8	0.011	19.3
C2	100 X 400	-	100 X 400	7.4	8 ϕ8	0.021	57.4
S2	60 X 400	40 X 400	100 X 400	7.4	8 ϕ8	0.021	60.0

* (a/d) is the shear-span-to-depth ratio.

The values of total maximum applied load (P) obtained from the different slab types are shown in Table 1. Figs. 1 and 2 show the typical load-deflection curves and crack pattern for strengthened slab Types S1 and S2 with their corresponding control slab Types C1 and C2.

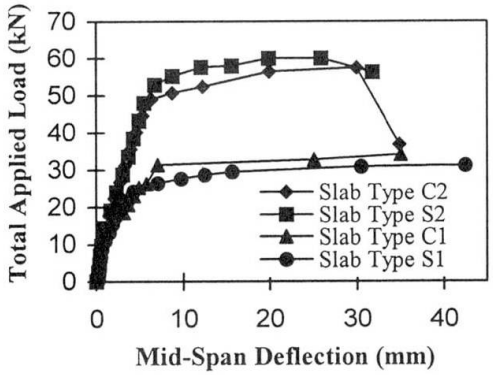

Fig. 1: Load deflection curves

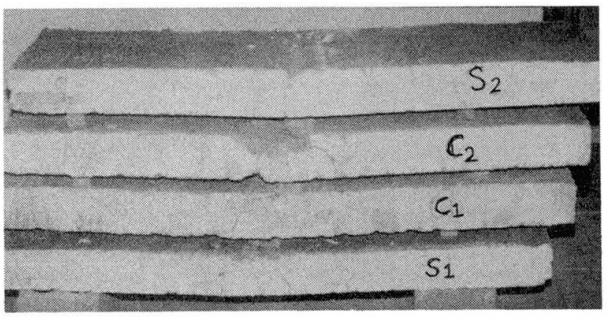

Fig. 2: Crack patterns for Types C1,S1,C2,S2

The test results and cracking patterns indicated that all test slabs were able to reach their full flexural behavior and failed in a ductile manner. The strengthened slab Types S1 and S2 acted as one unit under an increased loading. Their load carrying capacity, stiffness, ductility, and cracking patterns were similar to those obtained from the corresponding identical control slab Types C1 and C2 which were cast monolithically. Flexural cracks were developed in the lower part of the slabs. The flexural cracks widened and extended into the upper part under increasing loading. These cracks were extended in the strengthened slab Types S1 and S2 from the original slabs into the concrete overlay until they have been held in the compression zone. The test results have proved the adequacy of the expansion screws to provide the required positive anchorage between the two parts of the slabs; since no separation has occurred in any of the reported test slabs. The strengthened slab Types S1 and S2 were able to achieve up to 242% and 310% of their original strength compared to the original slab Types O1 and O2 respectively as indicated in Table 1.

It is concluded that the proposed strengthening technique can be easily adopted because of its simplicity in improving the structural behavior of slabs; especially in strengthening decks of existing bridges in order to increase their capacity to carry more demanding loading levels.

Hydraulic Lifting of Steel Box-Girders for Humen Bridge

Tang JIANGUO
Eng.
OVM Constr. Machinery Ltd
Liuzhou, Guangxi, China

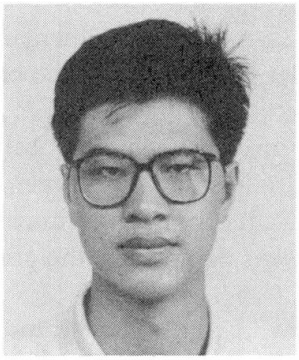

Tang Jianguo, born in 1970 received his science degree from Guangxi Institute of Technology.

Abstract:

Taking Humen Bridge of Guangdong in China for example,the article elaborates the new technology for steel box-girder-----hydraulic lifting technology,and includes applicational process、critical constructional technology、equipments as well as economic effect analysic.

1.Introduction

Humen Brige in Guangdong is a suspension bridge with a span of 888m.The reinforced steel box-girders are manufactured in factory by section. Standard sectional steel box-girder of each erecting unit is 24m in length,312t in weight.The erection of steel box-girder is one part of critical technology applied in the construction of upper structure for long span suspension bridge, winch cable-spanned crane are used in traditional erection.such hoisting structure is made up of wirerope、block and tackle、winch,featuring simple operation.mature technology and fast speed.Nevertheless it also has the following drawbacks:

(1)Lifting capacity is limited by wire rope、block and tackle and winch.For with the addition of lifted weigth,it is necessary to increase the diameter of wirerope and the multiplying power of block and tackle,which makes it difficult to satisfy structural requirements.

(2)It is affected greatly by the span of suspension bridge,For winch is generally placed on earth surface,with the increase of suspension bridge span and tower boby it is required to have long enough wire-rope,which makes the construction costs higher.

(3)Wide operating rang and different lay out of winch、lifting beam and hoisting weight cause the problems of communication and coordination.

in consideration of abve reasons it is necessary to search a new lifting method with regard to the lifting of sectional steel box-girder through deep research the new lifting technology for steel box-girder---hydraulic lifting technology adopting hydraulic lifting system for lifting structure instead of wirerope、block and tackle、winch,comes into the world.It needs continuous lifting jack as main unit and has been successfully applied for the project of Humen Bridge.

2.Constructional process of hydraulic steel box-girder lifting for Humen Bridge.

Adopt four 200t continuous lifting jack、two high-flow pump stations、one set of control system

and other relevant clamps as hoisting system.the process is as follows:
(1)Positioning and debugging of cranes:first position the cable-spanned cranes for hydraulic lifting,then debug hydraulic lifting system with full load to ensure the operation of each part is in accordance with design requirements.
(2)Lowering of the sling:release safe anchorage and two sets of wedges for continuous lifting jack.then lower the sling to water surface with four supplementary winches and connet with temporary hoisting point of steel box-girder.Finally release the binding rope used for transporting steel box-girder.
(3)Lifting of the steel box-girder:lift steel box-girder automatically and continuously.At the same time retrieve strands and make some adjustment for girder body horizontally if necessary.
(4)Installing of steel box-girder and boom:after lifing box-girder to place with continuous lifting jacks dischange load from jacks,which makes boom carry the girder's weight.It is the end of steel box-girder hoisting.

3.Critical technology for hydraulic steel box-girder lifting

(1)Uniform force carried by multiple strands:blank in equivalent length and mark at stipulated point,then install dead anchorage on the same point of each long enough strand.When strands are lowered together with sling,they remain equivalent length appoximately. So the pretighening problem is settled.
(2)The second lifting of upside-down cable
Because of the hoisting job practice strands need using repeatedly.With the help of winch on tower top the retraction of strants is achieved.
(3)Attached anchorages and clamps stipulated in job practice must be placed as rules require to ensure safe and reliable hoisting.
(4)Enough lifting speed and synchronous control make the technology widely applicable.

4.Economic effect analysis about using hydraulic lifting technology to hoist steel box-girder

Two sets of cable-spanned crane hoisted by winch and another two by hydraulic system were used in Humen Bridge.According to statistics gross weight of the former is 249t,the latter 100t,as a result that the use of the latter brings about the save of 149t material and ￥5,000,000 investment.Moreover,the change in design structure has led to the reduction of ￥1,000,000 investment on load test and 15 days for installation.

5.Conclusion

We have concluded the following by engineering practice.
(1)The hydraulic lifting technology for steel box-girder has the advantage of being not affected by the span of suspension bridges、lifting much heavier objects、simple structure、concentrative operating range and lower construction cost.so it is completely feasible.
(2)With regar to the future construction, it is considerable to add the length of steel box-girder section and decrease the joints number,which can shorten construction term and thus reduce costs.

Heat Straightening - an Unpopular Method of Repair of Steel Bridges

Henryk ZOBEL
Assoc. Prof.
Warsaw Univ. of Technology
Warsaw, Poland

Thakaa ALKHAFAJI
Dr Eng.
Warsaw Univ. of Technology
Warsaw, Poland

Agnieszka GOLUBINSKA
Civil Eng.
Warsaw Univ. of Technology
Warsaw, Poland

Henryk Zobel, born 1950, received his civil engineering degree from Warsaw Univ. of Techn. in 1972 and Ph.D. in 1978.

Thakaa Alkhafaji, born 1957, received her civil engineering degree from Moscow Autom. & Road Constr. Inst. in 1987, Ph.D. from Warsaw Univ. of Techn. in 1994.

Agnieszka Golubinska, born 1966, received her civil engineering degree from Warsaw Univ. of Technology in 1991.

Summary

Deformations of steel bridges relatively frequently result from the impact of oversized vehicle, fire or earthquake. These deformations are removed using various methods. One of them is heat straightening, sometimes combined with mechanical action. The paper presents application of this method for repair of plate girder and truss members. Although conclusions are not fully satisfied, this is the next step for more wide understanding of phenomena occuring during heating and cooling of steel members.

1. Introduction

Heat straightening is usually the most economical and practical method of field repair for a various type of damage. Unfortunately, even experienced personnel in steel fabrication industry, construction companies or maintenance services mostly do not know, what parameters of heating are adequate for a given kind of deformation. This knowledge is obtained from experience, which is not often shared. Unwillingness for application of heat for repair of steel structures is caused by limited knowledge related to work of structure in elevated temperature and impact of heating for steel properties. The fear of negative impact of heating for durability of bridges is also common. Most of mentioned above problems are myths which exist among bridge and structural engineers and technicians. The results of not numerous investigations and experience of a few only firms applying heat straightening confirm usefulness of this method. It should be emphasized that each case needs the individual design and choice of repair method .

2. Idea of Heat Straightening

The flame of the torch applied to the steel element causes its expansion. But this process is limited by cool part of this element. If the temperature is sufficiently high plastic deformations will generate and remain after cooling. The basic problem is to select proper pattern and parameters of heating to obtain required values and desired direction of deformations, which

remain in the structure. Although heating alone may be used to straighten a deformed member, external load may also be applied to increase the efficiency of the process.

3. Damage Classifications

Generally, there are two categories of damage: overall and local. First one consists of three types i.e. bending about „strong" axis, bending about „weak" axis and asymmetrical bending that results in torsion about the longitudinal axis of the member. The second group are bulges, crimps, buckles etc. One of the most common damage of plate girder is deformation of bottom flange ofter combined with the twist of the web against „weak" axis. In the case of truss, this is hitting the portal bracing at the approach of the truss. In some situations, the vehicle may travel partially through the truss span, striking intermediate sway frame bracing. The end post may be pulled inward enough to be bent beyond the elastic limit. Striking the sway frames may result in pulling the vertical truss members inward. In cases where the inward displacement is large enough, the top and the bottom chord members can be pulled down or up, respectively.

4. Heating Patterns

Two kinds of heat pattern are used: concentrated and continuous. The first are spot, strip and Vee; the second line and edge heats. They can be used individually or as a combination, depending on the structural configuration and damage pattern.

5. Factors Influenced the Heat Straightening Process

A lot of factors is necessary to take into account in design and repair of bridge structure. They can be put into 5 groups: technological parameters, geometry of the steel member, geometry of heated areas, change of steel properties in elevated temperatures, „accelerators" and „retardants" of the process. The large number of factors and their mutual coupling causes that problem is still, from mathematical and physical point of view, not sufficiently solved. It still remains more art than science.

6. Research and Practice

The main aim of computer analysis and experiments on heated and simultaneously compressed or tensioned truss members and plate girders was to determine the proper parameters of heating like its pattern, dimensions, location, number and spacing in dependence on size and location of damage in the bridge structure. The efficiency of single Vee or three Vee's combined with or without strip, line or edge heat patterns was investigated. The comparison of relations determining steel properties in chosen countries was also done. Authors of the paper realized successfully a repair of one bridge in Poland and also observed such process done in the U.S. The results of thermal-plastic analysis are comparable with practice in many cases but not always. To find better convergence it is necessary to improve thermal load model, to define more precisely change of steel properties in elevated temperatures, to use more correct statical scheme of bridge structures and to determine carefully boundary conditions. The investigation of about 15 bridges heat straightened in last 20 years proved that this method does not affect durability of steel bridges. No signs of damages related to heating were observed.

Construction of a V-Shaped Rigid-Frame Bridge with High Piers

Taakao IRUBE
Chief Eng.
TTK Co.
Tokyo, Japan

Born 1956, received his civil engineering Master's degree 1981 from Tokyo Metropolitan University.

Takira KAWATO
Constr. Mgr
Honshu-Shikoku Bridge Authority
Hyogo, Japan

Born 1954, received his civil engineering degree 1981 from Osaka Institute of Technology.

Summary
Nadagawa bridge is the V shaped rigid steel-frame bridge with five continuous spans having total length of 276 meters. The V shaped pier is 45.7 meters high and the highest one among similar type bridges in Japan.
The huge girder block erection method or the inclined cable erection method is generally used for construction of these types of bridges. However, for the erection of this particular bridge, the staging method providing cranes were used, and in order to stabilize the V shaped piers at correct position, the steel wires were provided. This paper presents outlines of this erection method, in particular of wire tensions control.

1. Outline of bridge
This bridge is located in Awaji Island on Kobe-Naruto route of the Honshu-Shikoku Highways, and is designed as to harmonize well with surrounding landscape. The type of this bridge is the V shaped rigid steel-frame bridge as shown in Fig.1 and 2.

2. Construction Methods
For the erection of this bridge, three construction methods were used. The staging method providing crawler crane was used in P6 (V-pier and girders), and the staging method providing tower crane in P7 (V-pier and girders), and the launching method in girders between P7 and A2 (Fig.3).

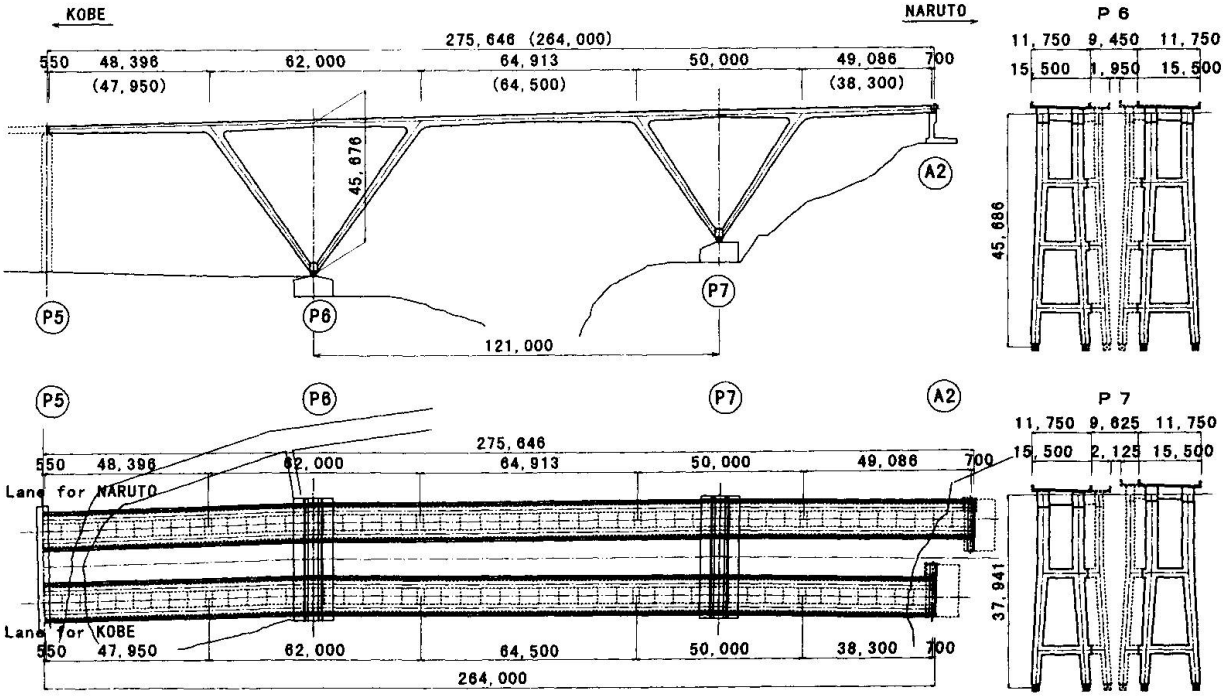

Fig.1 General View

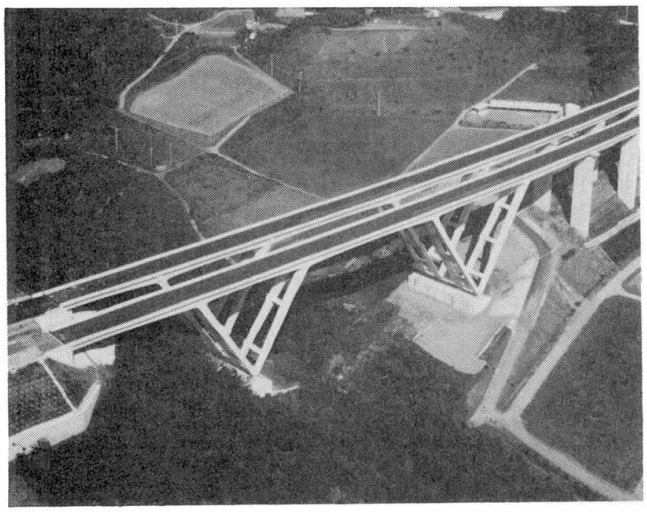

Fig.2 Nadagawa Bridge

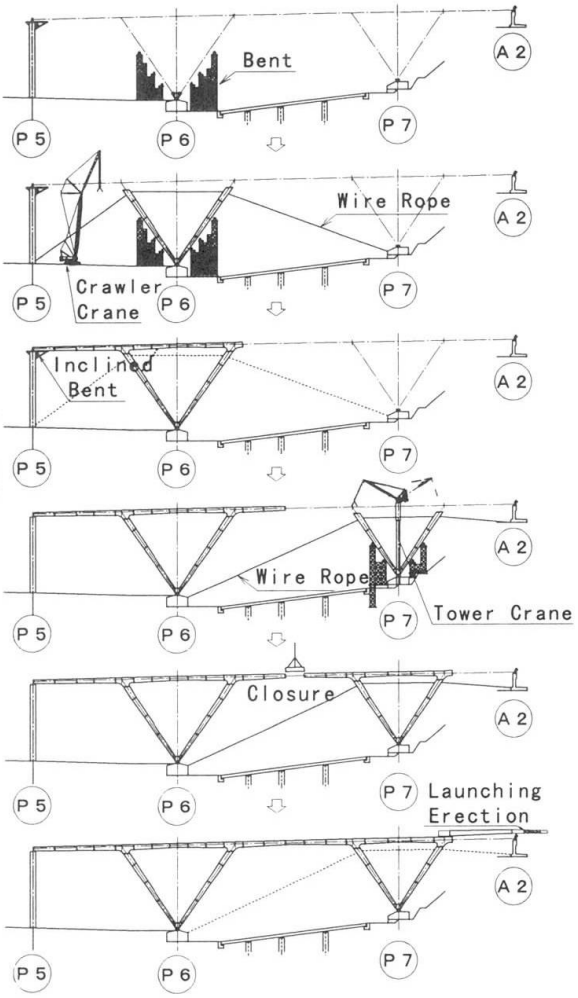

Fig.3 Stages of Construction

(1) Closure of side girder

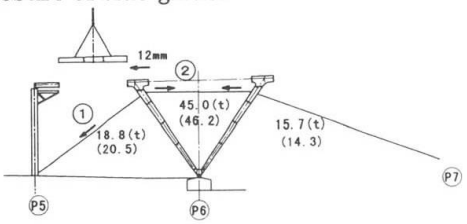

(2) Closure of girder in V-pier

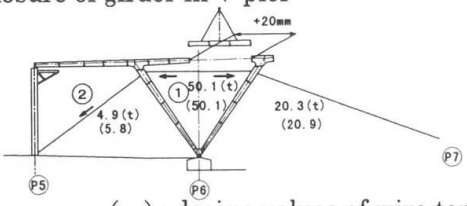

( ) : design values of wire tensions

Fig.4 Control of wire tensions

In first stage, the V pier was supported by bents, and then supported by wire ropes. In order to stabilize the V shaped piers at correct position, the steel wires were provided. The top end of these wires were anchored to the V shaped column and the bottom ends were anchored to the concrete foundation of adjacent piers. The stringent wire control was required in order to maintain wire tension at accurate values.

The shape of V pier were measured by 3-dimentional theodolite as coordinates and wire tensions were measured by strain gauges at tension bars in a pulling apparatus. The computer monitoring system which can constantly measure the wire tensions was introduced. It was controlled at each erection step so as to ensure the wire tensions and the shape of V pier within the design values. The controlling system of the wire tensions was useful to adjust the elevation and the gap of each girder at the stage of the closure erection(Fig.4).

3. Conclusion

This construction method has the advantage as shown below.

(1) This method is capable of erecting girders even at the site where the bents erection is difficult.
(2) It is possible to adjust the elevation and the gap of each girder at the stage of the closure erection with the help of wire ropes.
(3) It is unnecessary to build the temporary steel towers and the huge foundations of cable anchors as used in the ordinary cable erection method.

Aramid Fibers Used for Bridge Repair and Strengthening

Jorge H. SALAVERRIA
Research Assistant
Techn. Univ. of Catalunya
Barcelona, Spain

Joan R. CASAS
Prof.
Techn. Univ. of Catalunya
Barcelona, Spain

Summary

The paper presents the experimental tests designed to improve the existing techniques of bridge repair by the combination of external prestressing and aramid fibers (AFRP). The external prestressing substitutes the damaged prestressing steel and aramid strips will play, in the repaired bridge, the role of the corroded reinforcing steel. The first phase comprises the study of the bond characteristics of the composite when applied to a concrete surface considering different epoxi adhesive and placement. The sechond phase consists on the strengthening in shear and bending of a two span (7m + 7m) continuous prestressed concrete box-girder model previously damaged. The original beam was firstly loaded ocurring an important damage. After load removing, the beam is repaired and strengthened using AFRP and loaded again up to failure to compare the ultimate capacity.

1. SCOPE OF THE EXPERIMENTAL TESTS

The experimental work comprises two phases. In phase one the objective is to develop a theoretical model of the interface aramid-adhesive-concrete. To this end, a set of concrete-aramid specimens are considered. In the bottom face of the specimens a strip of aramid is glued using different adhesives and different preparation of the concrete and fiber surface before bonding. With the correct surface preparation before bonding and the most appropiate properties of the adhesive with the composite, the tension in the interfarce is increased to 3.5 MPa; this value is approximatelly the concrete tensile strength. Good bonding properties were obtained in the dynamic tests too, where the specimens resist more than 2 million cycles of a 2 Hz armonic force without debonding of the aramid strip. The force amplitude ranges from 0.3 to 0.7 of the failure load measured in the static tests.

Tests in the undamaged beam. The beam V1 is loaded up to failure. The two loads(Q) are only applied in one of the spans (Figure 1). During the test to failure different variables are continuosly monitored as load increases. The monitoring of slip of prestressing tendon at deviators is very important in order to compare the experimental results with those coming from a theoretical model, where the possibility or not of tendon slip should be considered.

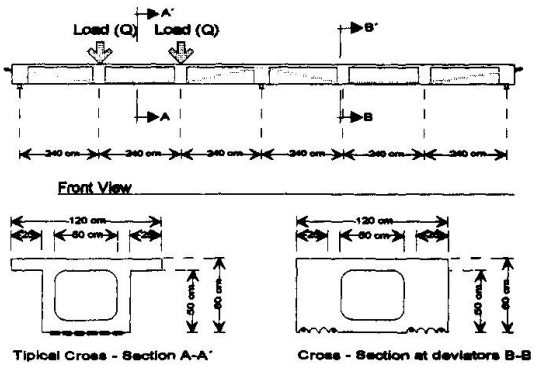

Figure 1. Definition of the two-span prestressed box girder beam.

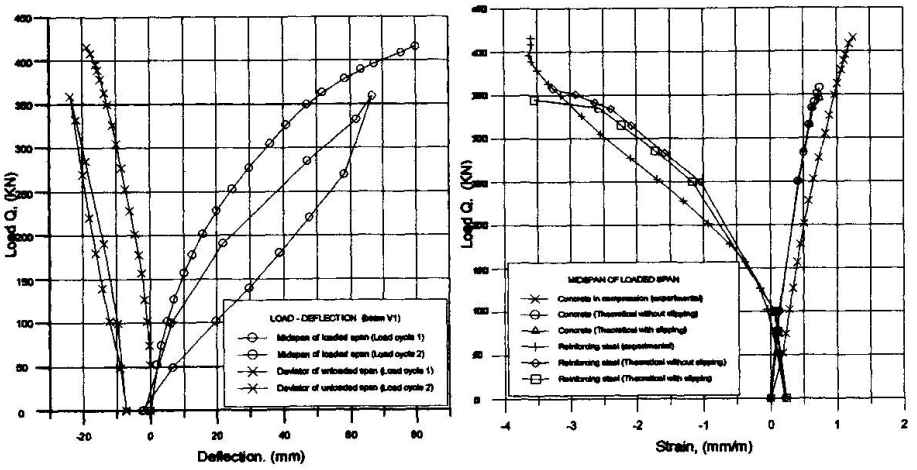

Figure 2. Results in the original undamaged beam in the test up to failure.

Results- In figure 2 are shown some load-deflection curves obtained in the original undamaged beam in the test up to failure. The strains in concrete and reinforcing steel measured with strain gages are presented too.

Repair and strengthening. Severe damage was provoked to the beam in the test up to failure. The repair method tried to simulate as close as possible the repair sequence that will be used in an existing bridge. The original reinforcing steel is replaced by bonding aramid strips (Length: 3000mm., Width: 20 mm., Thickness: 4 mm. each) .

Tests in the repaired beam. The same experimental arrangement and instrumentation as in the undamaged beam were disposed to obtain the experimental results in the same locations monitored in the previous test to compare the behaviour of undamaged and repaired beam.

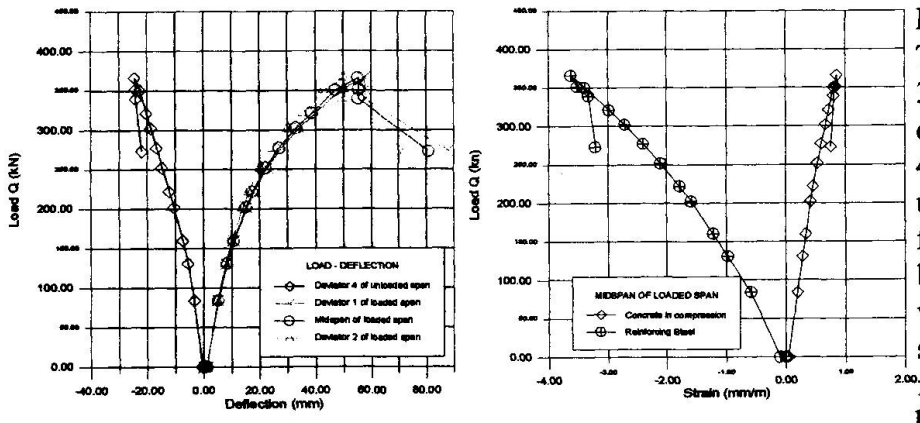

Figure 3. Experimental results in the repaired beam.

Results- (see figure 3) The ultimate load was 360 kN which is very close to the final load 400 kN in the undamaged beam. The final failure was quite brittle. The ultimate load was achieved by the sudden and progressive failure of the bonding between aramid strips and concrete. Once the strips failed, the load carried by them was suddenly transmitted to the prestressing steel that was beyond the yield limit, causing the final rupture of the beam.

2. CONCLUSIONS

The tests show how the repair and strengthening technique based on the use of AFRP strips and external prestressing seems to be very promising even for heavily damaged structures. In fact the ultimate load in the repaired beam was almost 90% the ultimate load in the undamaged beam. The strips externally bonded to the concrete seem to provide some crack control. Due to the brittleness of the rupture of concrete in tension, the failure of bonding concrete-aramid is brittle too, and so is the global failure of the repaired beam. The high tensile strength of the aramid material is under-used.

Estimation of the Remaining Fatigue Life of a Railway Bridge

Sang-Hyo Kim
Head of Dept of Civil Eng.
Yonsei Univ.
Seoul, Korea

Sang-Hyo Kim, born 1956, received his civil engineering degree from Yonsei Univ. in 1979 and Ph.D. from Univ. of Illinois in 1986.

Ho-Seong MHA
Researcher
Yonsei Univ.
Seoul, Korea

Ho-Seong Mha, born 1963, received his civil engineering degree from Yonsei Univ. in 1986 and Ph.D. from Oregon State Univ. in 1996.

Sang-Woo LEE
Grad. Student
Yonsei Univ.
Seoul, Korea

Sang-Woo Lee, born 1969, received his civil engineering degree in 1996 and MS from Yonsei Univ. in 1998.

Summary

The *Dangsan* steel railway bridge was located in Seoul, Korea, crossing the famous Han river for subway traffics (The old bridge was disassembled and a new bridge is under construction at the same location). Upon requests, the bridge had undergone many inspections near the end of its service life since it was reported that there were several fatigue cracks found, and the city authority considered deeply about the safety of the bridge. The remaining life of the bridge had been estimated through the field measurements and the corresponding fatigue test conducted. The results are briefly presented herein.

1. The Bridges

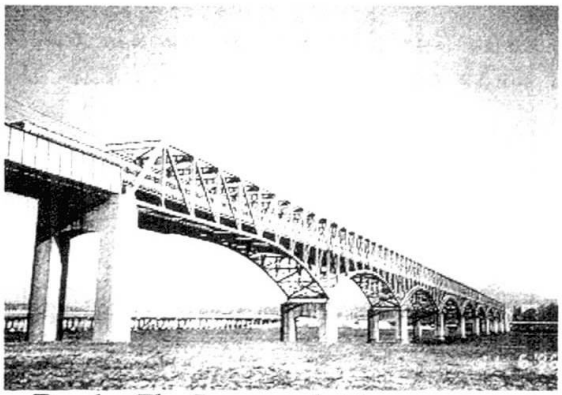

Fig. 1 The Dangsan bridge

The bridge consisted of three units of three-span-continuous steel Pratt truss with length 90-90-90m for its main spans in the middle and plate girder bridges on both ends. The picture, profile and corresponding FEM model are depicted in Fig. 1, 2, and 3, respectively. The bridge was made to serve the subway traffics only, and was experiencing about 510 trains daily in two way system.

Via both visual and ultra sonic inspections, most cracks were found from the floor systems (specially, stringers), and improper welding were also found. Based on the inspection and structural analysis, the critical members, which was assumed to dominate the remaining life of the whole bridge, were determined. Some peculiar details, of which the category was hard to be determined, were observed, and corresponding experimental models were manufactured to conduct fatigue test to determine the appropriate category for the details.

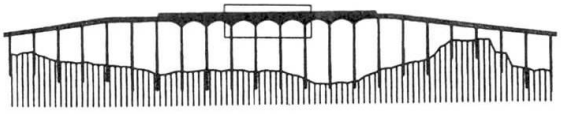

Fig. 2 Profile of the bridge

Fig. 3 FEM model

2. Fatigue test

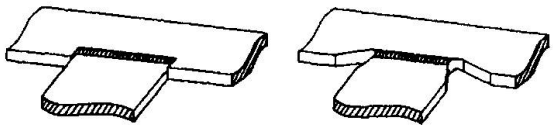

(a) *Model A* (b) *Model B*

Fig. 4 Fatigue Model

Some upper chords connected with bracings were found to have peculiar details at the connections of gusset plates due to the bad manufacture (See Fig. 4a). About 2cm of flange edges were cut off, and then the gusset plates were attached. Fatigue tests were carried out to identify the fatigue strength of these particular details. Based on visual inspections, experimental fatigue models were made to simulate the actual welding and manufacturing conditions by applying the improper cutting and welding to the flange edges. Repairing method was proposed by finishing the rectangular corner at the welding parts in the round shape according to AASHTO, which may improve the fatigue strength of the detail. Two models were prepared: with actual condition (model A); with proposed condition (model B) shown in Fig. 4a, b, respectively. In addition, the experimental models with typical details were also prepared for fatigue test to compare the results with those of other two models. Upon the test results, the Fatigue strengths for each model were measured and plotted on the AASHTO's S-N curves (Fig. 5). Fig. 5a is the result of the model A which simulates the actual detail condition, and Fig. 5b is the result of model B with the repaired detail. The model A shows that the fatigue strength is a little lower than Category E due to the improper details, but clearly higher than Category E'. The model B shows an apparent improvement.

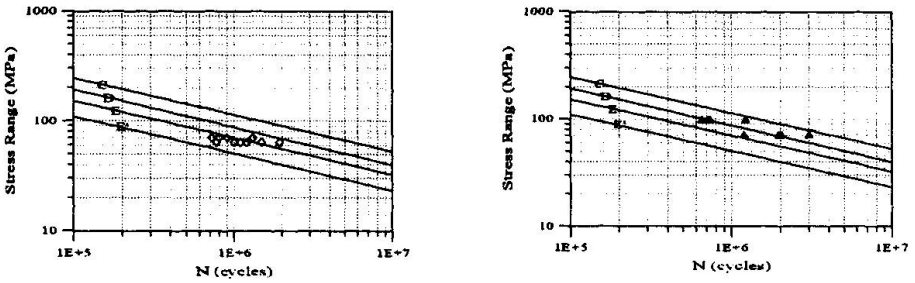

(a) *Model A* (b) *Model B*

Fig. 5 Measured fatigue strength

3. Estimation of Remaining Fatigue Life

The stresses due to the applied loads on the bridge vary randomly, and this results from the uncertain nature of the input variables, which are traffic schedules, passenger volumes, and so on. The coincident incidents of two trains crossing the bridge at the same location were also considered, since it produced the worst loading conditions. The coincident rate was numerically simulated based upon the provided time schedules of subway trains. It is not possible to obtain all the stress time histories for each loading condition from field measurements, due to the complexity of loading conditions. Consequently, a finite element method (See Fig. 3) was utilized to provide the time history for each loading condition, and the simulation results were modified according to the measured field data. Field measurements were conducted mainly through strain gages on the critical main members, which were selected from structural analysis. Two loading conditions for field measurements were considered: One was the normal traffic condition; The other was the controlled traffic condition. Under normal condition, tests were performed in a day while the trains traveled at the normal speed with passengers. The passenger volumes were obtained from visual survey at the station nearby. Under controlled situation, the tests were performed with the empty trains transferred to the site at night. The trains were traveling at speeds from 5km/h to 80km/h. Acoustic emission tests were also conducted to verify the possibility of crack growth, and some cracks were found to be growing. By using the stress ranges obtained from the loading simulations, the remaining fatigue lives of main truss members were estimated and found to be reasonable.

Retrofit of Corroded Splice Plates Using Epoxy Glued Escort Plates

Isao SUGIE
Civil Eng.
Hanshin Expressway Public Corp.
Osaka, Japan

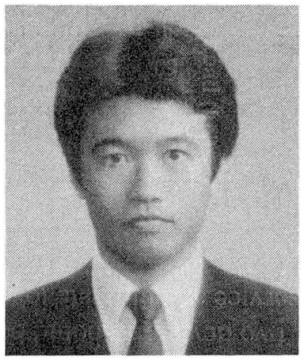

Isao Sugie, born 1962, received his Civil Engineering degree from Kobe Univ. in 1985 and MSc in 1987. He is currently chief engineer of the Maintenance division of HEPC.

Summary

Corrosion can be the most serious problem, in particular, for very complicated steel structures such as truss bridges. The Port Bridge in Osaka suffered water leakage and then serious corrosion at the joints of the cross beams, which are also floor beams for the deck plates, between the main truss members. As a result, the head of bolts seriously corroded and the splice plates became 3 to 5 mm thinner than the original. For the retrofit, additional reinforcing plates (escort plates) glued with epoxy resin was chosen. The effectiveness of this method was researched in laboratory tests.

1. Outline of corrosion

The Port Bridge is the third longest Gerber truss bridge in the world. It was constructed in 1975 and connected the reclaimed lands of Osaka Bay area with a 450 metre centre span as shown in fig.1.

As shown in fig.2, rain water entered from the scallops of the web plate of cross beam welded to the main truss members. There are no drainage holes around them, and the box beams have collected water inside them. As a result, corrosion has been advanced at the lower flange joints of the cross beams. This created two structural problems. One is the reduction of axle force of the high tension bolts. The maximum rate of measured reduction was 30 %, which is bigger than that due to relaxation (approximately 10 to 15%). Another is the reduction of thickness of the splice plates. The most corroded one was 5 mm thinner than the original. Finally, the stress limitation can not be guaranteed at the joints.

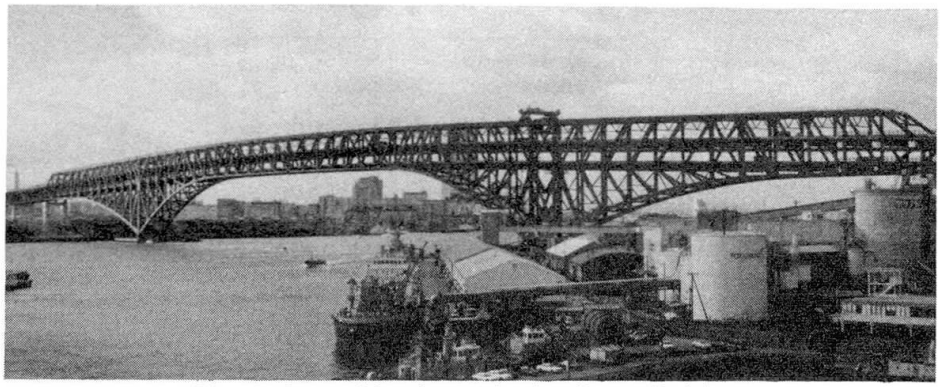

Fig. 1 Overall-view of the Port Bridge

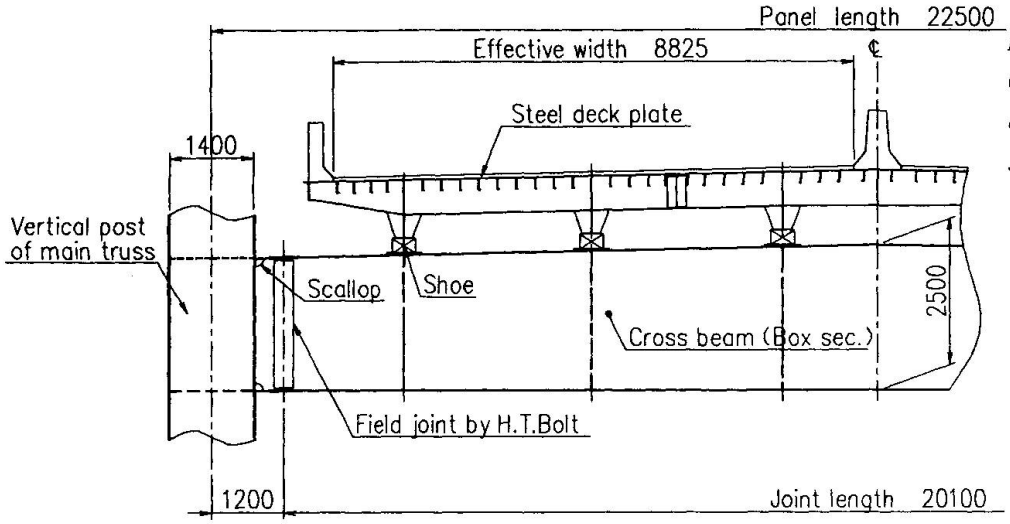

Fig. 2 General view around corroded joint

2. Retrofit concept

Fig.3 shows the retrofit using epoxy glued escort plates. In this method, the original splice plate can remain and only a row of bolts can be removed. These are replaced with new ones at the same time for fitting a long rectangular escort plate. The bolts should be replaced from the centre to the corners of the flange, so that re-distribution of the stress flow can be improved. Filler plates should be also fitted to make up for the lack of thickness of the corroded flange plates.

Other methods for retrofit have been considered such as replacement of the whole splice plates or reinforcing them with additional plates fixed by welding. They, however, were rejected for the following reasons.

(1) The working stresses due to dead loads are too large to remove the whole splice plate and all bolts from the lower flange at the same time.

(2) The influence of welding would be great, because high tension steel (HT70, HT80) was used.

Finally, using epoxy glued escort plates resulted in the most effective and practical method.

Laboratory tests have been done to examine the effectiveness of this method. The two bolts model test indicated that there were no remarkable difference between the sound specimen and the corroded ones reinforced by the escort plate.

It should be noted that using epoxy resin together with H.T.bolts may be able to reduce the number of bolts at the design stage.

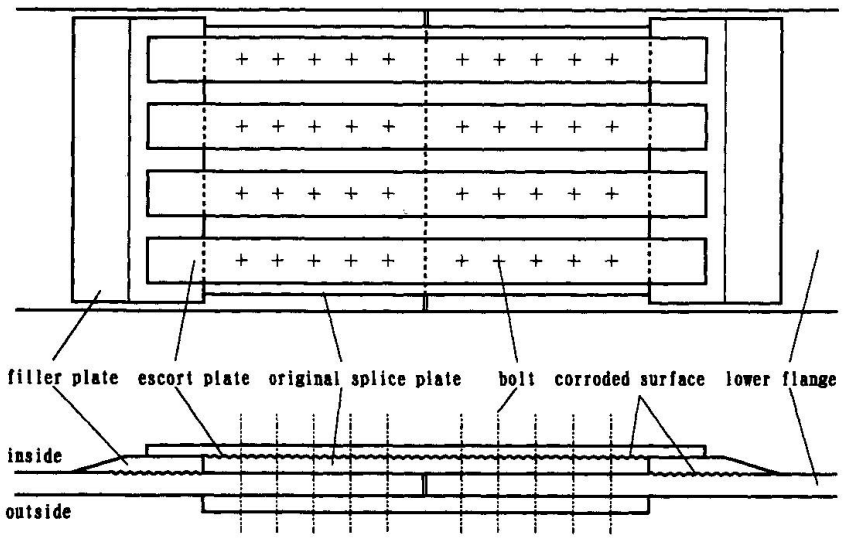

Fig. 3 Retrofit of corroded splice plates using epoxy glued escort plate

Shear Stress Distribution in Concrete/FRP Interface

Hamid VARASTEHPOUR
Head
Inst. Technology of Power & Water
Mashhad, Iran

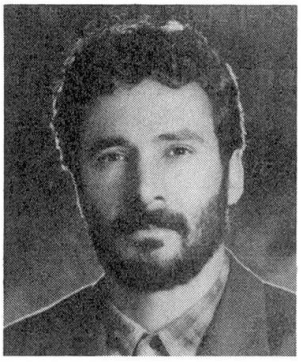

Hamid Varastehpour, born 1959 in Iran received his MSc in civil engineering form U.T.I. Iran in 1987 and Ph.D .from UCB France in 1995. He is currently head of the institute technology of power & water in Mashhad

Summary

Carbon fiber reinforced plastic (CFRP) can be bonded to the tension face of reinforced concrete beams to increase the flexural capacity. In this type of beams, high interface shear stress may result in debonding of plate and premature failure in concrete beam. To design of these beams failure mechanism and relationships between external load and shear strees distribution at concrete/plate interface must be considered. This paper present one important premature failure mode and the method to determine average of shear stress at interface.

1. Failure of concrete layer between the plate and steel

Different failure modes exist for a beam strengthened by FRP plate. First the classical rupture of the beam should be mentioned: either by the plate tensile failure (mode I), or by the concrete crush in the compression zone (mode II). However in this method of strengthening, possibility of premature failure exists at the interface because of the separation of plate (Zhang, 1995). The analysis of different beams shown, the crack pattern when the failure occurs could be defined by figure 1. The cracks propagate in tensile zone of the beam in the concrete layer between FRP plate and the reinforced steel. A part of concrete between two consecutive cracks is working similarly as a cantilever beam. These individual uncracked portions of concrete tend to bend under the influence of shear stresses at their end during the loading. When the concrete tensile stress at the section in contact with steel (point A) is higher than the concrete tensile strength (f't), debonding could appear suddenly. The above observations suggest a possible failure mode which is controlled by the characteristics of the individual teeth between two consecutively cracks in the concrete cover. If we neglect interaction between each teeth supposing an elastic behaviour for each canteliver beam, the tensile stress in the point A could be calculated as:

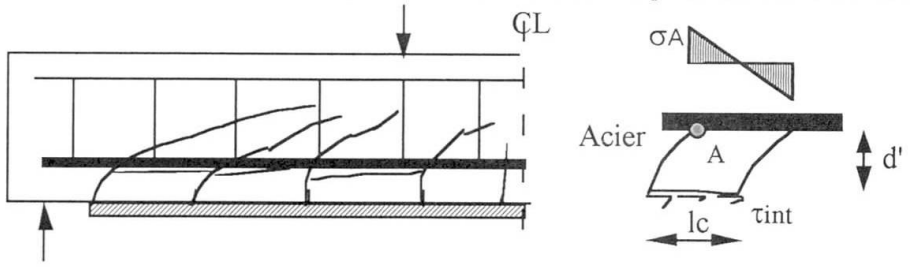

Fig.1: Cracks propagation and a teeth behaviour

$$\sigma_A = M_A \cdot (l_c / 2) / I_t \qquad (1)$$

where It is the second moment of area of the section, equal to $I_t = b.l_c^3 / 12$ and:

$$M_A = \tau_{int} \cdot l_c \cdot b_p \cdot d' \qquad (2)$$

where τ_{int} is the average interface shear stress which is reasonably assumed to be uniformly distributed and lc is the height of the section in cantilever beam equal to the flexural

crack spacings in the beam and finally d' is the concrete layer thickness between the FRP plate and the reinforced steel. With the substitution of equation 2 by equation 1 and by using $\sigma_A = f't$ (ultimate resistance of concrete in traction), the admissible shear stress at the interface is obtained:

$$\tau_{adm} = (f'_t \cdot l_c / 6d) / (b / b_p) \qquad (3)$$

This equation explains the debonding criteria due to the concrete cover failure and failure appears, when the shear stress value at the interface reaches τ_{adm}. This proposed theoretical model also depends on the crack spacing size (lc). The experimental result of the different large scale beams show that, lc is more or less equal to the average stirrup distance (S) in the shear zone.

2. Shear stress distribution at the interface

It is obvious that in order to anticipate the debonding of the plate, it is necessary to determine the distribution of the shear stresses at the level of the interface during the loading. In this part, we suggest a new equation to determine the maximal shear stresses at the interface plate/concrete on the basis of a parametric study (Varastehpour, 1996). To simulate the non-linear behaviour of material in the distribution of the maximum stress at the interface, we examined the effect of the different variables, such as rigidity and thickness of the plate, geometry of the section, the loading mode,etc. As a consequence of this parametric study, we introduce a factor β, made up of the different variables which have an important influence on the distribution of shear stress at the interface. Figure 2 shows the dispersion of the maximum normalized value of (multiplied by β) the shear stress for different examples determined by a non-linear software as a function of $\beta.\lambda.V$ on a logarithmic scale. By using regression analysis, the best fit line was traced in order to determine the relationship between shear force and shear stress.

$$\tau_{int} = \frac{1}{2} \cdot \beta^{0.5} \cdot (\lambda . V)^{1.5} \qquad (4)$$

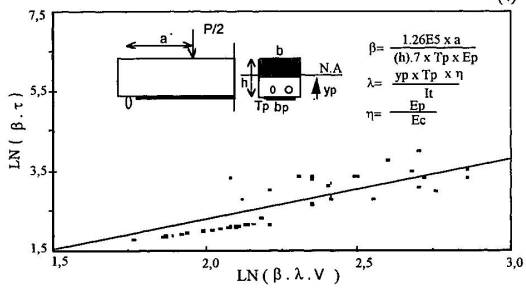

Fig.2 Regression to evaluate the shear stress-load relationships

5. Test results and conclution

The theoretical study of the beam strengthened with a FRP plate, allows to think that the mechanical behaviour (rigidity, resistance) depends strongly on the interaction of the plate/concrete interface. The ultimate capacity of the beam could be determined by the premature failure due to the debonding of the plate. The failure criterion defined in this paper show rupture of the concrete layer situated between the reinforced steel and the FRP plate. Equation [4] is suggested in this study. It allows us to estimate the distribution of the shear stress at the interface. To determine the separation load, it is necessary to solve this equation knowing the admissible interface stress (τ_{int}), and the relation between the applied load and the shear force. For example in the case of a beam under four points bending ($V=p/2$):

$$P_{sep} = \frac{3.2\,\tau_{adm}^{2/3}}{\lambda . \beta^{1/3}} \qquad (5)$$

The admissible shear stress, in this equation, is given by equation [3] according to the premature failure criteria. In the case of beams reinforced by thick plates, this separation load (P_{sep}) corresponds to the ultimate capacity of the beam. Figure 4 shown comparison of the ultimate load, result of differents test and theoretical value when we used classical method or equation [5].

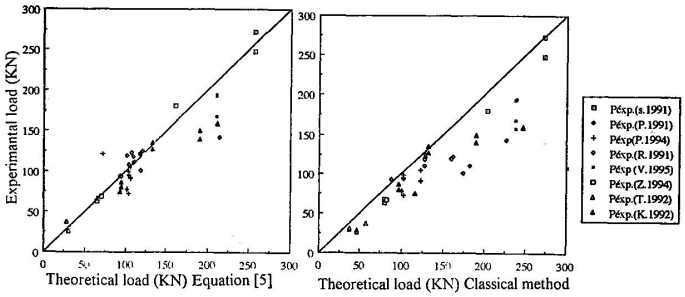

Fig 3: Comparison between experimantal and therotical result

REFERENCE

VARASTEHPOUR H., HAMELIN P.(1996)" Analysis and study of failure mechanism of RC beam strengthened with FRP plate", Second international symposium on composite material in bridges and structures, P. 555-563, 11 august. Montreal, CANADA

ZHANG S., RAOOF M., WOOD L.A. (1995)" Prediction of peeling failure of reinforced concrete beams with externally bonded steel plates", Journal of structures and buildings, Vo.110. No.3, P. 257-268, UK

Dynamic Response of a Full Scale Tested Bridge

Slavko ZDRAVKOVIC
Prof.
Civil Eng. Faculty
Nis, Yugoslavia

Slavko Zdravkovic, born 1947, received civil eng. degree from Univ. of Nis in 1972, Ph.D. from Univ. of Belgrade in 1981. He is an Expert of Fed. Ministry of Science, Tech. and Development.

Danilo RISTIC
Prof.
IZIIS, Univ. of Skopje
Skopje, Macedonia

Danilo Ristic, born 1950, received civil eng. degree from Univ. of Skopjie in 1974, Ph.D. from Univ. of Kyoto in 1988. He is Head of Dept for Civil Eng. Structure, IZIIS, Skopje.

Summary

Presented in this paper is dynamic testing of a reinforced-concrete bridge on the Kumanovo - Titov Veles motor way. The bridge is constructed of precast-prefabricated prestressed simple beams continued by a cast-in place deck structure. The objective of the test was to define the main dynamic characteristics of the structure necessary for the formulation of the mathematical model of this type of structures. Then, a mathematical model was formulated for the tested bridge. The model consists of 79 nodal points and 89 elements. The comparison between the computed and the measured values pointed to very good agreement of the results.

1. Description of the structure

The considered reinforced concrete bridge represents a precast system composed of prestressed simple beams continued by a cast-in-place deck structure with a thickness of 18 cm. Expansion joints exist over the abutments and over the central pier- S5.

The bridge has eight spans (4 x 31 x 2 x 38 + 31 + 26 = 257 m) as presented in Fig. 3. The bridge deck is in a horizontal curvature of R = 600 m, with longitudinal gradient of 1,4% and vertical gradient of 5%. The superstructure rests on the substructure via neoprene bearings that enable displacements in the longitudinal direction of the bridge only. Over piers S3 and S7, the bearings are immovable. The connection with the approach banks is made by cantilever wing walls and transition slabs with a length of 5.00 m.

2. Discussion on the experimental results

The obtained fundamental mode shapes lead to the conclusion that the bridge vibrates as a monolith structure under the given excitation level, i.e., the expansion joint is not activated to a sufficient extent that the two structural units behave separately.

As to damping capacity, coefficients of viscous damping of 0.92% to 1.72% were obtained, with the exception of the longitudinal direction in which 2.66% was obtained for the first symmetric mode. Analysing the obtained results and taking into account the geometrical characteristics of the piers, it is evident that the effect of interaction is most pronounced at the shortest piers (S_{13} and S_{14}). Considering the obtained values, the level of soil-structure interaction can be evaluated as considerably high, which means that the assumption of total fixation at the base is not thoroughly justified in formulating the mathematical model. This conclusion particularly refers to the transverse direction.

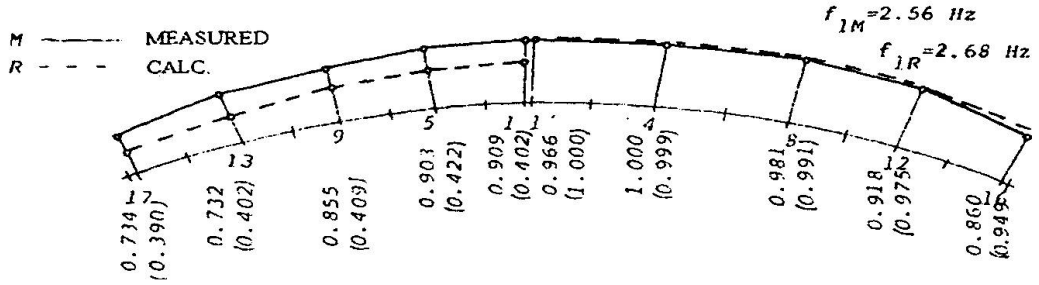

Fig.1 Fundamental horizontal mode under longitudinal excitation, tangential component

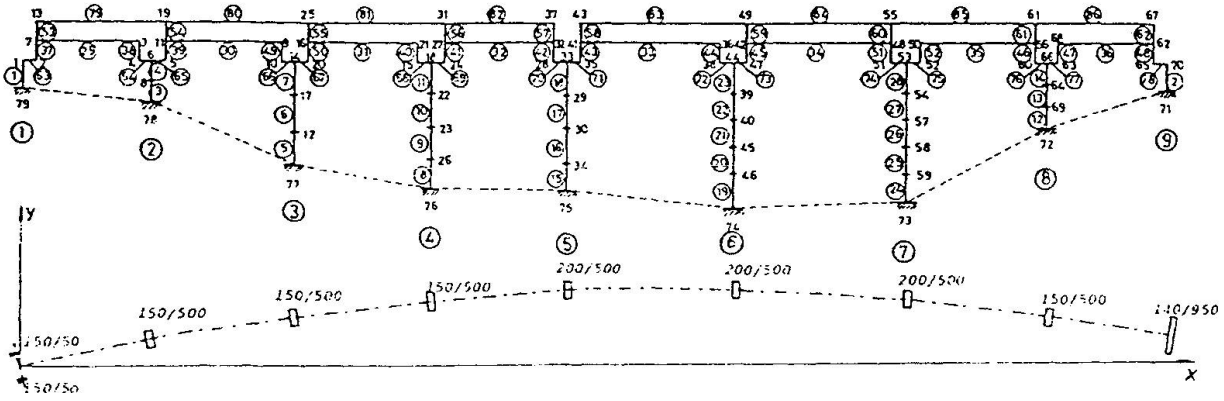

Fig.2 Formulated discrete mathematical model of the bridge structural system

3. Mathematical model formulation for two directions

Fig.2 shows a discrete mathematical model of a system consisting of 79 nodal points and 89 elements. In analysis of the natural vibrations of the system, the model enables interaction of the piers of the substructure through the deck structure which has a considerable horizontal rigidity, as well as, an independent behaviour of the left and the right part of the bridge by modeling of an expansion joint over pier S_5. The mathematical model represents a model of a space frame structure where six degrees of freedom of motion are considered for each node of the system. The same model was used for both longitudinal and transverse directions of vibration. The spectral theory was used for both directions in analysis of the dynamic response of the system.

A reliable proof that the mathematical model of the bridge has appropriately been selected is the comparison between the values computed through the mathematical model and the values obtained by the experimental testing of the full-scale structure.

4. Conclusions

Several important conclusions can be drawn: dynamic response of bridge structures is higly dependent on the structural system itself and for analysis purposes all the constituent components should be realistically modeled; experimental forced vibration tests of full scale structures provide very valuable experimental results for refinement of the formulated model; foundation soil and actual bridge configuration may produce significant soil-structure interaction effects which should be cosidered in the analysis, and based on sufficient experimental results on various bridge types, practical design methodology of bridge structures can successfully be improved.

Effect of Deviators in Long-Span Beams Strengthened by External Tendons

Kiang-Hwee TAN
Sen. Lecturer
National Univ. of Singapore
Singapore

Kiang-Hwee Tan, born 1955, received his doctorate degree in civil eng. from the Univ. of Tokyo in 1985. His research interests include external prestressing and fibre-reinforced polymer (FRP) reinforcement.

Chee-Khoon NG
Research Assist.
National Univ. of Singapore
Singapore

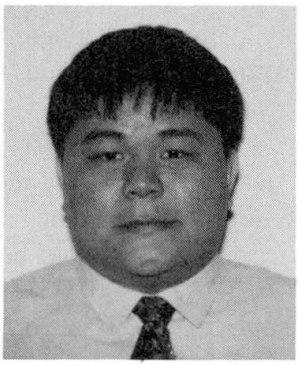

Chee-Khoon Ng, born 1970, received his civil eng. degree from the Univ. of Techn., Malaysia in 1994.

Summary

Careful attention should be placed on the provision of deviators in the flexural strengthening of beams using external tendons, particularly where the beam has very large span-to-depth ratios and second-order effects due to eccentricity variations under load are dominant. In this study, nine prototype T-beams with span-to-effective depth ratios ranging from 7.5 to 30 were prepared and strengthened in flexure using external tendons, with or without deviators positioned at various locations along the span. The beams were loaded at third points to failure. The provision of a deviator at the mid-span section ensured satisfactory service and ultimate load behaviour of the strengthened beams with span-to-depth ratio of less than 20. For beams with higher span-to-depth ratios, two deviators each at the third-span sections are required to achieve the desired performance.

Test Programme

Nine prototype T-beams shown in Fig. 1 were prepared. No deviator was provided in T-0A and T-0B. In ST-1, ST-2, ST-3, ST-4 and ST-5, a 100 mm-wide deviator was provided at mid-span. ST-5A had two deviators at one-third span sections; and ST-5B had three deviators at quarter span sections. The span-to-effective depth ratios, L/d_{ps0}, were 7.5, 9.0, 15, 22.5 and 30.0 for ST-1, ST-2, ST-3, ST-4 and T-0A, and ST-5, T-0B, ST-5A and ST-5B, respectively. All beams were tested under third-point loads.

Test Results and Discussion

The load-deflection characteristics were largely the same for all beams provided with a deviator at mid-span. Beams without deviators showed no difference in deflection characteristics prior to cracking compared to beams provided with deviators (Fig. 2). However, after cracking has occurred, beams without deviators showed a greater reduction in stiffness and a smaller ultimate load. All beams showed ductile behaviour at ultimate. The smaller ultimate deflection registered by ST-5 was due to the failure occurring away from the mid-span at a section where the effective tendon depth was considerably lower due to second-order effects.

The maximum deflection under an assumed service load, defined as the ultimate load divided by a factor of 1.7, was in general less than 1/250 of the span. For beams with a span to depth ratio of less than 20, it is less than 1/350 of the span. All beams registered maximum crack width under the assumed service load of about 0.09 to 0.12 mm, except for ST-2 and ST-5B, for which the maximum crack widths were 0.16 mm and 0.2 mm respectively. These are all well below the allowable value of 0.2 mm for partially prestressed beams. Fig. 4 shows the appearance of four beams after failure.

From the study, it was concluded that one deviator at mid-span is adequate for beams with span-to-depth ratio of less than 20. Otherwise, two deviators should be provided, one at each third-span section, so as to ensure satisfactory service and ultimate load behaviour of the beam.

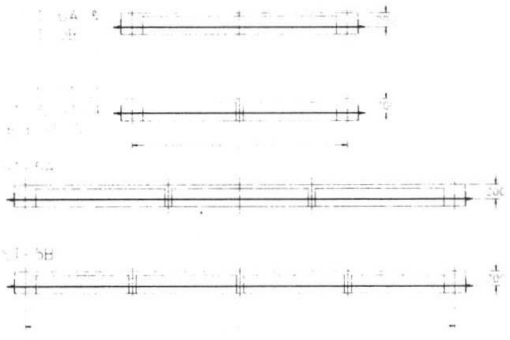

Fig. 1 External tendon and deviator configuration

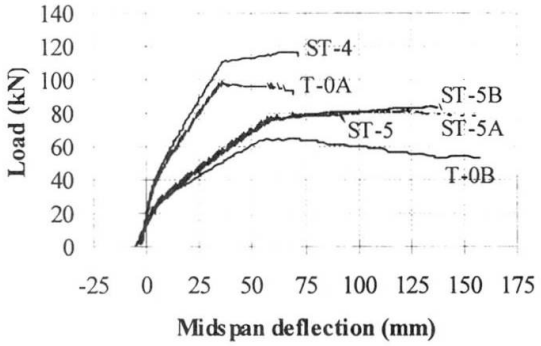

Fig. 2 Load-deflection curves

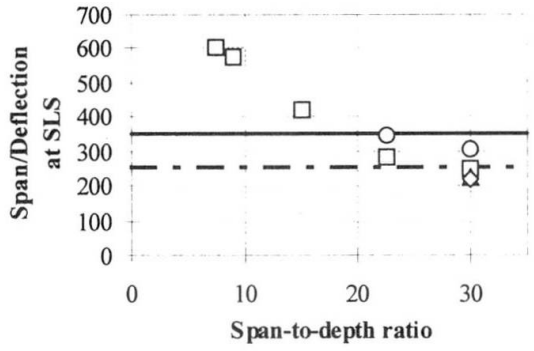

Fig. 3 Service load deflection

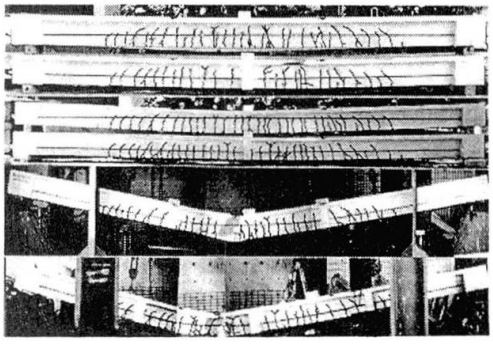

Fig. 4 Appearance of beams at failure

Importance of Higher Strength Steel Wire in Ultra Long Span Designs

William C.BROWN
Manging Director
Brown Beech & Assoc.
London, UK

Stafford CRAIG
Consulting Engineer
Brown Beech & Assoc.
London, UK

Summary

Studies in preparation are showing a requirement for ever increasing spans. The Messina bridge design has a clear span of 3300m and has demonstrated that the inherent aerodynamic problems associated with longer spans can be efficiently overcome. This work looks into the performance of bridge wire for such spans and beyond to demonstrate the advantages of enhancing current wire properties.

1. The influence of cable size on span

Practical considerations would indicate that a single cable diameter of around 1.25m is a reasonable limit in size to ensure good quality compaction. Thereafter multi cables - 2 or perhaps 3 at each side of the bridge will be required. (For a variety of sound reasons, only lines of cables at the sides of the deck should be seen as practical solutions for long spans). Thus the maximum weight may be seen in fig.1 as multiples of 8 tonnes/metre i.e. 16, 32, 48 etc., with the cost per metre of bridge rising accordingly.

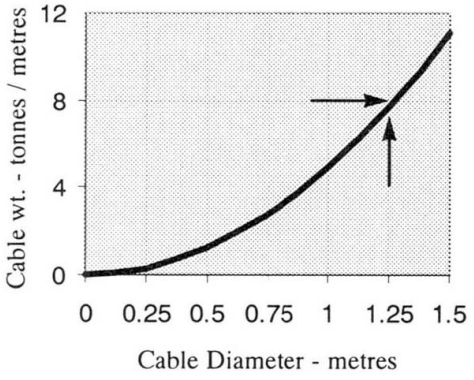

Fig 1 - Relationship of Cable Weight & Diameter

Next we have to look at what this means in terms of span, wire quality, traffic loading, deck weight and most importantly, aerodynamic stability.
Following the loss of the first Tacoma Narrows bridge, deck weights have tended to increase with span, principally to overcome problems associated with aerodynamics. A notable exception was the introduction of the Severn box in 1966 and now the design for the 3300m Messina Crossing has again reversed this trend. With its inherent stability, it sets a pattern for the future ultra-long crossings.
For the purposes of this note the suspended dead weight per traffic lane, including surfacing is therefore taken as 2.5 tonnes/lane. With a minimum of 6 lanes, this gives a deck weight of 15 tonnes/metre of bridge or with live load, 20 tonnes/metre. These are practical objectives for a stable steel deck following the Messina example.

2. Wire strength

However, the suspended structure and traffic has to be carried by the steel cable wire, with the available residual capacity after supporting its own weight and maintaining appropriate reserves for safety and durability. The quality of wire is clearly important. Fig. 2 indicates the influence of span and sag on residual capacity for current production wire (160 kg/mm2). The optimum value of the sag to span ratio depends on several influences - material, seizmic conditions etc but can be expected to lie between 1:10 - 1:11 (Messina for example is set at 1:11) and for this purpose of comparison is taken as 1:10.5.

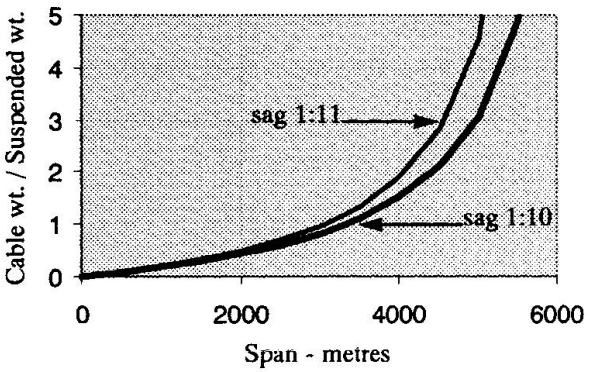

Fig 2 - Influence of Wire

We can now see the effect of varying the wire strength as shown in fig.3. This demonstrates the clear advantage of higher strength wire in the longer spans. A further refinement is to curtail wires over portions of the span where the force is less in the central region. The effects are shown and become more significant for the larger spans.

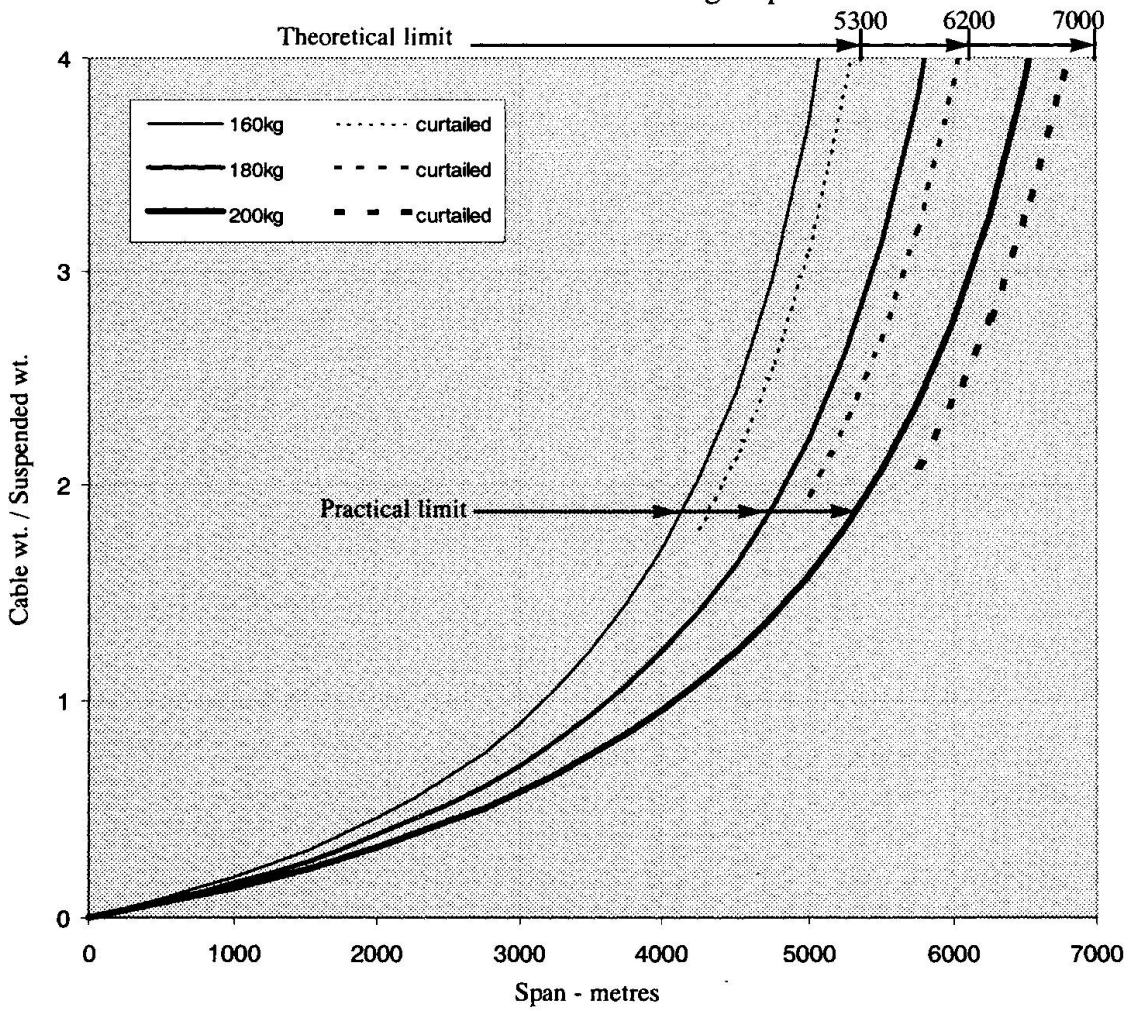

Fig 3 - Influence of Cable Strength